UNIVERSITY OF NEVADA, RENO
MACKAY SCHOOL OF MINES

NEVADA BUREAU OF MINES AND GEOLOGY

BULLETIN 110

INTRUSION-RELATED, POLYMETALLIC CARBONATE REPLACEMENT DEPOSITS IN THE EUREKA DISTRICT, EUREKA COUNTY, NEVADA

Peter G. Vikre

1998

Detailed descriptions of Cretaceous intrusion-related, skarn and polymetallic carbonate replacement deposits in the Eureka district, Eureka County, Nevada.

University and Community College System of Nevada
1998

Nevada Bureau of Mines and Geology

Jonathan G. Price, *Director/State Geologist*

Scientific Research Staff

Economic Geology
Stephen B. Castor, *Research Geologist*
John W. Erwin, *Geophysicist (Emeritus)*
Liang-Chi Hsu, *Research Mineralogist (Emeritus)*
Daphne D. La Pointe, *Research Geologist*
Keith Papke, *Industrial Minerals Geologist (Emeritus)*
Joseph V. Tingley, *Research Geologist*

Engineering Geology
John W. Bell, *Research Engineering Geologist*
Craig M. dePolo, *Research Geologist*
Alan R. Ramelli, *Research Geologist*

Environmental Geology and Hydrogeology
Donald C. Helm, *Adjunct Research Scientist*
P. Kyle House, *Research Geologist*
Paul J. Lechler, *Chief Chemist/Geochemist*
James G. Rigby, *Research Geologist*
Lisa Shevenell, *Research Hydrogeologist*

Geologic Mapping
Harold F. Bonham, Jr., *Research Geologist (Emeritus)*
Jim Faulds, *Research Geologist*
Larry J. Garside, *Research Geologist*
Christopher D. Henry, *Research Geologist*

Research and Administrative Support Staff

Administration and Publication Sales
Terri M. Garside, *Management Assistant*
Cheryl Steed, *Management Assistant*
Charlotte Stock, *Program Assistant*

Analytical Laboratory, Sample Curation, and Geologic Information
David Davis, Geologic Information Specialist
Paul J. Lechler, *Chief Chemist/Geochemist*
Mario Desilets, *Chemist and Quality Assurance Officer*
Bret Pecoraro, *Laboratory Assistant*

Cartography, Publication Support, Geographic Information Systems, and Databases
Ron Hess, *Information Systems Specialist/GIS Supervisor*
Gary Johnson, *Information Systems Specialist*
Janis Klimowicz, *Cartographer*
Dick Meeuwig, *Editor*
Susan L. Tingley, *Publication Manager/Senior Cartographer*
Kris R. Pizarro, *Cartographic Supervisor*
Robert Chaney, *Cartographer*
Jack Hursh, Jr., *Cartographer*

Editing: Dick Meeuwig
Typesetting: Jack Hursh
Graphics: Kris Pizarro

First edition, first printing, 1998, 500 copies
Printed by: Bear Industries, Sparks, Nevada

For sale by the Nevada Bureau of Mines and Geology, Mail Stop 178, University of Nevada, Reno, NV 89557-0088
(702)784-6691 x2 e-mail: info@nbmg.unr.edu

NEVADA BUREAU OF MINES AND GEOLOGY

BULLETIN 110

INTRUSION-RELATED, POLYMETALLIC CARBONATE REPLACEMENT DEPOSITS IN THE EUREKA DISTRICT, EUREKA COUNTY, NEVADA

Peter G. Vikre

1998

MACKAY SCHOOL OF MINES
UNIVERSITY OF NEVADA
RENO

CONTENTS

FIGURES

TABLES

ABSTRACT

The Eureka district, Eureka County, Nevada, includes carbonate replacement and minor vein deposits in Middle and Late Cambrian Eldorado Dolomite and Hamburg Dolomite from which significant amounts of lead, silver, gold, and zinc were recovered, and bulk-mineable, low-grade gold deposits in Late Cambrian and Early Ordovician limestones. The lower Paleozoic section at Eureka has been strongly deformed and dismembered by regional folding, thrust faults, and normal faults, both prior to and after mineralization, and intruded by Late Cretaceous granodiorite, the Ruby Hill stock, and by quartz porphyry. The radioisotopic ages of the intrusions are analytically indistinguishable at ~107 Ma, and both intrusions are spatially and temporally related to replacement deposits. Proximal to the contact with the Ruby Hill granodiorite stock, dolomite and limestone are altered to an early skarn assemblage dominated by diopsidic pyroxene ($Di_{75.1}$ $Hd_{24.3}$ $Jo_{0.6}$), grossularitic and andraditic garnets (Gr_{72} Al_{27} $(Sp+Py+Uv)_1$; Gr_{24} Ad_{74} $(Sp+Py+Uv)_2$; $Gr_{43.5}$ Ad_{55} Sp_1 $(Py+Uv)_{0.5}$), and subordinate magnetite; distally, dolomite, limestone, and calcareous shale are marbleized and hornfelsed. Pyroxene+garnet skarn is partly replaced by hydrous skarn consisting of quartz, pyrrhotite, pyrite, amphibole, chlorite, serpentine, dolomite, calcite, and other hydrated silicate minerals. Other intrusion-related alteration includes three vein sets and selvages in granodiorite and skarn that are composed of quartz, microcline, sericite, and sulfide minerals. Paragenetic relations among magnetite, pyrrhotite, pyrite, and sphalerite in both skarns and replacement deposits indicate local permutations in the stabilities of Fe-O-S minerals within an overall trend of progressive sulfidation, and suggest nearly synchronous formation of pyroxene+garnet skarn, hydrous skarn, veins in granodiorite and hydrous skarn, and replacement deposits following intrusion of the Ruby Hill granodiorite stock. Quartz porphyry, pervasively altered to quartz, sericite, and pyrite, is associated with no obvious contact alteration but contains irregular shear and breccia zones filled with lead and zinc sulfides, pyrite, sericite, and quartz.

Carbonate replacement deposits, which comprise the bulk of historical production, consist of lenses, pods, and pipes of pyrite, galena, sphalerite, several other sulfide and sulfosalt minerals, dolomite, subordinate calcite, and uncommon quartz and barite. Sulfide minerals are nearly completely oxidized to depths exceeding ~250 m (>800 feet). Metals in the important oxidized replacement deposits on Ruby Hill are enriched several times more than equivalent sulfide replacement deposits down-faulted and preserved at depth north of Ruby Hill. These deep sulfide replacement deposits are separated from the Ruby Hill stock by thrust and normal faults with hundreds of meters or more of displacement. The distribution of skarn assemblages and oxygen isotope depletion in dolomite indicates that the displacement by both fault sets largely if not entirely postdates intrusion of granodiorite, and that net displacement moved replacement deposits southward and apically, relative to the granodiorite stock, from their original sites. Most replacement deposits are confined to the lowest dolomites in the Paleozoic section but, other than semi-pervasive fracturing of dolomite, structural control of replacement deposits is subtle, contacts with enclosing dolomite are abrupt, and megascopic wall-rock alteration is absent. Individual sulfide replacement masses are enveloped by shells of ore metals enrichment and oxygen isotope depletion that are up to several times the dimensions of the sulfide masses, markedly enlarging exploration target size. In sulfide replacement deposits pyrite has replaced hydrothermal dolomite and pyrrhotite, remnants of which remain as inclusions. Pyrite has been partly replaced by sphalerite, galena, and other sulfide minerals, but the paragenesis of minerals younger that pyrite is largely indistinguishable. Silver in sulfide replacement deposits (and in productive quartz veins) occurs in various lead-antimony-arsenic-copper-bismuth sulfosalt minerals, and gold, unobserved in sulfide replacement deposits, mostly reports with pyrite in metallurgical tests. All sulfide minerals except galena are finely fractured and cemented with calcite, which upon slight weathering renders sulfide masses extremely friable. Productive vein deposits in the district are composed of quartz, and sulfide and sulfosalt minerals, some of which are common to hydrous skarn and sulfide replacement deposits.

Two sphalerite textural types, monotonically zoned sphalerite and finely banded sphalerite, and variations in Pb/Zn and Ag/Au in sulfide replacement deposits, are spatially related to granodiorite and to quartz porphyry, indicating that metal deposition was associated with the emplacement of both intrusions. Monotonically zoned sphalerite, which is spatially related to granodiorite, occurs in both hydrous skarn and in sulfide replacement deposits both north and south of Ruby Hill. Sphalerite textures and compositions, common sulfide mineralogy (pyrrhotite, pyrite, sphalerite, and galena) among hydrous skarn, hydrous skarn veins, and sulfide replacement deposits, and paragenetically early pyrrhotite inclusions in sulfide replacement deposits further support the interpretation that hydrous skarn and replacement deposits are coeval with the granodiorite intrusion.

Skarn mineral assemblages and fluid inclusion compositions ($XCO_2 \approx 0.075$) indicate that pyroxene+garnet skarn formed above 470°C, and hydrous skarn at lower temperatures, minimally 420°C. Minimum entrapment temperature (pressure-corrected) and salinity ranges for fluid inclusions in hydrous skarn (~340 to 385°C, $NaCl_{eq}$ = 6 to 13 wt.%) and sulfide replacement deposit minerals in the vicinity of Ruby Hill (~360 to 395°C, $NaCl_{eq}$ < 3.5 to 10.4 wt.%), determined by microthermometry, are broadly similar to temperatures derived from arsenopyrite+sphalerite+pyrite (+pyrrhotite) equilibria (averaging ~320 and 315°C for hydrous skarn and sulfide replacement deposits, respectively; maximum for hydrous skarn is ~385°C) and, in part, to sulfur isotope fractionation temperature modes (350 and 270°C for sulfide replacement deposits). The differences between skarn mineral equilibria temperatures and fluid inclusion entrapment temperatures, ~25 to 80°C, are perhaps a result of insufficient pressure corrections. Pressures of ~1 to 1.6 kilobars, determined from H_2O+CO_2+NaCl fluid systematics and hornblende Al^T geobarometry, indicate that granodiorite emplacement and formation of skarns and sulfide replacement deposits occurred

at minimum depths of 3.8 to 6.1 km (2.3 to 3.7 miles). Hydrogen and oxygen isotope compositions of fluid inclusion waters extracted from skarn and sulfide replacement deposit minerals are compatible with Cretaceous meteoric water, mixed with increments of magmatic water, that has exchanged varying amounts of oxygen with carbonate wall rocks.

Paragenetic and stable isotope relationships between pyroxene+garnet skarn, hydrous skarn minerals, hydrothermal dolomite, and sulfide minerals in sulfide replacement deposits, and Eldorado Dolomite enclosing sulfide replacement deposits indicate that hydrothermal dolomite initially crystallized in distal replacement deposit sites from Cretaceous meteoric water that partially exchanged oxygen with Cambrian dolomites. Economic quantities of base and precious metal sulfide minerals, which replaced hydrothermal dolomite and Cambrian dolomites in the same distal sites, pyroxene+garnet skarn, and hydrous skarn minerals were deposited from mixtures of magmatic and partially exchanged meteoric water. Compared to hydrous skarn water, sulfide replacement water, which also created the metal enrichment and oxygen isotope depletion shells enclosing sulfide replacement deposits, has similar deuterium compositions but lighter (more exchanged) oxygen isotope compositions. Differences in the degree of oxygen isotope exchange among waters that deposited hydrothermal dolomite, sulfide replacement deposit minerals, and hydrous skarn minerals may reflect, in addition to meteoric and magmatic water sources, contrasts in dolomite permeabilities.

Sulfur isotope compositions of pyrite, galena, and sphalerite in veins in granodiorite, hydrous skarn and veins in hydrous skarn, and in replacement deposits are consistently heavy, averaging ~14‰, and lead isotope compositions of sulfides and igneous feldspar are uniform and radiogenic. A permissive source of most sulfur and lead at Eureka is subjacent Late Proterozoic-Early Cambrian siliciclastic rocks which contain disseminated pyrite with similarly heavy sulfur and radiogenic lead isotope compositions. Small components of isotopically lighter sulfur and less radiogenic lead are required, and both were presumably derived from older Proterozoic rocks or magmas.

INTRODUCTION

The Eureka mining district lies immediately south and west of the town of Eureka, Eureka County, Nevada (fig. 1). It includes base and precious metal deposits in lower Paleozoic carbonate rocks that have been complexly deformed and displaced by several tectonic events, and altered by two intrusions. Recorded production is approximately 285,000 tonnes (313,000 tons) of lead, 6,360 tonnes (7,000 tons) of zinc, 910 tonnes (1,000 tons) of copper, 53.6 tonnes (1.65 million ounces) of gold and 1,266 tonnes (39 million ounces) of silver from ~1.7 million tonnes of ore during the period 1866-1964 (Nolan, 1962; Nolan and Hunt, 1968). These totals are understated owing to incomplete records prior to 1901 when much of the production took place, and most zinc was never recovered. The major metal deposits are classified as limestone replacement by Nolan (1962), and will be referred to as replacement deposits herein. Quartz vein, and in recent years, disseminated gold deposits have also been mined in the district.

The district measures about 22 km (13 miles) in a north-south direction and is 1.7 to 3.3 km (1 to 2 miles) wide (fig. 1). Most replacement ore production occurred at Ruby Hill and a reserve of several millions of tons of sulfide replacement exists in a block down-dropped by faulting north of Ruby Hill (Love, 1966). Smaller replacement deposits are situated north of Ruby Hill on Mineral Point and south of Ruby Hill on the north end of Prospect Mountain. Disseminated gold at the Windfall and Ratto Canyon deposits was mined in the 1970s and 1980s. In 1993, Homestake Mining Company announced the discovery of a significant disseminated gold resource, the West Archimedes deposit, east of Mineral Point (Dilles and others, 1996).

The spatial relations of metal deposits to intrusions, alteration of igneous and carbonate rocks, elevated temperatures of ore formation, metal zoning, and isotopic compositions of minerals and fluids indicate that igneous rocks are the heat source for the replacement and quartz vein deposits. This paper focuses on the stratigraphy, structure, alteration, and mineral deposits near Ruby Hill, where mine workings and drill holes provide sufficient exposures to reconstruct the tectonic and hydrothermal history of the district. Current interest in the district derives from the high grades of base metal ores, the significant amounts of gold and silver in those ores, and the disseminated gold deposits found in several parts of the district.

Early geologic examinations (King, 1878; Hague, 1883; 1892; Curtis, 1884; Walcott, 1884) are largely supplanted by the work of Nolan and others (1956), Nolan (1962), and Nolan and Hunt (1968); Nolan's (1962) geologic map of the district remains unsurpassed in scope and accuracy. Publications concerned with mining and exploration (Vanderburg, 1938; Binyon, 1946; Sharp, 1947; Johnson, 1958; Miesch and Nolan, 1958), and drill hole cores, logs, and maps in the possession of the Ruby Hill Mining Company and Homestake Mining Company were essential to this study. Surface mapping, underground mapping, and drill hole logging, which provided geological and structural data on the form and distribution of altered and mineralized rocks, were supplemented by several analytic methods that helped define mineral zoning and evolution of hydrothermal events at Eureka. Electron microprobe analyses, X-ray diffractometry, fluid inclusion microthermometry, analyses of both stable and radiogenic isotopes, and major and minor element analyses were used to determine the processes that altered rocks and formed ore.

GEOLOGY

More than 2,100 m (>7,000 feet) of Cambrian rocks underlie the Eureka district, although, because of deformation, in no place is the complete Cambrian section intact. Cambrian rocks comprise, from oldest to youngest, Prospect Mountain Quartzite, Pioche Shale, Eldorado Dolomite, Geddes Limestone, Secret Canyon Shale, Hamburg Dolomite, Dunderberg Shale, and the Windfall Formation (table 1; Nolan and others, 1956). The Cambrian siliciclastic and carbonate rocks are overlain by Ordovician through Early Cretaceous

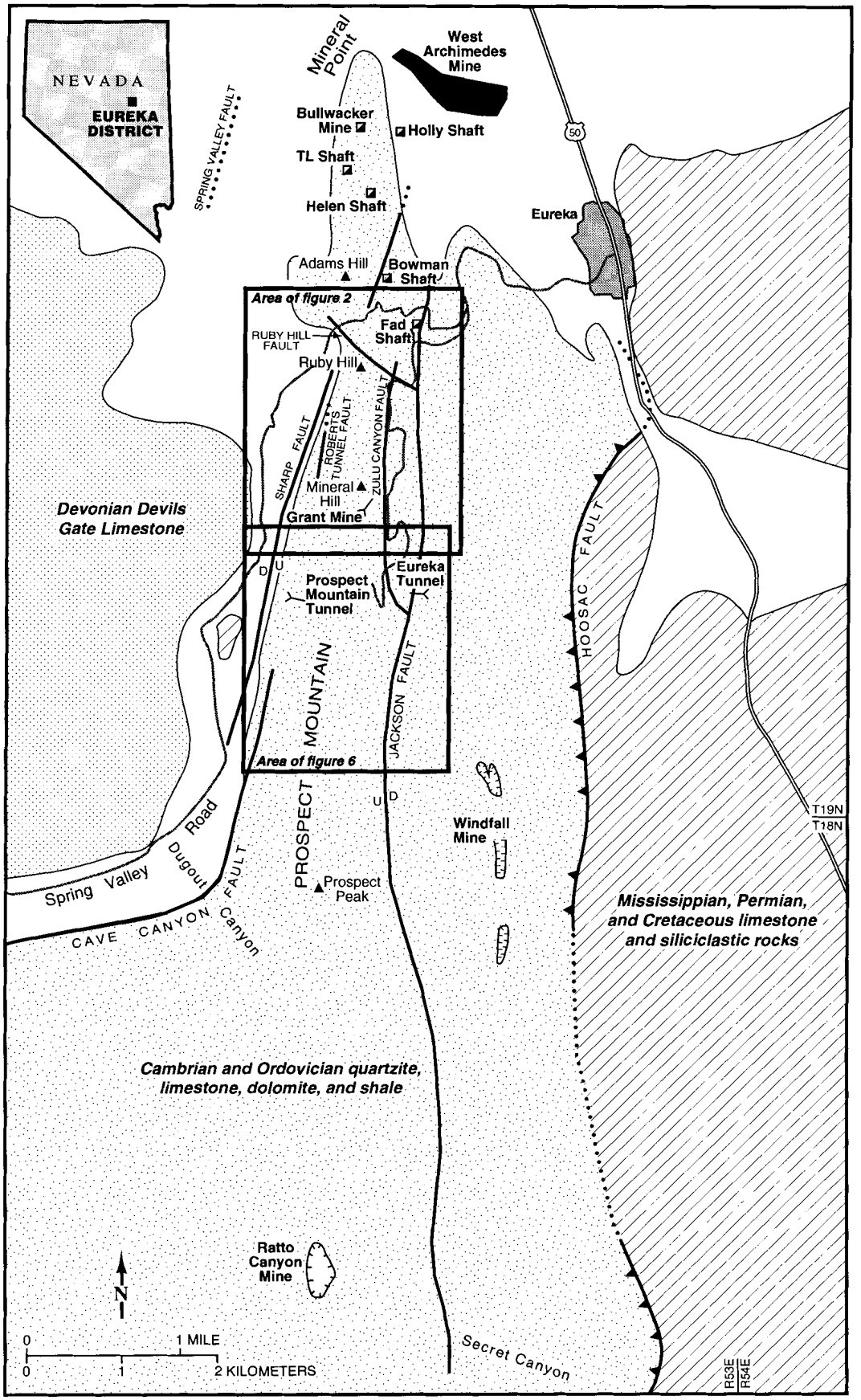

Figure 1. Map of the Eureka district, Eureka County, Nevada, showing generalized pre-Tertiary stratigraphy, major structural elements (after Nolan, 1962; Nolan and others, 1971, 1974), geographic points referred to in the text, and the areas of figures 2 and 6.

Table 1. Pre-Tertiary stratigraphic section of the Eureka district (modified slightly from Nolan and Hunt, 1968).

Cretaceous	quartz porphyry	——	sills and dikes
	granodiorite	——	intrusive stock south of Ruby Hill
	intrusive contact		
Cretaceous	Newark Canyon Formation	200±	freshwater conglomerate, sandstone, grit, shale, and limestone
	unconformity		
Permian	Carbon Ridge Formation	1,000±	thin-bedded sandy and silty limestone; some included sandstone and dark shale.
	unconformity—Ely Limestone absent		
Late Mississippian	Diamond Peak Formation	0–300	conglomerate, limestone and sandstone
	Chainman Shale	500± exposed	black shale with thin interbedded sandstone
	break in section		
Middle and Late Devonian	Devils Gate Limestone	500± exposed	thick-bedded limestone, locally dolomitized.
	Break in section—Nevada, Lone Mountain, and Roberts Mountains Formations absent		
Late Ordovician	Hanson Creek Formation	300± exposed	dark-gray to black dolomite
	unconformity?		
Middle to Late(?) Ordovician	Eureka Quartzite	300	thick-bedded vitreous quartzite
	unconformity		
Early and Middle Ordovician	Pogonip Group	1,600–1,830	chiefly cherty thick-bedded limestone at top and bottom; thinner bedded shaly limestone in middle
Late Cambrian	Bullwhacker Member	400	thin-bedded sandy limestone
Windfall Formation	Catlin Member	250	interbedded massive limestone, some cherty, and thin sandy limestone
	Dunderberg Shale	265	fissile brown shale with interbedded thin nodular limestone
Middle and Late Cambrian	Hamburg Dolomite	1,000	massively bedded dolomite; some limestone at base
	Clarks Spring Member	425–450	thin-bedded platy and silty limestone,with yellow or red argillaceous partings
Secret Canyon Shale			
	Lower Shale Member	220–225	fissile shale at surface; green siltstone underground
Middle Cambrian	Geddes Limestone	330	dark-blue to black limestone; beds ~8–30 cm thick; some black chert
	Eldorado Dolomite	2,500±	massive gray to dark dolomite; some limestone at or near base
Early Cambrian	Pioche Shale	400–500	micaceous khaki-colored shale; some interbedded sandstone and limestone
	Prospect Mountain Quartzite (base not exposed)	1,700±	fractured gray quartzite weathering pink or brown; a few thin interbeds of shale

sedimentary strata, Oligocene volcanic rocks, and Quaternary colluvium. Middle and Late Cambrian Eldorado Dolomite and Hamburg Dolomite are the important host rocks for the carbonate replacement and Windfall gold deposits. Lesser amounts of replacement ore and some gold deposits occur in carbonate rocks of the Late Cambrian Windfall Formation and Early and Middle Ordovician Pogonip Group.

Eldorado Dolomite, the host rock for the replacement deposits in and north of Ruby Hill, includes two varieties of dolomite and minor remnants of fine-grained and well-bedded limestone. One variety of dolomite is blue-gray, massive, and thick bedded. The second variety is lighter gray, coarser grained, displays little texture, and predominantly encloses the replacement deposits. Both varieties of dolomite are finely fractured, and both are interpreted to have been recrystallized, in part hydrothermally, from the fine-grained and well-bedded limestone (Wheeler and Lemmon, 1939; Nolan and others, 1956; Nolan and Hunt, 1968). The Hamburg Dolomite is similar in appearance to Eldorado Dolomite and is also finely fractured in the vicinity of replacement deposits. Some Hamburg Dolomite is also thought to be a product of hydrothermal alteration (Nolan and others, 1956). Hamburg Dolomite is marbleized and altered to pyroxene+garnet skarn and hydrous skarn south of Ruby Hill and on Mineral Hill, and contains replacement deposits in the vicinity of Prospect Mountain and on Mineral Point (fig. 1). Major oxide compositions of Eldorado Dolomite and Hamburg Dolomite are close to that of stoichiometric dolomite (Appendix).

Several igneous rocks intrude the Paleozoic section. A body of Cretaceous granodiorite (classified after LeMaitre, 1989; quartz diorite of Nolan, 1962; granodiorite porphyry of Langlois, 1971), known as the Ruby Hill stock, is exposed on the south slope of Ruby Hill and on the north end of Mineral Hill (table 2, fig. 2A). Although granodiorite is in close proximity to the large replacement deposits of Ruby Hill, it is separated from them by several postmineralization faults. North of Ruby Hill toward Mineral Point (fig. 1) an irregular mass of quartz porphyry, also Cretaceous in age (table 2), crops out near a second group of smaller replacement deposits on Mineral Point.

Although poorly exposed at the surface, granodiorite was encountered in many drill holes. Drill holes, coupled with the distribution of contact alteration and configuration of total field magnetic contours south of Ruby Hill (figs. 2A and 2B), indicate that granodiorite has lateral dimensions of hundreds to thousands of meters. The minimum vertical dimension, known from drill holes, exceeds 670 m (fig. 3), giving the intrusion stock-like proportions. Granodiorite consists of approximately 45 to 50% plagioclase (andesine), 24 to 27% quartz, 15% K-feldspar, 10% biotite and chlorite, and accessory hornblende, magnetite, epidote, sphene, apatite, and titanium oxide (Langlois, 1971; Appendix). Locally it has subporphyritic to glomeroporphyritic texture with hypidiomorphic 1- to 5-mm phenocrysts of quartz, plagioclase, biotite, and rare hornblende set in a slightly finer-grained quartz, plagioclase and K-feldspar matrix. K-Ar ages of biotite phenocrysts in granodiorite average 100.6 Ma (table 2). An $^{40}Ar/^{39}Ar$ biotite phenocryst age is 106.3±0.8 Ma (table 2). An $^{40}Ar/^{39}Ar$ age of biotite+feldspar (granodiorite) endoskarn is 105.0±0.5 Ma (biotite), and an $^{40}Ar/^{39}Ar$ age of a quartz+muscovite vein in hydrous skarn is 107.9±0.5 Ma (muscovite, table 2).

Quartz porphyry intrudes Late Cambrian Dunderberg Shale and Windfall Formation limestones in the vicinity of the Bullwacker, Holly, and Bowman Mines on Mineral Point (fig. 1). In drill holes quartz porphyry also intrudes Hamburg Dolomite, Windfall Formation, and Ordovician Pogonip Group rocks (table 1) north and west of the Fad Shaft (fig. 3). Based on surface exposures and drill hole intercepts, quartz porphyry masses have sill-like attitudes and dimensions. Lateral dimensions of quartz porphyry sills are up to hundreds of meters (Nolan, 1962), and vertical dimensions are tens of meters.

Quartz porphyry is composed of up to 10% rounded quartz phenocrysts, 3 to 5 mm in dimension, and 20 to 30% relict feldspar phenocrysts, 1 to 3 mm in dimension, that have been completely replaced by quartz, sericite, kaolinite, calcite, and sulfide minerals. Several percent chloritized biotite(?) phenocrysts occur in core from some drill holes. The phenocrysts are set in a fine-grained to microcrystalline matrix of quartz, sericite, kaolinite, calcite, and sulfide minerals. In places kaolinite forms a significant proportion of the rock (Langlois, 1971). Sulfide minerals are predominantly pyrite, but in the vicinity of mine workings and in drill core near replacement sulfide deposits, sphalerite and galena, in addition to pyrite, are disseminated in the matrix and occur in thin breccia and fault zones. Coarser-grained sericite (muscovite) occurs with sulfide minerals in some breccia and fault zones, and in selvages to those zones. No unaltered quartz porphyry has been observed in the Eureka district, and quartz phenocrysts are the only remaining major primary mineral. Chemical analyses of least altered samples show less than 63% silica (Langlois, 1971), suggesting an intermediate to mafic composition for the original rock. Quartz porphyry K-Ar muscovite ages average 100.3 Ma, and two $^{40}Ar/^{39}Ar$ muscovite ages average 107.5 Ma (table 2).

The ages determined for each intrusion by both methods are analytically indistinguishable (table 2), but it is not clear why an ~6 Ma age difference for the same rocks resulted from the two dating techniques. If the more precise $^{40}Ar/^{39}Ar$ ages are accepted, then granodiorite and quartz porphyry are both ~107 Ma.

Remnants of a variety of Oligocene eruptive rocks, ranging in composition from rhyolite to basalt, are scattered throughout the district, and dikes related to extrusive rocks have been encountered in mine workings and drill holes (EUD91-13, fig. 2A, table 2), and are locally exposed. Most eruptive rocks are unaltered but porphyritic dikes altered to clay minerals and alunite occur in the Windfall (Rustler Pit) and Ratto Canyon Mines (fig. 1), and at the Hamburg Mine (carbonate replacement deposit). These altered dikes texturally resemble radioisotopically dated Oligocene volcanic rocks (Blake and others, 1975), and two altered dikes penetrated in drill holes have Oligocene ages (731-890, Shadow Canyon, and EDT93-35, Zulu Canyon, fig. 2A, table 2). The altered hornblende-feldspar porphyry dike in Zulu Canyon is unusual in that the phenocrysts and matrix magnetite contain abundant pyrrhotite inclusions. Altered and presumed Oligocene dikes in two disseminated gold deposits, coupled with common structural

Table 2. Radioisotopic ages of Eureka district intrusive rocks and alteration minerals. Rock and mineral identifications are as given by the source; muscovite is considered compositionally equivalent to coarser-grained sericite. Some drill hole (DDH) locations are shown on figures 2A and 3.

Sample no.	Rock type	Location (DDH no.-ft.)	Mineral	K_2O%	$^{*40}Ar$ mol/gm	Percent $^{*40}Ar$	K-Ar Age(Ma) $^{40}Ar/^{89}Ar$ (Ma)	Source
USGS(D) PS64B-14	quartz diorite	Rogers Tunnel dump	igneous biotite	8.31	12.5×10^{-10}	96	102±3.0	1
		Ruby Hill stock	igneous biotite				101±2.0	2
USGS(M) AD39	quartz monzonite porphyry	DDH RH-713, 1388-98	igneous biotite	6.76	1.023×10^{-9}	85	99.8±2.0	3
713-1180	granodiorite	DDH 713 1180	igneous biotite	8.63	1.280×10^{-9}	90.6	100.2±3.0 *106.3±0.8*	4 6
706-1384.5	granodiorite	DDH 706 1384.5	vein selvage muscovite	9.75	1.483×10^{-9}	94.2	102.7±3.0	4
720-1952	granodiorite (biotite+feldspar endoskarn)	DDH 720 1952	igneous(?) biotite	4.87	7.134×10^{-10}	76	99.0±3.0 *105.0±1.0*	4 6
718-794	hydrous skarrn (quartz+musco-vite vein)	DDH 718 794	alteration muscovite				*107.9±0.6*	6
E-3	porphyritic dike		hydrothermal(?) muscovite				103±2	7
JDL-1-70	granodiorite porphyry	DDH 713-1705	vein selvage(?) microcline	10.79	1.331×10^{-11}	40.9	68.2±1.7	5
JDL-2-70	granodiorite porphyry	DDH 713-411	vein selvage(?) sericite	6.73	1.168×10^{-11}	57.5	95.3±2.4	5
713-1565	granodiorite	DDH 713-1565	vein selvage K-feldspar	13.80	1.417×10^{-8}	70.6	70.0±2.1	4
729-1854	quartz porphyry	DDH 729	alteration muscovite+quartz	5.60	8.515×10^{-10}	93.1	102.6+4.0	4
729-1902	quartz porphyry	DDH 729	alteration muscovite	6.67	9.950×10^{-10}	95.0	100.8±3.0 *107.9±1.0*	4 6
EUD91-2A	quartz porphyry	Bullwacker Dump	alteration muscovite	8.36	1.234×10^{-9}	94.7	99.7±3.0 *107.0±1.0*	4 6
JDL-1-69	andesite porphyry Bullwacker Sill	Mineral Point(?)	(alteration) sericite	7.72 (%K)	1.290×10^{-11}	55.4	98.1±1.8	5
EUD91-13	quartz-feldspar porphyry dike	Locan Shaft	igneous biotite	7.69	4.064×10^{-10}	76	36.8±1.1	4
731-890	altered felsic dike	DDH 731 Shadow Canyon	igneous biotite				*35.82±0.22*	6
EDT93-35	hornblende-feldspar dike	Zulu Canyon	igneous hornblende	0.990	4.436×10^{-11}	74	30.9±1.2	4

$^{*40}Ar$ = radiogenic ^{40}Ar

1 Marvin and Cole (1978)
2 Armstrong (1970)
3 Silberman and McKee (1971)
4 This paper; analyses by E.H. McKee
5 Langlois (1971)
6 This paper, $^{40}Ar/^{39}Ar$ age (Ma) plateau ages and total gas ages, analyses by New Mexico Geochronological Research Laboratory (Socorro, NM).
7 M.L. Silberman

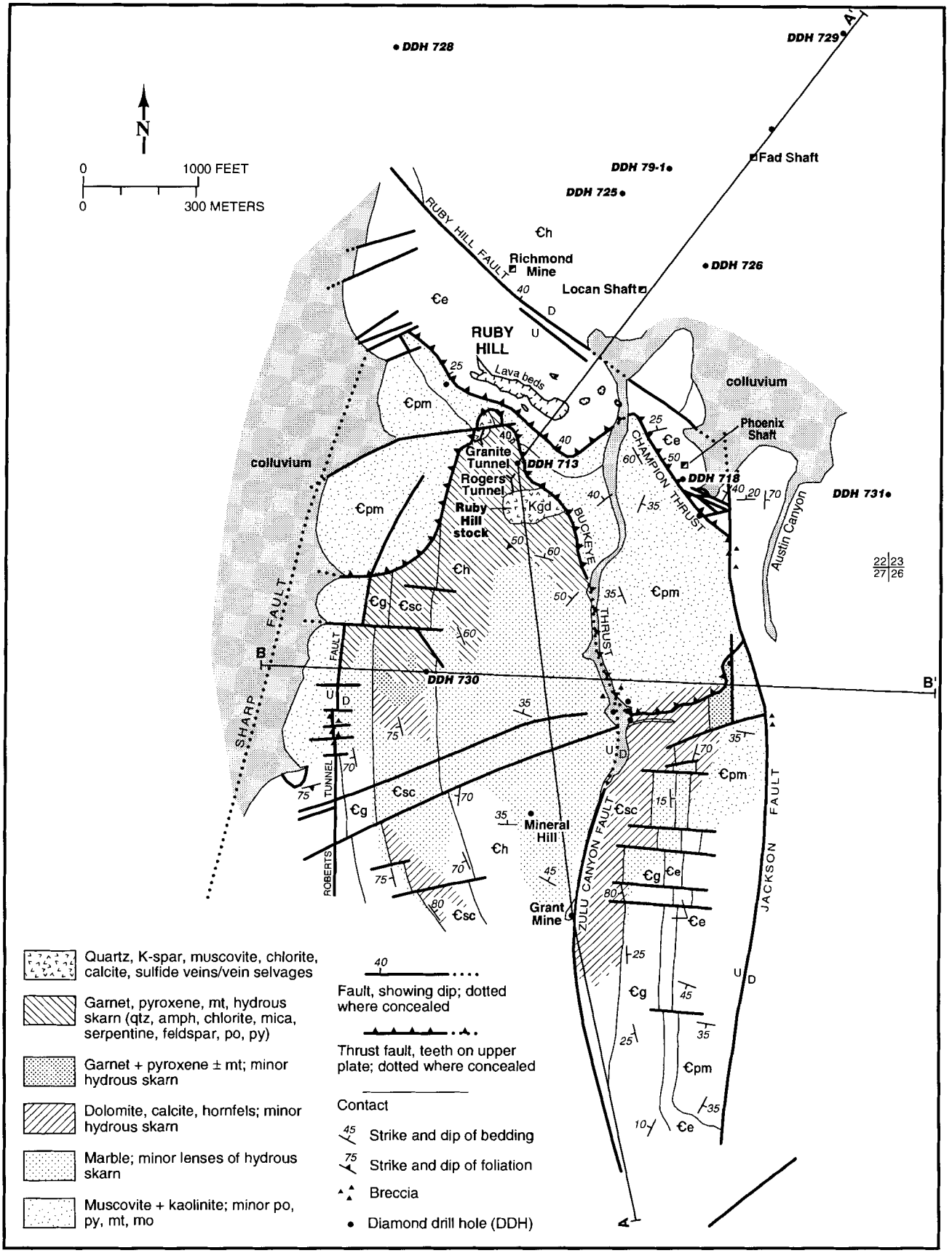

Figure 2A. Map of lithologies, structures, and contact zone alteration assemblages surrounding the Ruby Hill stock. Also shown are drill holes (DDH) from which subsurface data were obtained, geographic points referred to in the text, and lines of sections (figs. 3, 9A, 11, and 13). Lithologic designations are mostly those used by Nolan (1962): Kgd = granodiorite, €pm = Prospect Mountain Quartzite, €e = Eldorado Dolomite, €g = Geddes Limestone, €sc = Secret Canyon Shale, €h = Hamburg Dolomite, qtz = quartz, amph = amphibole, py = pyrite, mt = magnetite, mo = molybdenite. Location of the area of figure 2A is shown on figure 1.

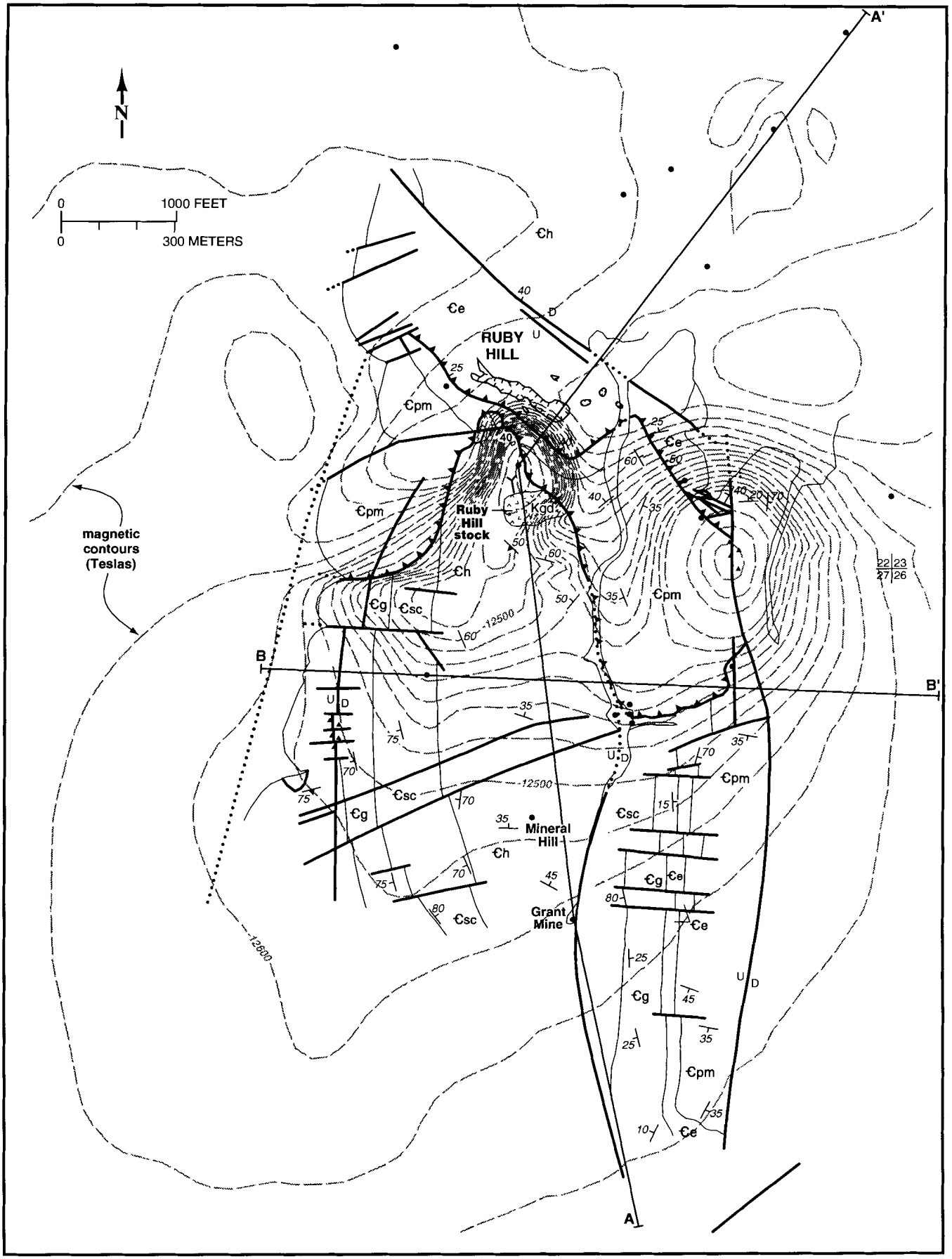

Figure 2B. Total field magnetic intensity (Teslas) contoured over the area of figure 2A (data from ASARCO files).

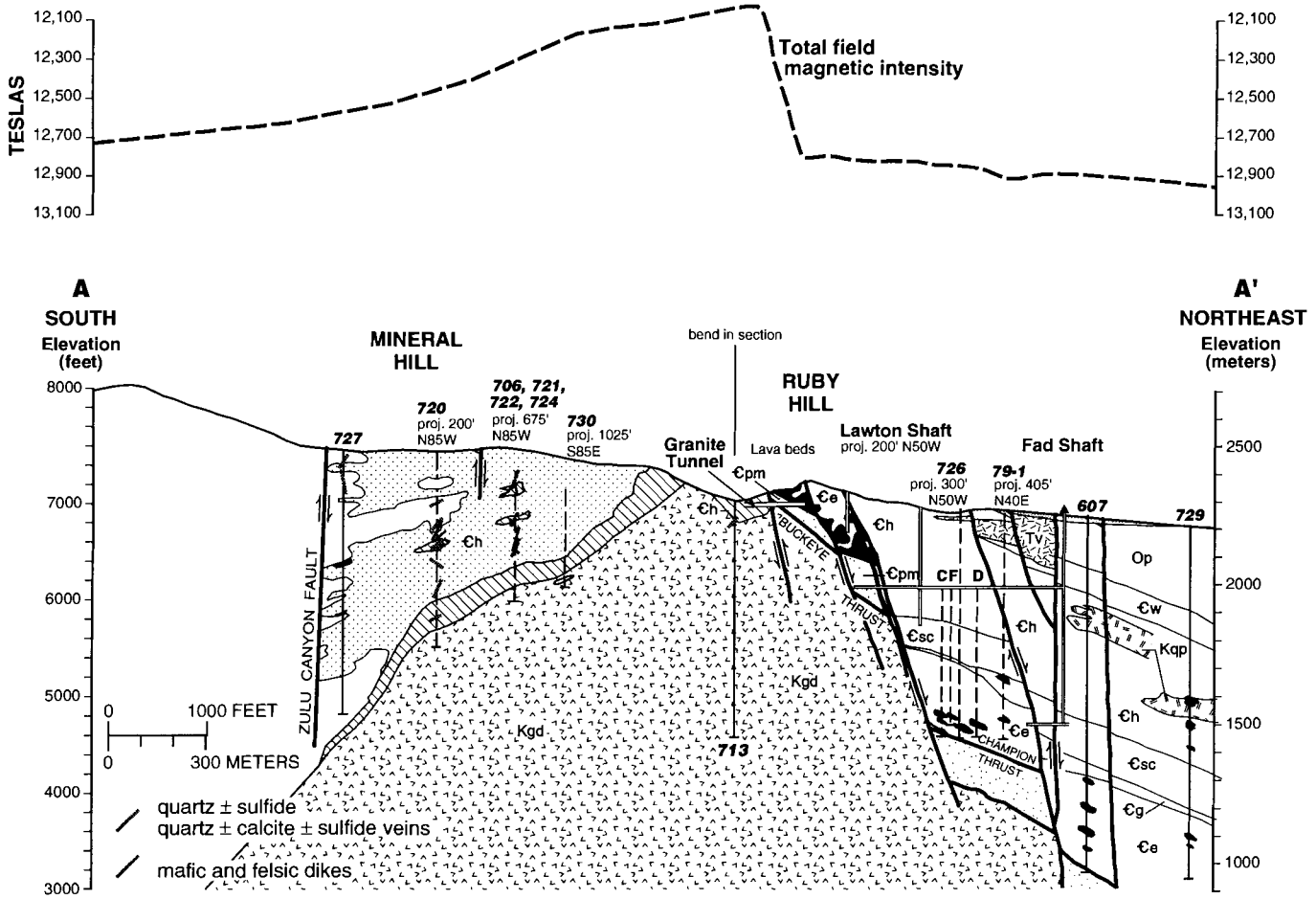

Figure 3. Sections A-A' and B-B' (on facing page) in the vicinity of the Ruby Hill stock, showing lithologies, contact zone alteration assemblages, structures, replacement deposits, drill holes, and mine workings from which subsurface data were obtained, and total field magnetic intensity profiles (Teslas). Filled (black) shapes in Ruby Hill and beaded on drill holes are oxide and sulfide replacement deposits, respectively. See figure 2A for locations of sections, most lithologic designations, and descriptions of contact zone alteration assemblages. Other lithologic designations: Kgp = quartz porphyry, Op = Pogonip Group, Tv = Tertiary volcanic rocks.

controls of disseminated gold deposits, several gold-mineralized faults, and altered dikes (described below) suggest that disseminated gold deposits and other gold mineralized structures are Oligocene.

STRUCTURE

Rocks in the Eureka district have been folded and faulted several times and the portion of the district near Ruby Hill is especially structurally complex. Prior to the Cretaceous, Paleozoic rocks were folded, tilted, overturned, and displaced by at least three low-angle thrust faults (Nolan, 1962). Farther to the south other thrust faults, including the Hoosac fault, have laterally displaced Paleozoic rocks (Nolan, 1962; Nolan and Hunt, 1968; Nolan and others, 1971, 1974; fig. 1). Intrusion of granodiorite in the Cretaceous further deformed the Paleozoic section. Basin-and-range normal faulting has segmented the district and Paleozoic rocks to the east into a series of alternating, north-trending horsts and grabens; nearly all of the Eureka district is confined to the westernmost horst (figs. 1 and 2A). The group of normal faults (Cave Canyon, Sharp, Roberts Tunnel, and Spring Valley faults) along the west side of the Eureka district horst trends northerly and separates early Cambrian rocks from Devonian Devils Gate Limestone to the west, indicating a displacement, barring tectonic foreshortening, of more than 750 m (>2,500 feet). The easternmost normal fault, the Jackson fault (and a branch, the Zulu Canyon fault), has even greater apparent displacement, based on stratigraphy. The Jackson fault trends northerly and juxtaposes Eldorado Dolomite and Hamburg Dolomite on the west with Ordovician Pogonip Group carbonate rocks to the east, indicating a total displacement on the order of 1,500 m (~5,000 feet). However, because of tectonic foreshortening, total displacement is probably less. These normal faults define the boundaries of the horst of Paleozoic rocks which contains Ruby Hill and nearly all metal deposits in the district (figs. 1 and 2A), and these faults, at least in part, coincide with Tertiary

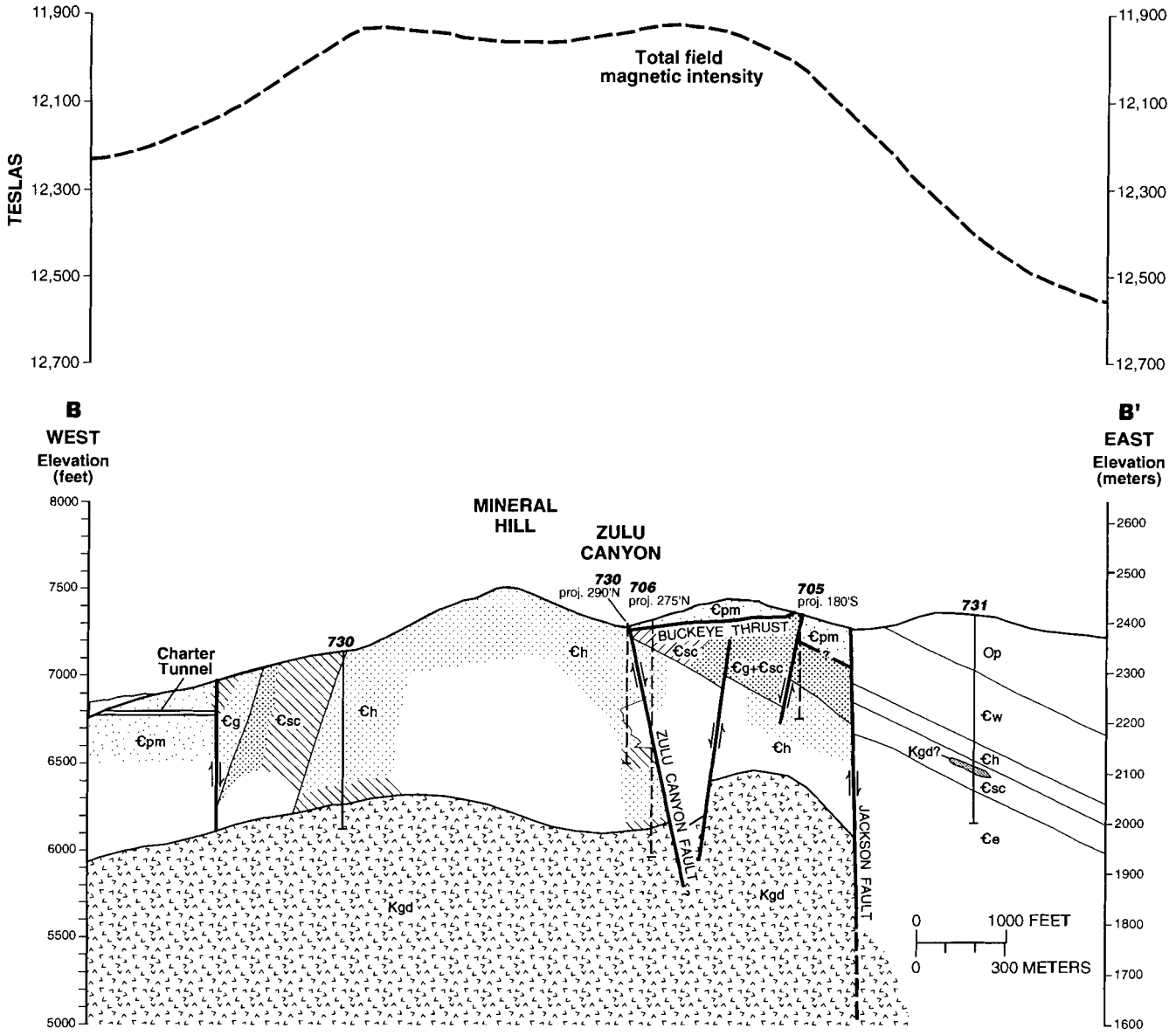

basin-and-range tectonism. The westernmost group of normal faults appear to postdate ore, but parts of the Jackson fault (between the Phoenix Shaft and upper Austin Canyon, fig. 2A) and Roberts Tunnel fault (fig. 1) are gold-mineralized.

Cambrian rocks in the vicinity of Ruby Hill can be divided into two structural domains, one north of the Ruby Hill granodiorite stock, and one south of the Ruby Hill granodiorite stock (fig. 2A). In the north structural domain the normal stratigraphic section, including the Prospect Mountain Quartzite through the Windfall Formation, has been displaced laterally along two parallel thrust faults, the Buckeye and Champion, and vertically by the northwest-trending Ruby Hill, Martin, and Office normal faults (Nolan, 1962; fig. 3). The north domain is bounded on the east by the Jackson normal fault and on the west by the Cave Canyon and Sharp faults.

South of the Ruby Hill granodiorite stock, overturned Cambrian rocks define the south domain. Hamburg Dolomite, Secret Canyon Shale, Geddes Limestone, Eldorado Dolomite, and Prospect Mountain Quartzite comprise a north-plunging antiform, cored by Hamburg Dolomite of Mineral Hill, that is bisected on the east limb by the north-south Zulu Canyon fault and on the west limb by the Roberts Tunnel fault (Nolan, 1962; fig. 2A). The south structural domain is also bounded on the east and west by the Jackson and Sharp-Cave Canyon faults, respectively. A separate sheet of Prospect Mountain Quartzite has been displaced over the antiform along the low-angle Buckeye thrust fault which continues northward and dips beneath Ruby Hill (figs. 2A and 3). The Buckeye thrust fault and the Ruby Hill stock largely obscure the relationship between the two structural domains. The Champion thrust fault separates Prospect Mountain Quartzite and Eldorado Dolomite in Ruby Hill. Both thrust faults are exposed in the Granite Tunnel (fig. 4).

The sequence of structural events in the vicinity of Ruby Hill can be determined by the distribution of hydrothermally altered and mineralized rocks. Contact zone skarn assemblages that replace Hamburg Dolomite adjacent to the Ruby Hill granodiorite stock formed in overturned rocks of the south

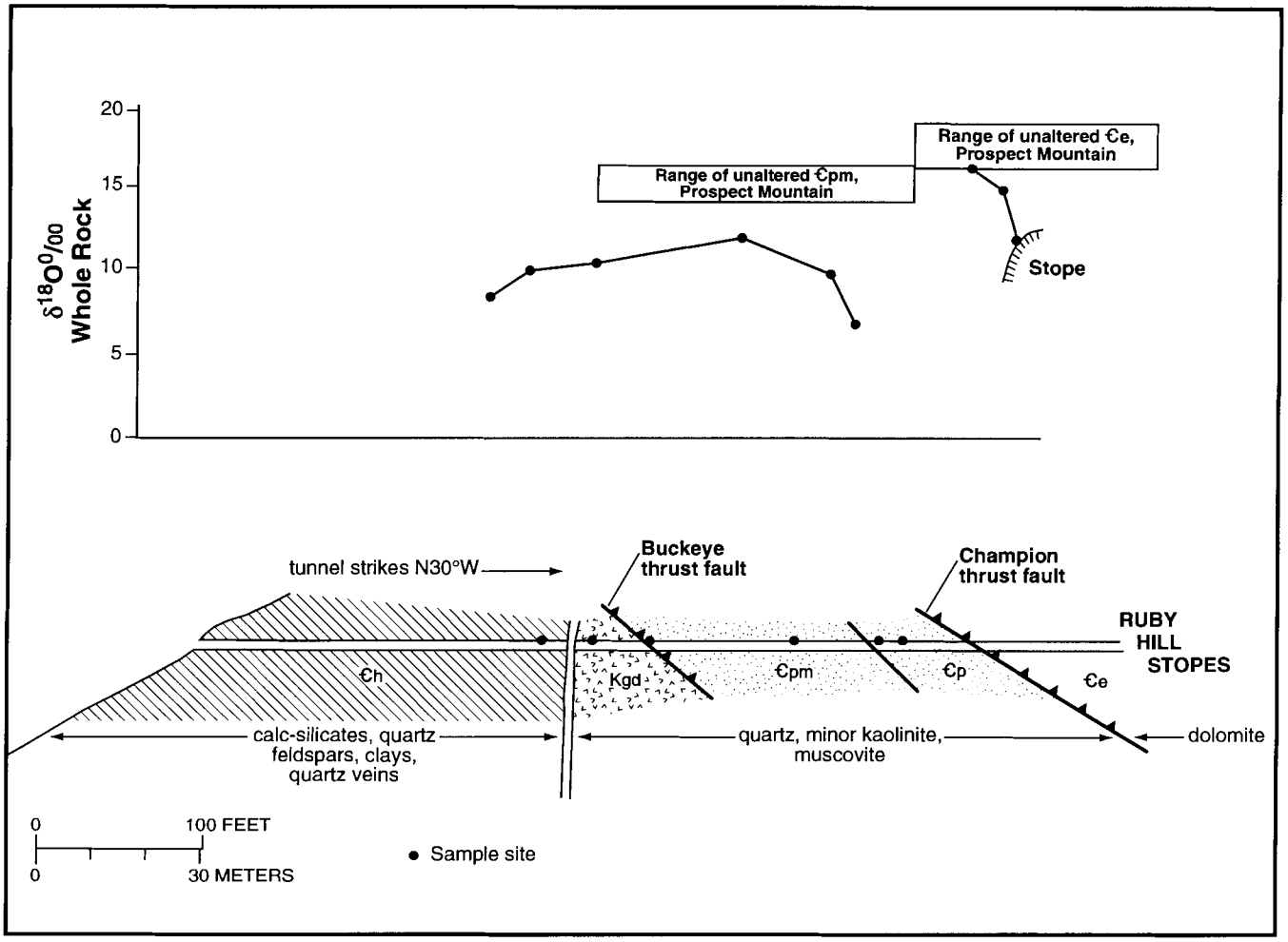

Figure 4. Section looking west through the Granite Tunnel in Ruby Hill, showing the Buckeye and Champion thrust faults, contact zone alteration assemblages, and oxygen isotope depletion associated with the Ruby Hill stock and replacement deposits in Ruby Hill. The location of Granite Tunnel is shown on figure 2A and isotope data are from table 8. The ranges of unexchanged or less extensively exchanged €pm and €e (rectangles) are derived from samples on Prospect Mountain.

domain antiform. Thus, south domain rocks were overturned and thrust-faulted into position prior to intrusion of the granodiorite, and later offset by the high-angle Zulu Canyon and Roberts Tunnel faults. Subsequently, the north domain of normally sequenced strata was thrust southward over the south domain antiform and Ruby Hill stock along the Buckeye, Champion, and subparallel thrust faults exposed in the Granite Tunnel (fig. 4). Two lobes of the Buckeye thrust sheet, composed of Prospect Mountain Quartzite and Pioche Shale, now flank the Ruby Hill stock to the east and west, partly covering the overturned south domain antiform of Mineral Hill and the northern traces of the Zulu Canyon and Roberts Tunnel faults (fig. 2A).

Some movement along the Buckeye thrust fault also predates intrusion of the Ruby Hill stock as both Prospect Mountain Quartzite and Pioche Shale in the hanging wall exposed on Ruby Hill and in the Granite Tunnel are intensely brecciated and altered to sericite and clay minerals (fig. 4). Quartz-sulfide veins that cut both the Ruby Hill stock and contact zone skarns also occur in hanging-wall quartzite of the Buckeye thrust fault. However, gouge in and planarity of the Buckeye thrust fault suggests an increment of postmineralization displacement. The Champion thrust fault apparently experienced post-Cretaceous movement as it separates unaltered Eldorado Dolomite from altered quartzite and shale of the Buckeye thrust fault hanging wall. The absence of calc-silicate alteration of Eldorado Dolomite coupled with oxygen isotope analyses of footwall and hanging-wall rocks in the Granite Tunnel (discussed in a later section) permit the interpretation that most, if not all movement on the Champion thrust fault postdated intrusion of the granodiorite.

The direction of movement along the postmineralization Champion thrust fault can be surmised from characteristics of altered rocks. Drill holes north of Ruby Hill show that the north structural domain extends at least several miles to the north and is displaced only by northwest-trending normal faults, such as the Ruby Hill, Martin, and Office faults, which successively down-drop Cambrian strata and replacement deposits to the north as much as 1,000 m (~3,300 feet; fig. 3). Thermal and mineral zoning in skarn and replacement deposits both north and south of the Ruby Hill stock indicate that the replacement deposits formed north of Ruby Hill in north domain rocks that have since

been displaced southward, perhaps hundreds, but probably not thousands of meters, along the Champion thrust fault.

Initial displacement on the Jackson fault apparently occurred after intrusion of the Ruby Hill stock because skarn and replacement deposits are cut off by the fault and no evidence of alteration or mineralization has been found by drilling east of the fault. Gold occurs in a silicified and ferruginous section of north-trending Jackson fault between the Old Jackson Shaft and prospects at the head of Austin Canyon (fig. 2A). This gold may be associated with the gold deposits which are localized by north-south faults at the Windfall and Ratto Canyon Mines 5 and 10 km (3 and 6 miles) south of Ruby Hill, respectively (fig. 1). Altered, north-striking porphyritic dikes that texturally resemble Oligocene eruptive rocks in the district (Blake and others, 1975) occur in the Windfall and Ratto Canyon Mines, and altered, porphyritic dikes were intersected in drill holes in Zulu and Austin Canyons (fig. 2A). The dikes in the drill holes have Oligocene radioisotopic ages (table 2) suggesting a genetic relationship between disseminated gold deposits and certain Oligocene eruptive rocks. The north-south Roberts Tunnel fault (figs. 1 and 2A), a high-angle fault parallel to the horst-bounding Jackson and Sharp faults, may also have been mineralized with gold in the Oligocene.

ALTERATION

Alteration of Cambrian carbonate and siliciclastic rocks, and Cretaceous intrusive rocks near Ruby Hill and on Mineral Point can be spatially divided into: (1) alteration of Cretaceous intrusive rocks, (2) alteration of the contact zone between Cretaceous intrusive and Cambrian carbonate and siliciclastic rocks, and , (3) alteration associated with replacement deposits. Alteration of granodiorite at Ruby Hill is largely confined to veins and vein selvages in the intrusion but also includes minor development of endoskarn evident in diamond drill holes (DDH) south of the Ruby Hill stock. Some veins similar to those in the intrusion also cut adjacent altered sedimentary rocks of the contact zone. Contact zone alteration of Cambrian carbonate and siliciclastic rocks is restricted to an annular zone bordering granodiorite, but carbonate rocks are extensively recrystallized to marble and minor hornfels farther from the stock. Replacement deposits are distal to but not contiguous with contact zone alteration. They consist of replacement of dolomite by hydrothermal dolomite, minor calcite, and sulfide minerals (now entirely to slightly oxidized) with no obvious wall-rock alteration, but measurable element exchange with wall-rock dolomite.

Alteration of Cretaceous Intrusive Rocks

Although granodiorite crops out only in two small exposures south of Ruby Hill, a much larger subsurface extent is indicated by the distribution of alteration minerals, by the configuration of magnetic contours, and by penetrations of the intrusion in nine rotary and diamond drill holes (figs. 2 and 3). Several of these drill holes cut thick sections of contact zone alteration and granodiorite below surface oxidation and the following descriptions are based largely on drill core.

Vein-related alteration of granodiorite is the product of three distinct vein types: (1) quartz-microcline-pyrite veins, (2) quartz-sericite-pyrite veins, and (3) carbonate veins. The first type consists of quartz, microcline, and pyrite veins, with subordinate amounts of calcite, sericite and molybdenite, that are enclosed by 2- to 8-cm-thick inner selvages of pink microcline, sericite, unaltered biotite, chlorite, pyrite, and molybdenite. These veins are up to 10 cm thick and their abundance increases with depth. The inner selvage microcline replaces primary quartz, feldspars, and most biotite, and has largely destroyed original subporphyritic texture, producing a xenomorphic texture. Small amounts of calcite, epidote, and clinozoisite locally replace plagioclase, and some biotite is partially altered to chlorite, calcite, epidote, magnetite, sphene, and pyrite in the inner selvages. Outer selvages are light gray to green and composed of sericitized feldspars, chloritized biotite, relict quartz, and pyrite. Within outer selvages the original subporphyritic texture of the rock has largely been retained.

The second vein type, consisting of quartz, sericite (muscovite), pyrite, and rare molybdenite, is flanked by selvages of these minerals which replace primary feldspars and biotite up to 30 cm from the vein. The selvages are divisible into an inner zone of pale green, coarse grained sericite, quartz, pyrite, and molybdenite in which original rock texture has been totally destroyed, and an outer zone of partly sericitized plagioclase and quartz. Primary feldspars and biotite may remain in the outer zone. Quartz-sericite-pyrite veins are usually at most a few centimeters wide but locally attain a thickness of approximately 10 cm. Sulfide minerals locally make up several percent of both quartz-microcline-pyrite and quartz-sericite-pyrite veins.

Sericite-dominated veins (type 2) cut quartz-microcline-pyrite veins (type 1), and sericite completely replaces selvage microcline where the two vein types are superimposed. Large volumes of granodiorite consist of coalescing selvages of the two vein types. Unaltered granodiorite is locally present between widely spaced veins. Quartz, pyrite, and molybdenite veins, apparently coeval with either quartz-microcline-pyrite (type 1) or quartz-sericite-pyrite (type 2) veins in granodiorite, cut skarn in the contact zone and probably correlate with sulfidation of skarn as described below. Some of these veins extend into Prospect Mountain Quartzite and Pioche Shale on the north side of Ruby Hill (fig. 4), although their abundance in the siliciclastic rocks is much lower that in the intrusion. Primary biotite from unaltered granodiorite, type 2 vein selvage sericite (muscovite), granodiorite endoskarn biotite, and skarn muscovite provided the Cretaceous radioisotopic ages of granodiorite (table 2).

Calcite and dolomite veins, the third vein type, cut both type 1 and type 2 veins, and carbonate minerals locally pervade older vein selvages, partly replacing microcline. Carbonate veins diminish in frequency with depth.

Quartz porphyry is pervasively altered to quartz, sericite, kaolinite, calcite, and pyrite, as described above. The contacts in drill holes are invariably sheared and no alteration is obvious

in adjacent carbonate rocks. Marble and hornfels are locally developed along quartz porphyry contacts on Mineral Point according to Langlois (1971). Matrix and vein selvage sericite (muscovite) provided the Cretaceous radioisotopic ages of quartz porphyry (table 2).

Contact Zone Alteration

Contact zone alteration consists of two proximal skarn assemblages, pyroxene+garnet skarn and hydrous skarn, and distal marble with lesser amounts of hornfels. The proximal alteration assemblages resulted from metasomatism of Hamburg Dolomite along the contact with granodiorite south of Ruby Hill. Cambrian siliciclastic rocks near the granodiorite stock were also altered but, because of protolith compositions, no calc-silicate minerals formed in them. Distal contact zone alteration consists of extensive volumes of marble and minor amounts of hornfels that formed from Cambrian carbonate rocks and shale (Hamburg Dolomite, Geddes Limestone, and Secret Canyon Shale) south of Ruby Hill. The distribution of both skarn assemblages, marble, and hornfels varies considerably in lateral extent and intensity, and is strongly controlled by lithology as well as distance from the stock (figs. 2A and 3). Skarn assemblages south of Ruby Hill are distributed annularly around intrusion exposures or subsurface apophyses (encountered in drill holes), and range in thickness from a few tens to more than 300 m (>1,000 feet). Skarn assemblages on the north and west sides of the Ruby Hill stock, where they are truncated by the Buckeye thrust fault, are more contiguous than on the south side of the stock. Marble and hornfels extend nearly 1 km (~3,300 feet) south of the Ruby Hill stock. The following description of contact zone alteration is based on both drill core and surface exposures.

Pyroxene+garnet skarn

Pyroxene+garnet skarn consists of massive to partial replacement of carbonate rocks proximal to the Ruby Hill stock by pyroxenes, garnets, and lesser amounts of magnetite. Pyroxene+garnet skarn that completely replaces Hamburg Dolomite adjacent to the north and west sides of the Ruby Hill stock consists of diopsidic pyroxene (average $Di_{75.1}$ $Hd_{24.3}$ $Jo_{0.6}$), grossularitic garnet (average Gr_{72} Al_{27} $(Sp+Py+Uv)_1$), and subordinate augite and clinoenstatite (figs. 2A, 3, and 5; table 3). These minerals reflect the addition of iron, aluminum, and silica to Hamburg Dolomite, which originally consisted of subequal amounts of calcium and magnesium carbonate (Appendix), during intrusion of granodiorite. On the north and west sides of the stock, magnetite, pyrrhotite, and pyrite are commonly intergrown with diopside and grossularite. Subequal amounts of magnetite and pyrrhotite also occur locally in nearly massive pods that measure up to several meters in dimension. These pods, which are absent south of the stock, are largely responsible for the strong and convoluted magnetic gradients on the north and west sides of the stock (figs. 2B and 3), and emphasize the lateral asymmetry of contact zone alteration. Magnetite and pyrrhotite are much less abundant south of the Ruby Hill stock exposure.

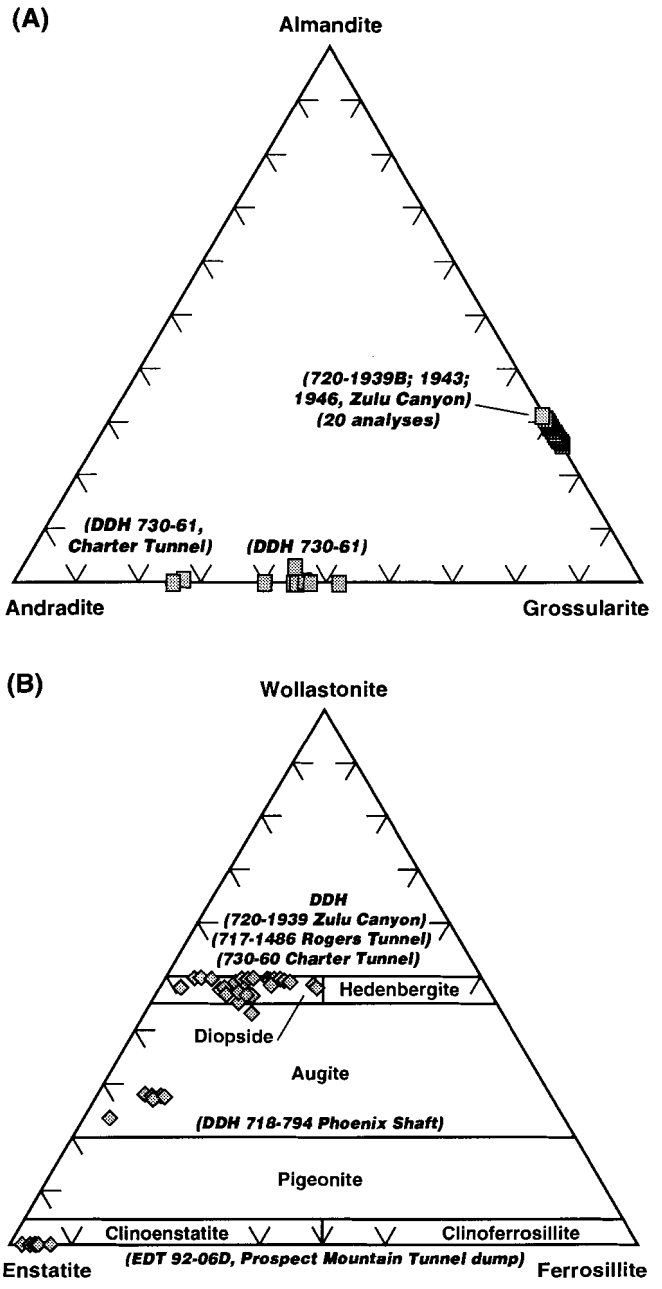

Figure 5. (A) Garnet compositions, expressed as mole percent end member grossularite, almandine, and andradite. (B) Pyroxene compositions, expressed as mole percent end member wollastonite, enstatite, and ferrosillite, determined by microprobe, in contact zone alteration assemblages. Representative compositions are given on table 3.

In two areas about 500 to 700 m (~1,650 to 2,300 feet) southwest and southeast of the Ruby Hill stock, pyroxene+garnet skarn completely replaces Hamburg Dolomite, Geddes Limestone, and Eldorado Dolomite (fig. 2A), and similar to pyroxene+garnet skarn north of the Ruby Hill stock, bedding in all three formations is entirely obliterated. These skarn exposures are characterized by diopside and andraditic garnet (average Gr_{24} Ad_{74} $(Sp+Py+Uv)_2$ and $Gr_{43.5}$ Ad_{55} Sp_1 $(Py+Uv)_{0.5}$) (figs. 2A, 3, and 5; table 3), and both occurrences relate to the relatively shallow subsurface presence

Table 3. Representative oxide compositions (in weight percent oxide) and average end member compositions (in mole percent) of pyroxenes, garnets, and amphibole from diamond drill holes in skarn near the Ruby Hill granodiorite stock, on Mineral Hill, and on Prospect Mountain. Analyses are by microprobe (T. Solberg, Virginia Tech. Univ.; P. Hansley and T. Cookro, Petrographic Consultants, Inc.). DDH (diamond drill hole) 720 is in Zulu Canyon, southeast of Ruby Hill; 718 is a the Phoenix Shaft; 730 is on Mineral Hill; EDT92-06D4 is from the Prospect Mountain Tunnel dump (figs. 2A and 3).

A. Representative oxide compositions

	PYROXENES			*GARNETS*			
Mineral	**Diopside**	**Augite**	**Clinoenstatite**	**Grossularite**	**Andradite**	**Grossularite-Andradite**	**Amphibole**
Location	720-1939AT4	718-988c	EDT92-06D4	720-1943c1	730-61n	730-61cc	730-913-4
SiO_2	52.50	57.63	35.24	37.63	37.06	37.80	49.20
TiO_2				0.08		0.09	0.15
Al_2O_3	0.25	0.36	0.03	23.58	6.16	12.18	6.72
FeO	9.62	4.38	3.12		22.02	14.97	4.15
Fe_2O_3				12.32			
Cr_2O_3						0.02	
MnO	1.24	0.33	0.20	0.21	0.52	0.40	0.08
NiO				0.05			
MgO	12.38	22.45	56.66	23.22	0.02	0.02	12.26
CaO	24.85	13.47	0.03		34.65	34.35	26.53
Na_2O	0.07	0.04				0.04	
K_2O	0.01	0.03					
TOTAL	100.92	98.70	95.28	97.09	100.44	99.88	99.09

B. End member compositions (based on 6 oxygens for pyroxene and 12 oxygens for garnets)

Cations

Si	1.960	Si	2.984	2.995	2.965
Ti	0.000	Ti	0.005	0.000	0.005
Al	0.011	Al	0.016	0.045	0.035
Fe	0.227	Fe	0.817	1.468	0.982
Cr	0.000	Cr	0.000	0.000	0.001
Mn	0.039	Mn	0.014	0.035	0.027
Ni	0.000	Ni	0.000	0.000	0.000
Mg	0.000	Mg	0.006	0.002	0.000
Ca	0.994	Ca	1.973	2.960	2.887
Na	0.000	Na	0.000	0.000	0.006
K	0.000	K	0.000	0.000	0.000

Average percent end member

diopside	75.1	andradite		74	55
hedenbergite	24.3	grossularite	72	24	43.5
johannsenite	0.6	almandine	27		
		pyrope+spessartine +uvarovite	1	2	1.5
number analyses averaged	37		20	3	8

of granodiorite (fig. 3). With increasing distance from the stock margin, pyroxene+garnet metasomatism of Hamburg Dolomite and Geddes Limestone grades into marble, and marble grades into unaltered dolomite and limestone. Metasomatism and metamorphism of Secret Canyon Shale, however, extends much farther south than marbleization of adjacent Hamburg Dolomite and Geddes Limestone. One area of skarn and hornfels in Secret Canyon Shale west of Mineral Hill is separated by hundreds of meters of marble from the sub-annular zones of pyroxene+garnet skarn that are nearly contiguous with the Ruby Hill stock (fig. 2A). Distal metamorphic assemblages in Secret Canyon Shale both west and east of Mineral Hill include recrystallized dolomite and calcite layered with anorthite, quartz, and minor diopside, minerals which reflect the alternating silty limestone and argillaceous shale layers which compose the thin-bedded Secret Canyon Shale (Nolan, 1962). However, because of the overall close spatial association to the Ruby Hill stock, metasomatized and metamorphosed Secret Canyon Shale are considered contemporaneous with pyroxene+garnet skarn.

Large volumes of Hamburg Dolomite, Geddes Limestone, and the silty limestone layers of the Secret Canyon Shale south of the Ruby Hill stock are recrystallized to marble (fig. 2A). Marble consists predominantly of pure, coarse-grained (up to 0.5 cm), white dolomite, although calcitic marble is locally abundant. Within marbleized Hamburg Dolomite nearest the south side of the stock, irregular pods and lenses of pyroxene+garnet skarn (with maximum dimensions of tens of meters), are largely replaced by hydrous skarn. The close spatial association of marble with pyroxene+garnet skarn, and distal, generally annular distribution of marble about the Ruby Hill stock suggests that pyroxene+garnet skarn and marble are contemporaneous.

Because of subtle mineralogical changes, the distribution and paragenesis of contact alteration of Pioche Shale and Prospect Mountain Quartzite were not determined in detail. Minerals in Pioche Shale that may be contemporaneous with Ruby Hill stock skarns are sericite, kaolinite, and iron oxides (figs. 2A and 4). Several thousand meters south of the Ruby Hill stock Pioche Shale is composed of quartz, albite, phlogopite, and minor kaolinite and calcite, a modal composition closer to its original mineralogy (Nolan, 1962). Other than sericite and kaolinite in shaly beds near the top of the unit, no changes in original mineralogy of the Prospect Mountain Quartzite are discernible near the stock (figs. 2A and 4). However, 1 to 3% pyrite, and lesser amounts of magnetite and pyrrhotite (observed in drill core) have been added to Prospect Mountain Quartzite for up to hundreds of meters south of Ruby Hill, and iron oxides, resulting from weathering of these hypogene minerals, color much of the quartzite south of Ruby Hill red-orange. Pyrite, at least, appears to have been widely introduced in the relatively chemically inert quartzite as a result of intrusion of the Ruby Hill stock.

Although no skarn, marble, or granodiorite are exposed on the surface, minor amounts of skarn are found on mine dumps from workings in the northern part of Prospect Mountain. Dump samples of skarn from the Diamond Mine (Prospect Mountain Tunnel, Ruby Hill Tunnel, Eureka Tunnel) and from dumps near the top of Prospect Mountain (Wabash, Silver Connor) consist of clinoenstatite, magnetite, serpentine, pyrrhotite, quartz, pyrite, and minor amounts of chalcopyrite and molybdenite that replace Hamburg Dolomite (figs. 1 and 6, table 3). These skarn occurrences and the distribution of magnetic contours relative to outcropping and drilled granodiorite to the north (figs. 2A and 3) indicate the subsurface presence of granodiorite beneath Prospect Mountain.

Hydrous skarn

Hydrous skarn consists of quartz, hydrated silicates, and sulfide minerals that both replace pyroxene+garnet skarn and marble, and occur in irregular veins that cut pyroxene+garnet skarn. Hydrous skarn that replaces pyroxene+garnet skarn developed in both carbonate rocks (Hamburg Dolomite, Geddes Limestone) and in silty limestone-shale (Secret Canyon Shale) near the Ruby Hill stock consists of, in addition to quartz, one or more generations of amphibole (magnesio-hornblende and tremolite), chlorite (pycnochlorite, diabardite, clinochlore), pyrrhotite, pyrite, serpentine (antigorite), molybdenite, and muscovite (fig. 2A; table 3). In pyroxene+garnet skarn these minerals entirely replace pyroxene and garnet, rim pyroxene and garnet, and mimic crystal boundaries and cleavages of both

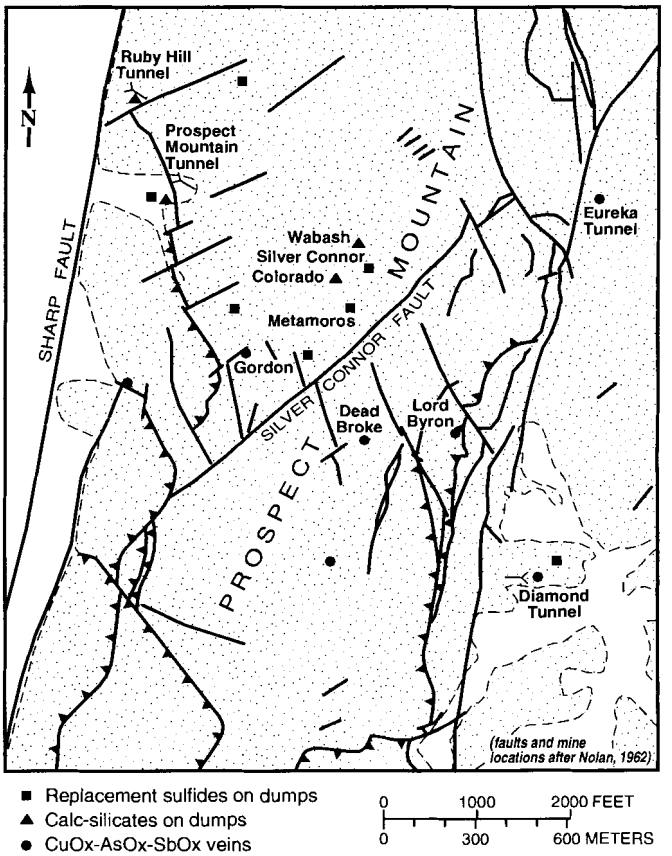

Figure 6. Map showing the location of sulfide replacement deposits, quartz veins, and calc-silicate minerals on mine dumps on the north end of Prospect Mountain. Location of the area of figure 6 is shown on figure 1.

minerals. Hydrous skarn minerals that formed more distal to the Ruby Hill stock in Secret Canyon Shale near Mineral Hill (fig. 2A) include chlorite, tremolite, and kaolinite. Hydrous skarn minerals reflect the addition, or redistribution of water, sulfur, and iron to pyroxene+garnet skarn, Hamburg Dolomite, Geddes Limestone, and Secret Canyon Shale.

Because of several common minerals and distribution, the three vein types that occur in granodiorite and veins that cut pyroxene+garnet skarn, most abundant on the north side of the Ruby Hill stock, are considered to be coeval with hydrous skarn. Although no individual veins were traced from granodiorite to skarn, veins in pyroxene+garnet skarn, up to 15 cm thick, consist of quartz+pyrite±molybdenite, the same mineralogy that comprises type 1 veins in granodiorite. Seams and lenses of molybdenite with minor amounts of quartz also cut pyroxene+garnet skarn. Microcline and sericite, fairly abundant in veins in granodiorite, are virtually absent in veins in skarn, although minor amounts of muscovite in one sample of hydrous skarn were locally abundant enough to yield a radioisotopic age (sample 718-794, 107.9±0.6 Ma, table 2). Other type 1 quartz veins that cut pyroxene+garnet skarn contain epidote and ripidolite.

The lenses of pyroxene+garnet skarn in marbleized Hamburg Dolomite south of the Ruby Hill stock are largely replaced by hydrous skarn assemblages consisting of quartz, biotite, chlorite, and sulfide minerals, and veins of calcite, chlorite, epidote, tremolite, and serpentine (fig. 2A). Other thin zones of calc-silicate minerals, micas, and iron sulfides are scattered irregularly in marble.

Paragenesis of iron minerals

The relationships among magnetite and sulfide minerals in pyroxene+garnet skarn, in hydrous skarn, and in replacement deposits, are complex, and differ on the north and south sides of the Ruby Hill stock. In general, the textural relations among magnetite, pyrrhotite, and pyrite on the north side of the stock are indicative of progressive sulfidation of magnetite, although local perturbations in magnetite and pyrrhotite stabilities, and in pyrrhotite and pyrite stabilities, are evident. In some occurrences magnetite coexists in apparent textural equilibrium with pyrrhotite, while in most occurrences pyrrhotite clearly has either replaced magnetite completely or partially along crystal margins and internal fractures. Other examples of replacement are evident where pyrrhotite and rare laths of molybdenite partially replace diopside±magnetite, preserving diopside crystal forms and cleavages.

In most occurrences where pyrrhotite coexists with pyrite on the north side of the stock, pyrite and minor amounts of molybdenite, chalcopyrite, sphalerite, quartz, and calcite replace pyrrhotite. Thus, most, if not all contact zone pyrite can be assigned to hydrous skarn mineral assemblages. Replacement of pyrrhotite by pyrite commences along internal fractures and progresses to a fine-grained porous aggregate of pyrite grains which results from volume reduction during the nearly isochemical replacement (Murowchick, 1992). Not uncommonly, however, pyrrhotite and pyrite contain inclusions and thin veins of each other, in addition to remnant inclusions of magnetite. This mutual veining and replacement suggests that some sulfidation of magnetite took place near the isobarically divariant stability point of magnetite+pyrrhotite+pyrite.

On the south side of the stock where magnetite is much less abundant, pyrrhotite and pyrite occur disseminated in marble and in lenses of hydrous skarn minerals in marble. Pyrrhotite in hydrous skarn lenses ranges from massive to disseminated, and is intergrown with calcite of several grain sizes in irregular layers and bands. In these occurrences pyrrhotite is invariably replaced by pyrite and minor amounts of sphalerite, chalcopyrite, barite, and other rare sulfide minerals (galena, stibnite, tennantite, seligmannite, and boulangerite; table 4). Thus, both pyrrhotite and pyrite south of the stock occur in hydrous skarn assemblages.

Mineralogical correlation of skarn and replacement deposits

In sulfide replacement deposits north of Ruby Hill, where pyrite, sphalerite, and galena are the dominant sulfide minerals, inclusions of pyrrhotite in pyrite and sphalerite are not uncommon, suggesting that pyrrhotite was the initial sulfide mineral deposited in replacement sites. All sulfide minerals associated with sphalerite in hydrous skarn, including several of the rare sulfide minerals in hydrous skarn south of the Ruby Hill stock (e.g., seligmannite and boulangerite), occur in varying abundances in both replacement deposits and in vein deposits south of the Ruby Hill stock (Mineral Hill and Prospect Mountain (table 4; figs. 1 and 6)). The composition of sphalerite, another unifying factor among hydrous skarn and replacement deposits is discussed below. All of these relationships indicate that pyrrhotite was stable during both pyroxene+garnet and hydrous skarn formation, and during the initial stage of distal sulfide replacement of dolomite. Although more than one generation of pyrrhotite may be present, the formation of pyroxene+garnet skarn, hydrous skarn, and sulfide replacement deposits appear to be nearly synchronous, and the transition from pyroxene+garnet to hydrous skarn to replacement of carbonate rocks by sulfide minerals is largely marked by increased sulfur activity.

Conditions of skarn formation

Based on experimental data, the equilibrium temperatures of calc-silicate mineral assemblages commonly found in skarns can be determined if the amount of CO_2 (expressed as mole fraction CO_2, or XCO_2) in fluid present during mineral precipitation is known (e.g. Einaudi and others, 1981, figs. 5 and 6). At Ruby Hill, XCO_2 measured in fluid inclusions in veins in granodiorite and in hydrous skarn minerals averages about 0.075 (discussed in a later section). At this CO_2 abundance and 1 to 2 kilobars total pressure, tremolite and antigorite of hydrous skarn formed at temperatures greater than about 420°C. If $XCO_2 = 0.075$ is valid for earlier pyroxene+garnet skarn, then garnet formed at or above ~470°C.

Alteration Associated with Replacement Deposits

Alteration of dolomite adjacent to sulfide replacement deposits north of the Ruby Hill stock is not visually obvious. The contacts of sulfide replacement deposits, regardless of form, with enclosing dolomite are abrupt as is characteristic of most carbonate replacement deposits (Titley, 1993). Aggregates of massive sulfide or oxide minerals formed from sulfide minerals during weathering virtually terminate on a grain boundary scale within dolomite, and adjacent carbonate crystals show no evidence of metasomatism or recrystallization. However, minor element enrichment and oxygen isotope depletion in dolomite wall rocks (discussed in subsequent sections) constitute analytically measurable wall-rock alteration.

Minor amounts of hydrothermal dolomite and subordinate calcite are internal to replacement deposits. Both dolomite and calcite are generally white and relatively coarse-grained, and contain abundant primary fluid inclusions in growth planes. The carbonate minerals are intergrown with metal sulfide and oxide minerals or occur in homogeneous masses measuring centimeters to tens of centimeters in dimension. No other non-sulfide minerals are present in sulfide replacement deposits as only dolomite and calcite were stable, or incompletely replaced, during sulfide mineralization. The release of CO_2 during carbonate dissolution and sulfide mineral replacement, coupled with relatively low temperatures, suppressed the precipitation of wollastonite and other calc-silicate minerals in Eureka district replacement deposits. Calc-silicate minerals are also absent or uncommon in other sulfide replacement deposits in carbonate rocks (e.g. Megaw and others, 1988; Thompson and Arehart, 1990; Titley, 1993).

Within the replacement deposits thin (micrometers wide) veins and films of calcite cement sulfide minerals along grain boundaries and internal fractures. Replacement deposits encountered north of the Ruby Hill fault were extremely friable and flowed in drill holes and on the Fad Shaft 2250 (foot) level (Binyon, 1946; Love, 1966). Microscopic examination of numerous samples from the 2250 level shows that the friability results from dissolution of the intergranular calcite. Calcite dissolution is probably effected by modern groundwater that is slightly acidic from incipient sulfide oxidation, as the sulfide replacement deposits are saturated with groundwater under high pressure (an unresolved deterrent to mining; Love, 1966). Pyrite, because of its brittleness relative to galena and sphalerite, is nearly always comminuted and cemented by calcite. Sphalerite and galena are not nearly as extensively cemented by calcite, and some masses of these sulfides remain competent. Coupled with the tendency of galena to deform and not fracture, the low solubility of galena in the surface weathering environment explains its presence on mine dumps and in the oxidized ores of Ruby Hill when all other sulfides are completely oxidized.

Fine-grained silica, or jasperoid, commonly marginal or internal to carbonate replacement deposits elsewhere in the American cordillera (Titley, 1993), is absent at Ruby Hill and an extremely rare component of Prospect Mountain replacement deposits. However, silica alteration occurs with gold mineralization north of Ruby Hill. Jasperoid is a component of gold ore in the West Archimedes deposit (~3 km north of Ruby Hill, fig. 1; Dilles and others, 1996). About 1 km north of Ruby Hill on the north side of Adams Hill irregular masses of fine-grained quartz that replace Hamburg Dolomite near the contact with overlying Dunderberg Shale were mined for gold and silver, with lesser amounts of lead (Silver Lick, Bowman, Cyanide, Wales, and Helen Mines). Relative metal abundances in the Adams Hill ores differ markedly from those in Ruby Hill, Mineral Point and Prospect Mountain replacement deposits. Ore in them commonly contained >1 oz/ton (34 g/tonne) gold, tens of oz/ton silver, and only small amounts of lead. Nolan (1962) attributed the precious metal mineralization in this silica to zoning based on a north-south progression of increasing precious metal and decreasing lead content of ores on Mineral Point. Since no quartz occurred with replacement ores in the district, the age, paragenetic position, and significance of Adams Hill ores are not known. Examination of fluid inclusions in quartz north of Adams Hill reveals liquid/vapor indicative of low temperature homogenization.

Stratigraphic and Structural Controls of Replacement Deposits

All significant replacement deposits in the Eureka district occur within two Cambrian carbonate rock formations, Eldorado Dolomite and Hamburg Dolomite, and the most important deposits are in Eldorado Dolomite. Confinement of carbonate replacement deposits to a small number of stratigraphic units within thick sedimentary rock sections is common in other districts in the North American cordillera, and large volumes of apparently similar carbonate rocks are not mineralized (Megaw and others, 1988; Titley, 1993). A regional control of replacement deposits in Eldorado Dolomite may be the presence of relatively impermeable, overlying Secret Canyon Shale. Secret Canyon Shale may have constituted an aquaclude as evidenced by the water damming ability of the shale encountered in sinking the Fad Shaft (Love, 1966). For reasons that are unclear, most replacement deposits near Ruby Hill are situated in the lower part of the Eldorado Dolomite. Distinctive lithofacies within Eldorado Dolomite that were preferentially replaced by sulfide minerals have not been identified, and any local stratigraphic control of sulfide mineral replacement is extremely subtle. Both dolomites are positioned at the bottom of a thick sequence of lower Paleozoic carbonate rocks, and may have been preferential sites for replacement because of their proximity to potential, subjacent source rocks (discussed in a later section).

A primary structural control on the distribution of replacement deposits in the Eureka district was thought to be zones of fractures in otherwise massive Eldorado and Hamburg Dolomites (Nolan, 1962), although fractured dolomite extends far beyond clusters of replacement deposits at Ruby Hill and on Prospect Mountain. Replacement sulfide deposits in the down-dropped blocks north of the Ruby Hill fault are usually situated within zones of fractured dolomite, some of which contain disseminated pyrite. Faults cutting or tangential to replacement deposits that could have served as fluid conduits

have not been recognized. Permeability for fluid flow was apparently provided by crushed zones and networks of thin fractures that pervade much of the Eldorado Dolomite, and possibly enhanced by high temperatures during mineralization (Maxwell and Verall, 1953; Hanson, 1995).

REPLACEMENT AND VEIN DEPOSITS

Metals produced in the Eureka district were mined from replacement deposits, quartz veins, and disseminated gold deposits. Most production came from oxidized replacement deposits on Ruby Hill. Lesser production was derived from replacement deposits, also largely oxidized, on Mineral Point and Prospect Mountain (fig. 1), from quartz veins south of Ruby Hill (e.g., Grant Mine, fig. 1) and on Prospect Mountain (e.g., Dead Broke Mine, fig. 6), and from low grade disseminated gold deposits several kilometers south and north of Ruby Hill (Windfall, Ratto Canyon, and West Archimedes Mines, fig. 1). Forms of replacement deposits, and their mineralogy and parageneses were determined from field examination and study of specimens from drill core and mine dumps. Sulfide minerals preserved in replacement deposits north of Ruby Hill, and in replacement and vein deposits north and south of Ruby Hill were studied in detail in order to determine pre-weathering paragenetic and pre-tectonic spatial relationships between replacement sulfide minerals, skarn mineral assemblages, and igneous rocks.

Replacement Deposits

The replacement ores of Ruby Hill were oxidized to the lowest mining levels, about 250 m (~800 feet) below the surface. Replacement ores on Mineral Point and on Prospect Mountain were also highly oxidized, and only small amounts of unoxidized sulfide minerals were mined at the three locations. In Ruby Hill and on Prospect Mountain much ore was recovered from the floors of caves where oxidation of sulfide minerals and removal of sulfur and zinc residually enriched lead, silver, and gold in the ores. The historically mined grades of 0.5 to 2 oz/ton (17 to 68 g/tonne) gold, tens of oz/ton (hundreds of g/tonne) silver, and tens of percent lead (Curtis, 1884; Vandenburg, 1938; Nolan, 1962) were undoubtedly derived from oxidation of sulfide deposits with grades as much as 4 times lower, as evidenced by the tenor of sulfide replacement deposits encountered by drilling north of Ruby Hill (fig. 3). A resource of 3.1 million tons at 3.7% lead, 8.3% zinc, 0.16 oz/ton (5.4 g/tonne) gold, and 5.6 oz /ton (190 g/tonne) silver is estimated to exist about 600 to 800 m (~2,000 to 2,600 feet) below the surface in the down-dropped block north of Ruby Hill (Love, 1966).

Forms of replacement deposits

Replacement deposits enclosed by dolomite in and north of Ruby Hill occur as coherent but inhomogeneous masses of oxide and/or sulfide minerals mixed with lesser amounts of hydrothermal dolomite and subordinate calcite (described above), and inclusions of unreplaced wall-rock dolomite. Geometries and distribution of replacement deposits correspond to no predictable pattern, recognizable structural control, or favorable lithofacies, although all are confined to the Eldorado Dolomite within tens to a few hundred meters above the Champion thrust fault. On a local scale both the oxidized deposits in Ruby Hill and the deep sulfide deposits north of Ruby Hill are extremely irregular in shape, and collectively form an anastomosing series of sub-tabular to semi-horizontal bodies with large lateral dimensions, that are discreet or loosely connected by pipes and chimneys (Curtis, 1884; Love, 1966; fig. 7). In deep sulfide deposits pure aggregates of sulfide minerals are generally no more than a few to a few tens of centimeters in dimension, but masses consisting of 50 to 75% sulfide minerals and 25 to 50% hydrothermal dolomite±calcite

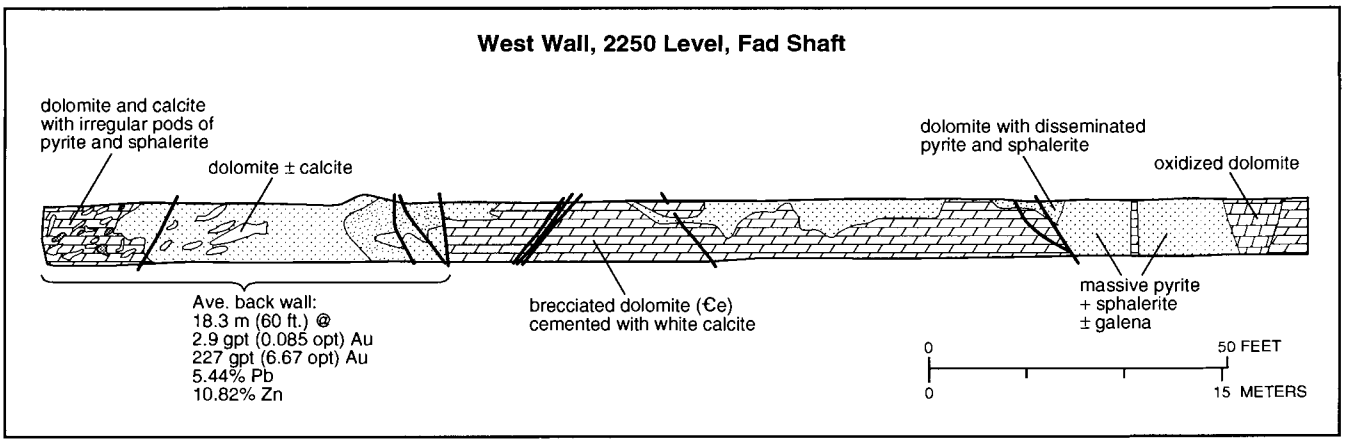

Figure 7. Rib map of the 2250 (foot) level (now flooded) from the Fad Shaft, showing the distribution of sulfide replacement of Eldorado Dolomite in the down-dropped block north of Ruby Hill. Section is modified from a map by R.A. Lillibridge, dated 9/30/65 and provided by the Ruby Hill Mining Company. Designation of some wall rock as limestone may reflect remnant limestone in Eldorado Dolomite that occurs throughout the district (e.g., Nolan, 1962). Location of the Fad Shaft is shown in figures 1 and 2A. gpt = grams per tonne; opt = troy ounces per short ton.

and dolomite wall-rock fragments have dimensions of meters to tens of meters. Within Ruby Hill, oxidized replacement deposits have a vertical range in Eldorado Dolomite of >250 m (>800 feet), and north of Ruby Hill sulfide replacement deposits have a known vertical range of ~ 400 m (~1,320 feet, fig. 3).

At the north end of Prospect Mountain (fig. 6) replacement deposits occur entirely in Hamburg Dolomite as masses of iron oxides, carbonate minerals, and rare quartz in pipes, tabular zones, and small pods. Tabular replacement deposits are generally less than 2 m wide, dip at high angles, and may extend tens of meters laterally and below the surface. Pipes and pods have surface expressions of as little as 1 m in maximum dimension, but may extend to depths of hundreds of meters. Most of them plunge 60° or more. Much of the ore mined consisted of cave fill cemented by iron oxides similar to that exposed in a high wall at the Metamoros Shaft (fig. 6). Prospect Mountain replacement deposits generally have greater height/width aspects, occur over a larger vertical range, and are smaller than the replacement deposits in and north of Ruby Hill. These contrasting shapes, stratigraphic positions, and sizes probably reflect subtle differences in the mechanical controls of replacement between the two dolomite host rocks, as well as proximity to granodiorite. On the Wabash, Colorado, and Prospect Mountain Tunnel dumps on Prospect Mountain (fig. 6) calc-silicate-sulfide assemblages indicate that some replacement pipes, or at least the mine workings exploiting them, are close to the Ruby Hill granodiorite stock. The distribution of magnetic contours around and south of the Ruby Hill stock also shows that the granodiorite extends beneath the northern part of Prospect Mountain.

Oxidized replacement deposits

Lead, zinc, gold, and silver values in oxidized replacement ores of Ruby Hill, Mineral Point, and Prospect Mountain occur in cerrusite, anglesite, and plumbojarosite, and in lesser amounts of mimetite, bindheimite, hemimorphite, and smithsonite (Nolan, 1962; Nolan and Hunt, 1968). These minerals are mixed with limonite, goethite, hematite, dolomite, calcite, aragonite, and copper oxides, and small amounts of barite, wulfenite, and unreplaced wall-rock dolomite. All metallic oxide minerals formed from weathering of sulfide minerals, as remnant nodes of galena, pyrite, and sphalerite enclosed by iron, lead, zinc, and arsenic oxides exist on mine dumps. No silver minerals or gold have been recognized in oxidized replacement deposits.

Sulfide mineral paragenesis

Sulfide replacement deposits north of Ruby Hill, on Prospect Mountain, and on Mineral Point consist mainly of subequal amounts of pyrite, sphalerite, and galena, with subordinate amounts of hydrothermal dolomite, calcite, arsenopyrite, tennantite, pyrrhotite, quartz, and chalcopyrite (fig. 7). Locally, relatively pure pods of pyrite, galena, and sphalerite with dimensions of tens of centimeters exist within sulfide replacement masses north of Ruby Hill and in Prospect Mountain. Grain size of pyrite, sphalerite, and galena and hydrothermal dolomite ranges from ~1 to 4 mm in Ruby Hill deposits; sulfide aggregates in quartz porphyry tend to be slightly coarser grained.

In sulfide replacement deposits north of Ruby Hill pyrite, intergrown with small amounts of arsenopyrite, is partly replaced by or intergrown with sphalerite and galena. These sulfide minerals replace both hydrothermal dolomite±calcite and Eldorado Dolomite that encloses sulfide masses. On a microscopic scale, pyrite contains inclusions of sphalerite, chalcopyrite, and pyrrhotite. Sphalerite contains inclusions of chalcopyrite, pyrite, tennantite, and rare pyrrhotite, which is sometimes elongated and entrained along cleavages. Tennantite also fills fractures in and is intergrown with sphalerite. Rare inclusions of seligmannite ($CuPbAsS_3$, table 4) occur in galena. Galena locally encloses pyrite and sphalerite aggregates and cements fractured pyrite and sphalerite.

Pyrite, arsenopyrite, and sphalerite in the replacement deposits north of Ruby Hill are invariably finely fractured and cemented with calcite. Calcite-filled cracks in these minerals are up to tens of micrometers wide and may be as dense as tens of cracks per square centimeter. Locally, finely comminuted pyrite and sphalerite are entrained in calcite matrix, further illustrating that the precipitation of late, fracture-filling calcite followed a sulfide deformational event. Galena is entirely unfractured, perhaps a result of plastic instead of brittle deformation, but there is no evidence of annealed or strained galena crystals. Whereas other sulfides in drill holes (Binyon, 1946; Love, 1966) and on the Fad Shaft stockpile (derived from the 2250 level) are finely comminuted because of dissolution of late calcite cement, galena masses are generally competent.

Pieces of a post-sulfide breccia consisting of subrounded clasts of sulfides and subangular dolomite+pyrite clasts, mostly <1 cm in dimension, in a matrix of finely comminuted dolomite are found on the Fad Shaft 2250-level stockpile. The breccia is probably from a postmineralization fault zone.

Examination of remnant sulfide masses from dumps on Prospect Mountain showed that sulfide species, textures, and paragenesis are generally similar to those preserved at depth north of Ruby Hill. Chalcopyrite is somewhat more abundant in Prospect Mountain sulfide replacement deposits as reflected by the relatively common occurrence of copper oxides on dumps. Quartz is a minor component of some replacement deposits and small amounts of acanthite and miargyrite occur as inclusions in galena from the Diamond Tunnel dump (fig. 6).

Replacement sulfide minerals that are spatially related to quartz porphyry intrusions north of Ruby Hill and on Mineral Point consist of individual crystals, aggregates, and intergrowths of galena, sphalerite, and pyrite, which are commonly coarser grained, especially those in breccia and fault zones within quartz porphyry, than sulfide minerals in replacement deposits in dolomite. On Mineral Point and in TL Shaft ores (fig. 1) galena is the predominant sulfide where it is intergrown with and contains inclusions of pyrite and sphalerite. Sphalerite in or spatially associated with quartz porphyry is characterized by fine growth bands (described below), and contains inclusions of pyrite, chalcopyrite, arsenopyrite, and tennantite. Arsenopyrite is uncommon but locally cements fractured pyrite, whereas fractured pyrite, arsenopyrite, and sphalerite are cemented by calcite. In general, parageneses in

quartz porphyry-related sulfide replacement deposits and in sulfide replacement deposits in dolomite near Ruby Hill are similar, although galena is more abundant in replacement deposits in and near quartz porphyry, and sphalerites in the two groups of deposits differ in texture and composition.

Galena and sphalerite are the main sources of lead and zinc, respectively, in all replacement deposits. Silver occurs in small amounts in tennantite, galena, acanthite, and miargyrite (table 4). Gold, unobserved microscopically, occurs mostly in pyrite, based on metallurgical tests. In order to determine the abundance of gold and other minor elements in sulfide minerals from replacement deposits, as well as in other hydrothermal sulfide minerals (pyrite in veins in granodiorite, pyrite in hydrous skarn, and pyrite in disseminated gold deposits) gold, silver, arsenic, antimony, mercury, tin, and bismuth concentrations were determined by fire assay and atomic absorption spectrometry (AAS; fig. 8, table 5). The major sulfide replacement minerals (pyrite, sphalerite, and galena) contain moderate to high concentrations of all minor elements analyzed, with pyrite containing the largest amounts of gold, and pyrite and galena containing the largest amounts of silver. Pyrite in veins in granodiorite and in hydrous skarn contains very low concentrations of all minor elements analyzed, with the possible exception of arsenic. Because of small sample size only a few analytic data were obtained for pyrite in one disseminated gold deposit (Ratto Canyon). Gold at Ratto Canyon apparently occurs in sites other than pyrite, which contained ~0.07 ppm gold (0.07 g/tonne), as the sample from which pyrite was extracted assayed more than 1 oz gold/ton (>34 g gold/tonne).

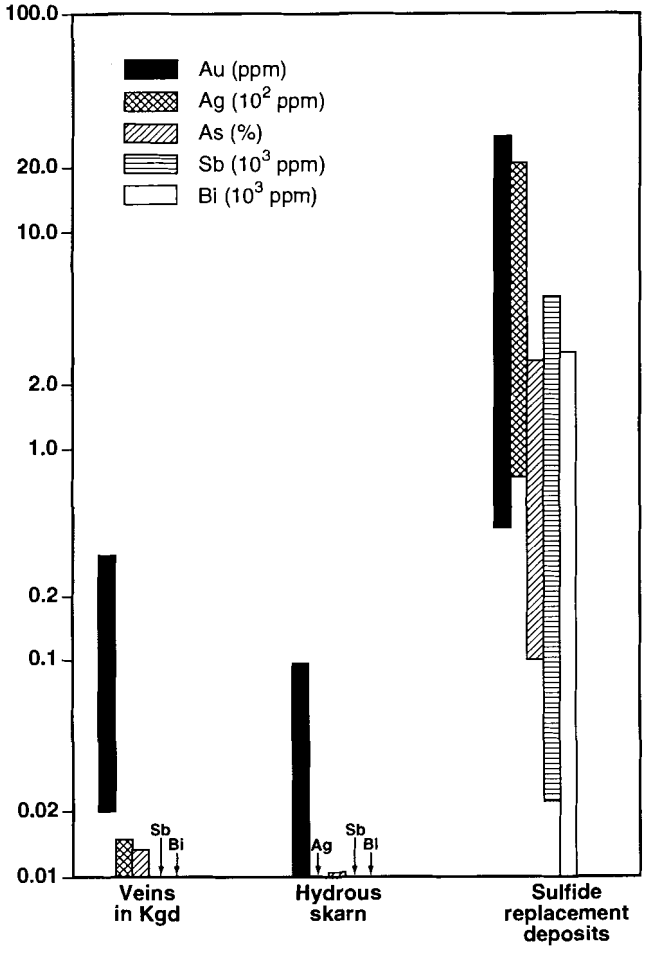

Figure 8. Gold, silver, arsenic, antimony, and bismuth concentrations in pyrite from veins in granodiorite, hydrous skarn, and sulfide replacement deposits.

Vein deposits

Veins on Prospect Mountain, on Mineral Hill, and in Zulu Canyon (figs. 1, 3, and 6) consist predominantly of quartz and subordinate amounts of calcite and sulfide minerals, range in width from a few centimeters to ~ 1 m, and have variable strikes and dips. Most veins were prospected and minor lead and silver production is recorded from the Grant, Dead Broke, Gordon, Lord Byron, Eureka Tunnel, and a few other vein mines (fig. 6; Nolan, 1962). Veins are completely oxidized near the surface but sulfide minerals in dump samples include stibnite, galena, sphalerite, pyrite, tetrahedrite, tennantite, jamesonite, zinkenite, boulangerite, and several phases with atomic proportions that correspond to no known minerals (table 4). Microscopic electrum and anatase were observed in vein samples from the Grant Mine and Eureka Tunnel dumps, although the neither mine has recorded gold production (Nolan, 1962). Galena is the source of most vein lead production, whereas silver is distributed among galena, tetrahedrite, jamesonite, galenobismutite, and boulangerite (table 4). Stibnite predominates and pyrite is uncommon in veins of the Grant, Dugout, and Gordon Mines, and in the veins in Zulu and Secret Canyons (figs.1 and 2A). A Eureka Tunnel vein contains breccia clasts of marble, tremolite, and magnetite, supporting the presence of contact zone alteration and granodiorite underlying Prospect Mountain in the vicinity of the mine workings (fig. 6). Based on fluid inclusion microthermometric measurements and other evidence presented below, veins on and north of Prospect Mountain may have been formed during hydrothermal event(s) separate from those that accompanied intrusion of granodiorite and quartz porphyry.

In most veins anhedral sulfide minerals fill interstices of subhedral quartz crystals. In other veins aggregates of sulfides are intergrown with fine-grained quartz, and some veins include both textures. In several mines quartz+stibnite± calcite veins up to 1 m wide are cut by thin (several centimeters wide), coarse-grained, quartz+galena veins, which also contain minor tennantite and pyrite. The thin quartz+galena veins also occur independently, and galena in them fills irregular openings among quartz subhedrons in vein centers. Within individual veins no paragenesis is evident other than the tendency of sulfide minerals to cluster toward vein centers.

Sphalerite Textures and Compositions

Sphalerite is widely distributed in the Eureka district and occurs in most hydrothermal mineral assemblages: hydrous skarn, veins in hydrous skarn and marble, veins in granodiorite, sulfide replacement deposits, shear and fault zones in quartz porphyry, and quartz veins in dolomite. The textures and compositions of the various occurrences of sphalerite in the vicinity of Ruby

Table 4. Compositions in weight percent of sphalerite, arsenopyrite, pyrrhotite, and other sulfide minerals in Eureka district DDH core and mine samples. Analyses are by microprobe (T. Solberg, Virginia Tech. Univ.). Some drill hole (DDH) locations are shown on figures 2A and 3.

Sample no.	No. of analyses	Location	Fe	As	Co	Zn	Cd	Mn	Ni	Cu	Ag	Sb	Pb	Bi	S	Se	Sum	Stoichiometry and probable phase
SPHALERITE																		
79-1-1724	3	DDH, Fad Shaft	8.8			58.2	0.5	0.8							33.4		101.3	
79-1-1724	2		6.9			59.5	0.6	0.7							33.3		101.0	
79-1-1724	2		4.8			61.9	0.5	0.5							33.7		101.4	
706-771	4	DDH, Zulu Canyon	0.6			67.4	0.5	0.1							33.6		102.2	
718-764	3	DDH, Phoenix Shaft	7.7			58.7		3.4							34.1		103.9	
720-284.6	4	DDH, Mineral Hill	7.7			60.2	0.6								34.0		102.5	
720-284.6	1		6.8			61.7	0.5								34.2		103.2	
720-305	2		0.5			65.9	0.6	0.1					0.9		33.5		101.5	
720-1073	2		2.0			65.5	0.7	0.1							33.7		102.0	
720-1073	2		4.5			62.9	0.6	0.1							33.5		101.6	
720-1583	2		0.6			66.3	0.5								32.9		100.3	
720-1946	2		8.8			58.7	0.4	0.2							33.5		101.6	
721-399	2	DDH, Zulu Canyon	2.3			64.2	0.7	0.4							33.0		100.6	
721-399	2		0.5			66.8	0.5								33.2		101.0	
721-442	1		0.4			66.9	0.6	0.1		0.2		0.1			33.0		101.3	
722-346	1	DDH, Zulu Canyon	1.3			65.4	0.5								33.0		100.2	
723-1846	2	DDH, S. of Holly Shaft	7.4			60.0	0.4	0.5							34.2		102.5	
724-772	2	DDH, Zulu Canyon	4.6			62.5		0.2							33.3		100.6	
724-772	1		8.1			58.7		0.4							33.9		101.1	
724-793	2		1.8			65.9	0.6	0.6		1.5					33.0		103.4	
724-793	1		4.1			62.8	0.5	0.6		0.3					33.0		101.3	
724-793	1		7.6			60.5	0.2	0.2							33.3		101.8	
726-2278	2	DDH, Fad Shaft	4.5			61.8	0.6	0.5							32.9		100.3	
729-3034	3	DDH, N. of Fad Shaft	5.3			61.8	0.6	0.5							33.3		101.5	
DH8-2125	4	DDH, Fad Shaft	1.5			65.9	0.6	0.5							33.2		101.7	
EDT92-06A	5	Prospect Mtn. Tunnel dump	1.8			65.2	0.6								32.9		100.5	
EUD91-1C	2	Bullwacker Mine dump	2.6			64.9	0.2	0.3							31.6		99.6	
EUD92-10P1	4	Grant Mine dump	0.3	0.1		66.4	0.6						0.5		34.1		102.0	
EUD91-11A	3	Fad Shaft stockpile	6.9			59.8	0.5	0.5							33.3		101.0	
EUD91-11A	2		5.6			61.3	0.4	0.3							32.6		100.2	
EUD91-11C	1		6.2			61.9	0.6	0.4							32.1		101.2	
EUD91-11C	1		10.7			56.9	0.4	0.3							32.7		101.0	
EUD91-11E	2		7.5			59.9	0.5	0.3							32.5		100.7	
EUD91-11H	3		2.5			64.9	0.5	0.3							32.0		100.2	
EUD91-11H	1		8.3			58.7	0.4	0.6							31.7		99.7	
EUD91-11H	1		5.1			60.4	0.7	1.1							32.1		99.4	
EDT92-04	2	Grant Mine dump	0.60			66.69	0.56	0.02							33.44	0.02	101.33	
EDT92-16B	3	Dead Broke Mine dump	1.12			65.47	0.26				0.10				33.44		100.39	
EDT92-20	2	Richmond Mine dump	4.81			63.20	0.37	0.08							33.66		102.12	
	1	Richmond Mine dump	8.23			59.89	0.42	0.07							33.82		102.43	
EUD92-88	4	Prospect on Prospect Ridge	4.15			63.77	0.53	0.05					0.26		33.35		102.11	
ARSENOPYRITE																		
79-1-2190	1	DDH, Fad Shaft	36.5	42.7								0.2			22.2	0.1	101.7	
713-222	2	DDH, Ruby Hill	35.6	43.0											21.9	0.2	100.7	
724-793	2	DDH, Zulu Canyon	36.1	41.9											22.6	0.2	100.8	
726-2278	2	DDH, Fad Shaft	36.5	41.1											22.9	0.2	100.7	
729-3034	1	DDH, N. of Fad Shaft	35.9	41.2											23.3	0.1	100.5	
DH8-2125	4	DDH, Fad Shaft	35.1	42.1											22.6	0.1	99.9	
EUD91-1C	1	Bullwacker Mine dump	35.1	43.2								0.1			20.9	0.2	99.5	
EUD91-11C	3	Fad Shaft stockpile	35.7	40.7											22.8	0.1	99.3	
EUD91-11E	3		35.4	41.7								0.2			22.2	0.1	99.6	
EUD91-11H	2		36.2	40.4								0.2			23.2	0.1	100.1	
EUD91-11H	1		37.4	42.1			0.2					0.2			22.3	0.1	102.3	

Table 4. ***Continued***

Sample no.	No. of analyses	Location	Fe	As	Co	Zn	Cd	Mn	Ni	Cu	Ag	Sb	Pb	Bi	S	Se	Sum	Stoichiometry and probable phase	
PYRRHOTITE																			
79-1-1748	2	DDH, Fad Shaft	60.7	0.1	0.1										39.3		100.2		
79-1-1748	1		60.6	0.1	0.1										39.3		100.1		
706-780	4	DDH, Zulu Canyon	61.1	0.1	0.1				0.1						40.0		101.4		
713-222	2	DDH, Ruby Hill	60.9												39.0		99.9	$Fe_{.90}S$	
718-526	3	DDH, Phoenix Shaft	60.6	0.1											39.2		100.5		
718-764	2	DDH, Phoenix Shaft	59.1												39.8		98.9	$Fe_{.85}S$	
720-1943	2	DDH, Mineral Hill	59.5												38.3		97.8	$Fe_{.89}S$	
720-1946	1		61.2												39.3		100.5	$Fe_{.89}S$	
724-761	3	DDH, Zulu Canyon	61.3												38.9		100.2		
724-793	5		60.8												38.9		99.7	$Fe_{.90}S$	
DH8-2125	2	DDH, Fad Shaft	61.0												39.1		100.1		
EDT92-06E	3	Prospect Mtn. Tunnel dump	61.1		0.2										39.9		101.2		
TENNANTITE																			
724-793	2	DDH, Zulu Canyon	1.0	20.4		8.5	0.2			41.6	1.5	0.2			28.0	0.1	101.5	$Cu_{9.8}As_{4.1}Zn_{2.1}(Fe,Ag)_{0.6}S_{13}$	
726-2278	3	DDH, Fad Shaft	1.1	21.0		8.4	0.2			42.4	1.7	0.2	0.2		28.2	0.1	103.5	$Cu_{9.8}As_{4.1}Zn_{1.8}(Fe,Ag)_{0.6}S_{13}$	
729-3034	3	DDH, N. of Fad Shaft	1.6	19.0		7.3	0.1			41.8	1.8	2.9			28.0	0.1	102.6	$Cu_{9.8}As_{3.8}(Zn,Sb,Ag,Fe)_{3.3}S_{13}$	
729-3034	1		1.6	16.2		6.9	0.3			39.9	2.4	6.6			27.7	0.1	101.7	$Cu_{9.4}As_{3.3}(Zn,Sb,Ag,Fe)_{3.3}S_{13}$	
EUD91-1C	2	Bullwacker Mine dump	2.2	20.0		8.5				43.0			1.4		27.8		102.9	$Cu_{10}As_{4.1}Zn_{2.1}Fe_{0.6}S_{13}$	
EUD91-11H	2	Fad Shaft stockpile	1.7	20.3		7.8	0.3			42.1	1.8	0.4			28.9		103.3	$Cu_{9.4}As_{3.9}(Zn,Ag,Fe)_{2.3}S_{13}$	
GALENA																			
79-1-2190	1	DDH, Fad Shaft									0.2		85.3		13.4		98.9		
720-1073	3	DDH, Mineral Hill									1.1	0.3	84.3		13.9		99.6		
720-1583	1			0.1							0.7	0.3	85.1		12.8		99.0		
DH8-2125	3	DDH, Fad Shaft		1.3						0.2	0.5		85.0		13.9		100.9		
EUD91-1B	1	Bullwacker Mine dump									0.5	0.5	83.1		13.1		97.2		
EUD91-11A	1	Fad Shaft stockpile								0.1		0.1	86.4		13.6		100.2		
EUD91-11C	1			0.2							1.3	3.3	80.8		13.6		99.2		
EUD92-01B	4	Diamond Tunnel dump									0.6	0.4	86.5		14.0		101.5		
EDT92-21	1	K-K/Lawton Mine Dump						0.15			0.12	0.29	87.46		13.64		101.66	PbS	
OTHER SULFIDES																			
EUD91-1C	1	Bullwacker Mine dump	2.0							68.0			0.2		30.3		100.5	$Cu_{1.1}Fe_{.04}S$	chalcocite?
EUD92-01B	2	Diamond Tunnel dump	0.1								76.1	3.1	4.3		13.1		96.7	$Ag_{1.8}Pb_{.05}Sb_{.07}S$	acanthite
EUD92-01B	1	Diamond Tunnel dump	0.5			0.4					37.2	40.7			21.3		100.1	$AgSbS_2$	miargyrite
EUD92-01B	2	Diamond Tunnel dump	0.8				0.1			1.4		19.4	60.2		17.8		99.7	$Pb_{5.9}Sb_{3.1}S_{11}$	
EUD91-6	2	Eureka Tunnel dump	1.0	1.3		6.6				30.9	11.0	27.0			24.2		102.0	$Cu_{8.3}Sb_{3.9}Zn_{1.8}Ag_{1.8}S_{13}$	tetrahedrite
EUD91-6	1	Eureka Tunnel dump		0.6						1.0	7.7	30.7	42.9		19.9		102.8	$Pb_{2.3}Sb_{2.8}Ag_{0.8}S_7$	jamesonite?
EUD91-6	1	Eureka Tunnel dump		0.1						1.8	89.4				9.0		100.3	Ag_3S	
EUD91-6		Eureka Tunnel dump	0.6	0.8		4.9				4.0	49.0	22.9			20.0		102.2	$Ag_{2.9}Cu_{0.4}Zn_{0.5}Sb_{1.4}S_4$	
DH8-2125	1	DDH, Fad Shaft	51.7							10.4					38.1		100.2	$Fe_{0.8}Cu_{0.1}S$	
EUD91-11C	1	Fad Shaft stockpile	16.8							14.4		0.3	47.4		21.3		100.2	$CuPbAsS_3$	seligmannite
EUD92-10P1	2	Grant Mine dump	1.0								0.1	71.7			28.3		101.1	Sb_2S_3	stibnite
EUD92-10P1	1	Grant Mine dump		0.7							0.6	46.1	30.9		23.1		101.4	$Pb_{0.8}Sb_{2.1}S_4$	zinkenite
720-1583	2	DDH, Mineral Hill	1.6	1.1		6.1	0.4			27.1	15.0	29.6	0.1		23.3		104.3	$Cu_{7.9}Sb_{4.2}Ag_{2.4}(Fe,As,Zn)_{2.7}S_{13}$	tetrahedrite
720-1907.3	2	DDH, Mineral Hill	49.2												50.1		99.3	$\sim Fe_2S$	
718-522	3	DDH, Phoenix Shaft	49.1												50.9		100.0	$\sim Fe_2S$	
EDT92-06E	1	Prospect Mtn. Tunnel dump	48.3												51.1		99.4	$\sim Fe_2S$	
713-1520	2	DDH, S. of Ruby Hill								0.1	7.4		25.6	50.4	16.4		99.9	$Bi_{1.9}PbAg_{0.5}S_4$	galenobismutite
721-442	2	DDH, Zulu Canyon		0.2								29.9	53.8		19.0		102.9	$Pb_{4.9}Sb_{4.5}S_{11}$	boulangerite?
721-399	3	DDH, Zulu Canyon		0.4						13.8		28.0	42.4		19.8		104.4	$CuPbSbS_6$	
722-346	4	DDH, Zulu Canyon		0.2						1.4	3.8	29.9	43.9	4.9	19.1		103.2	$Pb_4Sb_{4.4}Bi_{0.4}Ag_{0.6}Cu_{0.4}S_{11}$	boulangerite?
EDT92-04	1	Grant Mine Dump		0.57	0.72		6.87			28.84	15.48	27.18			23.51		103.17	$Cu_{8.1}Sb_{3.9}(Zn_{1.9}Ag_{2.6})S_{13}$	tetrahedrite
EDT92-10B	3	Gordon Mine dump			0.42					2.67	2.23	32.87	42.81		20.11	0.04	101.15	$Pb_{2.3}Sb_3S_7$	jamesonite?
	1	Gordon Mine dump		0.14	2.80		7.73			40.78	2.89	23.95			24.73		103.02	$Cu_{10.8}Sb_{3.3}Zn_{2.0}S_{13}$	tetrahedrite
	1	Gordon Mine dump		0.05	1.32		7.75			33.85	7.21	28.31			24.32		102.81	$Cu_{9.1}Sb_{4.0}(Zn_{2.0}Ag_{1.1})S_{13}$	tetrahedrite
	1	Gordon Mine dump		0.06				0.16			0.19	27.40	53.84		18.32		99.97	$Pb_5Sb_{4.3}S_{11}$	amesonite?
	1	Gordon Mine dump			0.24					1.19	20.87	22.29	39.17		13.57		97.33	$Pb_{3.1}Sb_{3.0}Ag_{3.2}S_7$	
	1	Gordon Mine dump			0.65					17.09	13.71	17.92	30.40		12.30		92.07	$Cu_{7.7}Sb_{4.2}Pb_{4.2}Ag_{3.6}S_{11}$	
	1	Gordon Mine dump			0.44		0.05			0.15	0.05	38.41	41.93		20.53		101.56	$Pb_{1.3}Sb_{2.0}S_4$	zinkenite?; plagionite?
EDT92-19	2	Silver Conner Mine dump					0.13			100.69	0.05	0.14			0.17		101.18	Cu	copper

Table 5. Minor element concentrations (in ppm) in optically homogeneous (at ~600 magnification) pyrite, galena, sphalerite, and arsenopyrite from granodiorite (Kgd), contact zone skarn, replacement deposits, and disseminated gold deposits. Some drill hole (DDH) locations are shown on figures 2A and 3. Fire assay and atomic absorption spectrometry analyses by Cone Geochemical Inc. (Lakewood, CO).

Sample no.	Mineral	Au	Ag	As	Sb	Hg	Sn	Bi
Intrusion vein sulfides								
713-1269p	pyrite	0.31	1.5	134	2	0.06	<1	2.4
713-1287p	pyrite	0.02	<0.2	26	<1	0.01	<1	0.8
717-1658p	pyrite	0.03	0.3	103	5	0.08	<1	0.9
Contact zone skarn sulfides								
713-222p	pyrite	0.10	0.9	114	7	0.12	<1	9.0
Replacement deposits sulfides								
718-2466p	pyrite	17.0	2007	2.5%	990	1.38	480	2760
725-2517p	pyrite	19.2	248	1.83%	22	14.0	32	<0.2
726-2276g	galena	3.9	1294	1.55%	390	4.6	390	63.4
726-2393s	sphalerite	2.4	1206	4800	142	151	1260	<0.2
79-1-1748p	pyrite	1.3	72	980	50	10.6	31	326
EDT93-34	pyrite	27.2	718	2000	420	90.0		
EDT92-07	pyrite	9.0	100	2600	5000	1.67	2	461
EDT92-11	pyrite	0.41	158	1480	810	0.89	1	0.5
EDT92-14a	arsenopyrite	6.6	7.8	25.3%	173	0.24	4	28.2
EDT92-15	arsenopyrite	4.0	33.7	21.1%	1740	1.82	6	501
Disseminated gold deposits								
EUD91-12p	pyrite	0.06	10	1.14%	5	6.1		
EUD91-12p1	pyrite	0.08						

Hill were compared in order to determine if sphalerite was deposited by a common or several hydrothermal fluids. These sphalerites conform to two textural types that are readily identified under the microscope: monotonically zoned sphalerite, and finely banded sphalerite.

Monotonically zoned sphalerite

Monotonically zoned sphalerite, the most common textural type, consists of a core and up to two overgrowths that have characteristic colors and uniformly zoned (core to rim) compositions. In 100-μm-thick section, cores are generally dark red-brown to opaque, the medial overgrowth is amber to light brown, and the outer or rimming overgrowth is light yellow to green in color (table 6). The iron content of each growth zone varies, but within zones compositional ranges are relatively small and nowhere overlap those of adjacent zones. Sphalerite cores in sulfide replacement deposits north of Ruby Hill contain 10.7 to 18.2 mole% FeS (6.2 to 10.7 wt.% Fe), medial overgrowths contain 5.5 to 10.3 mole% FeS (3.2 to 6.0 wt.% Fe), and rims contain 2.3 to 4.5 mole% FeS (1.3 to 2.6 wt.% Fe). Sphalerites in hydrous skarn and veins in hydrous skarn south of Ruby Hill have cores that contain 11.7 to 15.2 mole% FeS (6.8 to 8.9 wt.% Fe), medial overgrowths that contain 7.1 to 8.5 mole% FeS (4.1 to 4.9 wt.% Fe), and rims that contain 0.7 to 3.8 mole% FeS (0.4 to 2.2 wt.% Fe) (table 6, fig. 9A). In individual crystals the medial and rim zones may partially to completely envelope cores, but more commonly only parts of one or two of the three zones are present. Where two or more zones are present, contacts between them are indistinct and gradational over a lateral distance of several tens of micrometers, and the zones themselves are hundreds of micrometers thick. In larger aggregates of sphalerite, the medial and rim zones usually coalesce around clusters of cores.

Monotonically zoned sphalerite occurs in sulfide replacement deposits, hydrous skarn, and veins in hydrous skarn. Similar compositional ranges for growth zones of sphalerites from these three deposit types and assemblages, both north and south of the Ruby Hill stock, indicate that monotonically zoned sphalerite and, by association, the hydrothermal minerals with which it occurs, belong to a common hydrothermal event. Based on its distribution, monotonically zoned sphalerite is spatially related to granodiorite (fig. 9A).

Finely banded sphalerite

Sphalerite in or spatially related to quartz porphyry north of Ruby Hill, the second textural type, has a pronounced finely

banded texture that corresponds to tens of growth layers per crystal. The growth layers have sharp boundaries, individual thicknesses of 30 to 50 μm, and relatively homogeneous intralayer compositions (fig. 9B, table 6). The number, width, and composition of growth layers optically distinguishes finely banded sphalerites from monotonically zoned sphalerites. Iron content within growth layers ranges from 1.7 to 15.5 mole% FeS (1.0 to 9.1 wt.% Fe) and displays no clear gradient with age. While sphalerite in quartz porphyry (DDH 729, fig. 9B) is exclusively the finely banded variety, finely banded sphalerite in some occurrences (DDH 79-1, fig. 9A) occurs with monotonically zoned sphalerite, where it appears to be the younger textural type. The occurrence of both sphalerite textural types in the same sulfide replacement deposit suggests separate but overlapping mineralizing events related to both granodiorite and quartz porphyry, as supported by spatial relationships and metal ratios (below). However, while sphalerite textures indicate that quartz porphyry is younger than granodiorite, radioisotopic ages are inconclusive (table 2).

Unoxidized sphalerite in replacement deposits and veins in Prospect Mountain and on Mineral Hill is uncommon and only a few samples were examined. No Prospect Mountain or Mineral Hill sphalerite is finely banded, and none contains more than 5.5 mole% FeS (3.2 wt.% Fe, table 6). Although these low iron sphalerites may correspond to the rim zone of monotonically zoned sphalerites, arguments presented below suggest that the Prospect Mountain and Mineral Hill vein sphalerites are younger than the Cretaceous sphalerites.

Arsenopyrite Compositions

Arsenopyrite is a minor component of sulfide replacement deposits north of Ruby Hill, on Mineral Point, and on Prospect Mountain, where it coexists with sphalerite, pyrite, and locally pyrrhotite. It also occurs with sphalerite, pyrite, and pyrrhotite in hydrous skarn near the Ruby Hill stock. Compositions of arsenopyrite (expressed in atom percent As), sphalerite (expressed in mole percent FeS), and pyrrhotite (expressed in atom percent Fe) that coexist with pyrite can be applied to the experimental data of Scott (1983) and Barton and Skinner (1979) to obtain estimates of depositional temperatures. Arsenopyrite that coexists with sphalerite, pyrite, and pyrrhotite in hydrous skarn adjacent to the Ruby Hill stock and in sulfide replacement deposits has a compositional range of 28.2 to 31.1 atom% As (tables 4 and 6), and an average of 29.4 atom% As. Arsenic content of arsenopyrite from hydrous skarn is at the higher end of this range. The iron content of sphalerite that coexists with arsenopyrite and pyrrhotite in hydrous skarn has a compositional range of 7.9 to 12.2 mole% FeS (4.6 to 7.1 wt.% Fe), and an average of 10.0 mole% FeS (5.8 wt.% Fe, tables 4 and 6). The iron content of sphalerite that coexists with arsenopyrite in sulfide replacement deposits has a compositional range of 7.8 to 18.2 mole% FeS (4.5 to 10.7 wt.% Fe), and an average of 13.5 mole% FeS (7.9 wt.% Fe, tables 4 and 6). The average iron content of pyrrhotite in hydrous skarn and in sulfide replacement deposits is 46.9 atom percent (table 6). Coupled with arsenopyrite compositions, average pyrrhotite composition corresponds to a maximum depositional temperature of ~375°C and a minimum depositional temperature of ~308°C (by graphical solution) of arsenopyrite+pyrrhotite in hydrous skarn and sulfide replacement deposits. The range of arsenopyrite and sphalerite compositions corresponds to a maximum depositional temperature of ~385°C (by graphical solution) for hydrous skarn arsenopyrite+sphalerite+pyrite, and minimum temperatures of <300°C for the same assemblage in sulfide replacement deposits (at 1 kilobar, Scott, 1983). Average arsenopyrite and sphalerite compositions give approximate depositional temperatures in hydrous skarn and in sulfide replacement deposits of 320 to 315°C, respectively. Although sulfide mineral equilibrium temperatures in hydrous skarn and sulfide replacement deposits are somewhat consistent, they are lower than depositional temperatures estimated from silicate mineral equilibria in pyroxene+garnet and hydrous skarn.

Metal Zoning

The distribution of metals in and adjacent to sulfide replacement deposits north of Ruby Hill, and in other replacement deposits in the district with recorded production, was determined by analysis (fig. 10) and from production records and drill hole data, respectively (Nolan, 1962; Nolan and Hunt, 1968). These data were collected in order to assess the extent of metal distribution haloes encompassing sulfide replacement deposits, and to determine if metal abundances in the deposits varied with proximity to granodiorite and quartz porphyry. Metal distribution patterns display several spatial consistencies. Regarding metal distribution haloes, the downhole distribution of gold, silver, lead, and zinc in DDH 726 (fig. 10) shows that anomalous amounts of one or more of these elements, relative to unmineralized Eldorado Dolomite in DDH 728, occur near, as well as within, sulfide replacement deposits. Other gold, silver, zinc, and minor lead anomalies at about 600 to 680 m (~2,000 to 2,250 feet) below the surface may relate also to nearby replacement sulfide masses that were not intercepted in the drill hole. The significance of minor element anomalies in drill holes is that they may identify altered and mineralized sections of megascopically unaltered Eldorado Dolomite near Ruby Hill on a scale of meters to possibly tens of meters distal to sulfide replacement deposits.

Regarding spatial relationship of replacement deposits to Cretaceous intrusions, Pb/Zn and Ag/Au in both oxide and sulfide replacement deposits in Ruby Hill and on Mineral Point were compiled from production records (Nolan, 1962) and drill hole analyses. The ratios were organized by spatial proximity to granodiorite and to quartz porphyry in order to determine if the intrusions are associated with different metal signatures in sulfide replacement deposits. In detail contoured metal ratios are rather complex, perhaps because of incorrect assignment of ratios to intrusions, but by increasing the contour interval to smooth irregularities, the contours form distinct patterns around replacement deposits spatially associated with each intrusion (fig. 11). Sulfide replacement deposits interpreted to be spatially related to granodiorite are characterized by Pb/Zn and Ag/Au

Table 6. Partial compositions, textures, and colors of sphalerite, and compositions of arsenopyrite and pyrrhotite, in Eureka district DDH core and mine samples. Compositions derived from data on table 4. Some drill hole locations are shown in figures 2A and 3.

Hole/ Sample no.	Minerals	wt.% Fe	Sphalerite color[1]; paragenesis	mole% FeS	atom% As	Average atom % Fe	Average mole fraction Fe
706-771	sphalerite	0.63	dark brown; discrete anhedrons with pyrite in 1 cm dolomite vein in dolomite	1.13			
706-780	pyrrhotite	61.10				46.71(4)	0.9342 ± 0.0017
713-222	arsenopyrite				30.91 29.52		
	pyrrhotite	60.90				47.22(2)	0.9444 ± 0.0008
718-526	pyrrhotite	60.60				46.50(3)	0.9299 ± 0.0021
718-764	pyrrhotite	59.10				45.95(2)	0.9190 ± 0.0022
	sphalerite	7.84	opaque; inclusions and thin veins in massive pyrrhotite marginally	14.04			
		7.43	replaced by pyrite	13.31			
720-284.6	sphalerite	7.68	opaque; discrete anhedrons in dolomite	13.75			
		6.83		12.23			
720-1073	sphalerite	1.81	pale, yellow-green rim; coarse grained subhedrons in dolomite	3.24			
		2.19		3.92			
		4.55	darker, amber core; coarse grained subhedrons in dolomite	8.15			
		4.50		8.06			
720-1583	sphalerite	0.52	v. pale yellow; discrete anhedrons in banded carbonate + calc-silicates	0.93			
		0.65		1.16			
720-1943	pyrrhotite	59.50				47.10(2)	0.9420 ± 0.0025
720-1946	pyrrhotite	61.20				47.12	0.9424
sphalerite		8.85	opaque; intergrown with pyrite replacing massive pyrrhotite	15.85			
		8.67		15.53			
721-399	sphalerite	1.26	pale lt. brown; coarse grained anhedrons in 5 mm	2.26			
		1.82	galena + stibnite vein in dolomite	3.26			
		0.37					
		0.72		1.29			
721-442	sphalerite	0.39	pale lt. brown; anhedral, intergrown with stibnite, boulangerite(?) and quartz, in 5 mm vein cutting dolomite	0.70			
722-346	sphalerite	1.34	v. pale yellow green; anhedrons dissem. in dolomite breccia with pyrite, stibnite, and boulangerite(?)				
723-1486	sphalerite	7.36	opaque; massive, intergrown with pyrite euhedrons and minor galena	13.18			
724-761	pyrrhotite	61.30				47.44(3)	0.9488 ± 0.0030
724-772	sphalerite	8.11	dark, nearly opaque; discrete anhedrons in banded quartz + carbonate	14.53			
		4.24	pale amber brown; discontinuous bands of anhedrons in banded	7.59			
		4.87	quartz + carbonate	8.72			
724-793	sphalerite	1.70	mottled amber brown/opaque; intergrown with pyrite replacing pyrrhotite;	3.04			
		4.05	chalcopyrite, dolomite, calc-silicates, rare arsenopyrite euhedrons	7.25			
		1.97	also present	3.53			
		7.58		13.58			
	arsenopyrite				28.88 29.50		
	pyrrhotite					47.36(5)	0.9472 ± 0.0090
726-2278	sphalerite	5.93	dark, nearly opaque cores; massive with pyrite, chalcopyrite, tennantite, and arsenopyrite inclusions; fractures filled with dolomite	10.62			
		3.15	amber overgrowths; massive with pyrite, chalcopyrite, tennantite, and arsenopyrite inclusions; fractures filled with dolomite	5.64			
	arsenopyrite				28.79 28.30		
726-2370	sphalerite	5.32	opaque; minor inclusions in massive comminuted pyrite; fractures in pyrite	9.53			
		5.97	filled with dolomite, minor galena inclusions	10.69			
727-305	sphalerite	0.50	amber brown; anhedrons intergrown with coarse grained dolomite in 3 mm vein cutting limestone	0.90			
DH-82125	sphalerite	1.45	opaque; inclusions in massive fractured pyrite intergrown with dolomite;	2.60			
		1.56	other inclusions of galena, arsenopyrite, and pyrrhotite	2.79			
		1.31		2.35			
		1.35		2.42			
	arsenopyrite				29.88 30.13 29.38 28.86		
	pyrrhotite					47.14(2)	0.9428 ± 0.0002

Table 6. ***Continued***

Hole/ Sample no.	Minerals	wt.% Fe	Sphalerite color[1]; paragenesis	mole% FeS	atom% As	Average atom % Fe	Average mole fraction Fe
79-1-1724	sphalerite	8.25 8.99 9.32 6.84 6.94	opaque; intergrown with fractured pyrite and coarse grained dolomite in matrix of angular clast dolomite breccia	14.78 16.10 16.69 12.25 12.43			
79-1-1740	sphalerite, scan	1.0-5.9	growth zoned, most of crystal 3-5 wt.% Fe; lighter amber layers contain 3 wt.% Fe and lie distal to dark amber layers which contain 3-5 wt.% Fe and lie adjacent to brecciated dolomite				
79-1-1748	pyrrhotite	60.70				46.96(2)	0.9392 ± 0.0002
79-1-2190	arsenopyrite				29.69		
	sphalerite	3.82 5.83	opaque; inclusions in massive galena + intergrown pyrite and arsenopyrite euhedrons; galena fills cracks in pyrite, arsenopyrite	6.84 10.44			
729-1896	sphalerite, scan	2.0-9.1	growth zoned, alt. bands of brown, amber brown, lt. yellow brown; intergrown with galena and pyrite; brown, amber brown layers contain 4-9 wt.% Fe and lie adjacent to quartz porphyry, light brown to yellow layers contain < wt.% Fe and are distal to brown and amber brown layers				
729-3304	sphalerite	6.46 4.42	dark brown; fractured anhedrons intergrown with very coarse grained dolomite and minor pyrite; rare tennantite, pyrrhotite inclusions	11.57 5.03 9.01			
	arsenopyrite			28.57			
EUD91-1B	sphalerite arsenopyrite	5.12	dark red-brown; massive, intergrown with pyrite, arsenopyrite, galena; finely fractured, filled with dolomite	9.17 28.07	28.28		
EUD91-3A	sphalerite	3.11 2.02	amber-yellow; dissem. with pyrite euhedrons, minor tennantite, and chalcopyrite in dolomite breccias	5.57 3.62			
	arsenopyrite			30.93			
EUD91-11A	sphalerite	7.17 6.98 6.62	dark red brown; massive, replaces massive pyrite; both finely fractured and cemented with dolomite.	12.84 12.50 11.86			
EUD91-11C	sphalerite	6.22 10.66	opaque; massive, replaces massive pyrite and skeletal galena; minor seligmannite inclusions in galena; arsenopyrite also present	11.14 19.09			
	arsenopyrite				29.79 27.41 28.47		
EUD91-11E	sphalerite	6.68 8.23	very dark brown to opaque; anhedral clots with pyrite inclusions, intergrown with dolomite; minor inclusions of arsenopyrite and tennantite; fractured and cemented with dolomite	11.96 14.74			
	arsenopyrite				28.82 29.63 29.97		
EUD91-11H	sphalerite	2.64 2.39 2.36 8.32	yellow green rims; intergrown with pyrite adjacent to dolomite amber to dark brown cores; distal to dolomite and in places sharply contacts yellow green rims; arsenopyrite, tennantite also present	4.73 4.28 4.23 14.90			
	arsenopyrite				29.07		
EDT92-04	sphalerite	0.60	opaque; dissem. with tetrahedrite in quartz + dolomite veins (15 cm)	1.07			
EDT92-06A	sphalerite	1.77	opaque; massive, intergrown with galena, chalcopyrite, coarse-grained dolomite and minor calc-silicates	3.17			
EDT92-06E	pyrrhotite	61.10				46.75(3)	0.9350 ± 0.0015
EDT92-16B	sphalerite	1.12	dark brown; intergrown with pyrite and inclusions in galena in center of 30 cm quartz vein	2.00			
EDT92-20	sphalerite	4.81	thin, dark brown overgrowths	8.61			
		8.23	opaque cores; massive with pyrite inclusions; largely oxidize	14.74			
EDT92-88	sphalerite	4.15	opaque; inclusions in massive galena; largely oxidized to anglesite	7.43			

[1] Transmitted light, 100-µm-thick section.

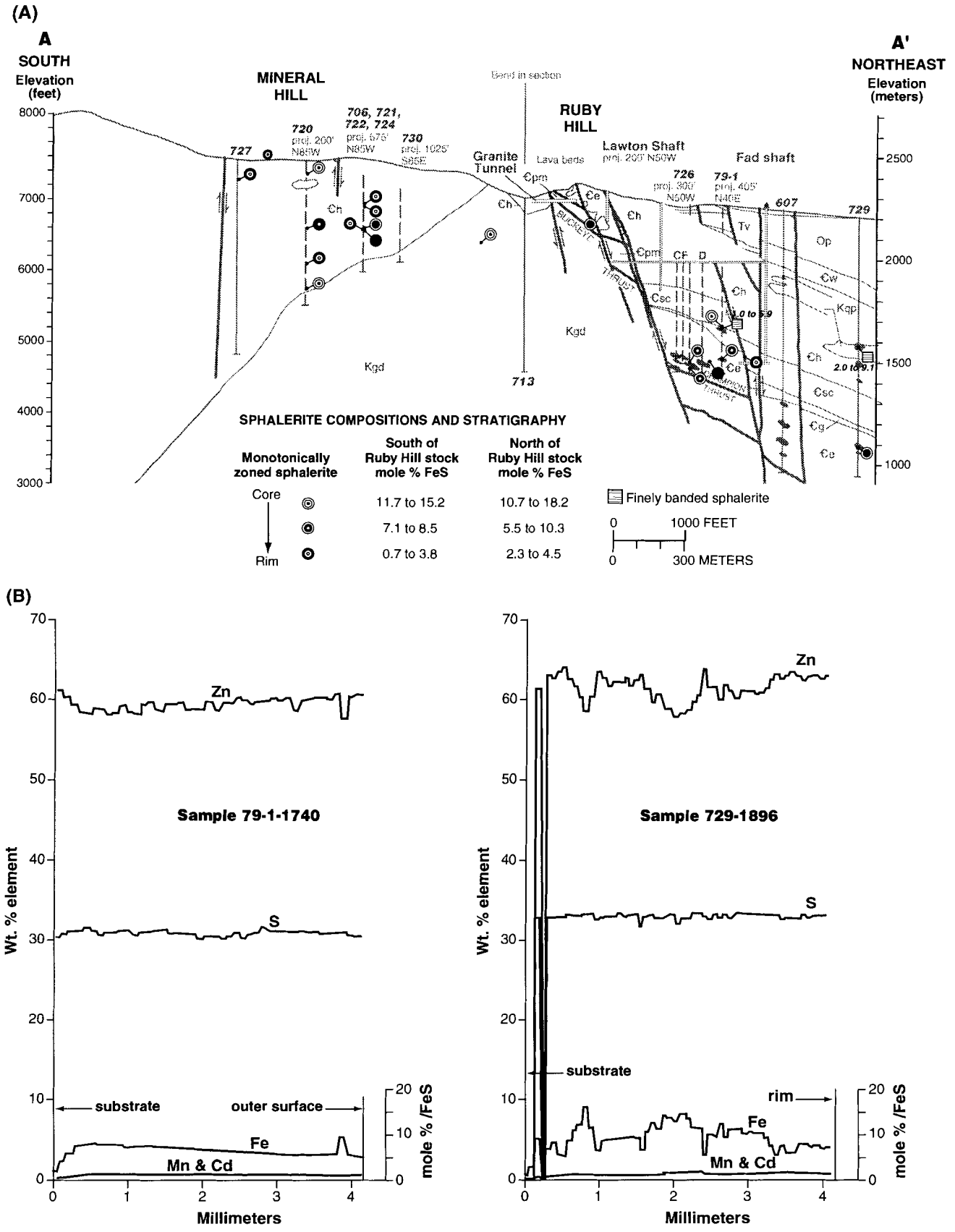

Figure 9. (A) Section A-A' (fig. 3) showing sphalerite types and compositional ranges of monotonically zoned sphalerite (in mole percent FeS). Filled and partially filled symbols on the section that are not specifically reproduced in the explanation represent sphalerites consisting of more than one concentric compositional range (e.g., filled symbols are sphalerites containing all three concentric zones). Data are from tables 4 and 6. (B) Major and minor element compositions of finely banded sphalerites in DDH 79-1 and 729 (fig. 3), determined by electron microprobe. Analyses were made along approximately 4-mm-long traverses oriented orthogonally to banding.

that decrease from the margins of replacement deposits inward. In sulfide replacement deposits north of Ruby Hill Pb/Zn is ≤ 0.8, and Ag/Au is < 100. In the oxidized ores of Ruby Hill Pb/Zn is > 3 and Ag/Au is < 20. These different ratios resulted from removal of zinc and possibly silver, and residual concentration of gold during weathering of the oxidized deposits. Among individual sulfide replacement deposits associated with granodiorite north of Ruby Hill, lead abundance relative to zinc decreases toward the north (DDH 607 and DDH 729, fig. 11), a trend pointed out by Nolan and Hunt (1968), and precious metals tenor also decreases. No metal zoning is apparent among individual quartz porphyry replacement deposits, although the data base is relatively small, but replacement deposits interpreted to be spatially associated with quartz porphyry north of Ruby Hill have Pb/Zn ≥ 0.8, and Ag/Au ≥ 100 (fig. 11).

When metal ratios in the replacement deposits and drill intercepts on Mineral Point, which are near quartz porphyry, are added to those north of Ruby Hill, spatial affiliations of metal ratios to the two intrusions are more distinct (fig. 12). Granodiorite-related sulfide replacement deposits are zinc-rich compared to quartz porphyry replacement deposits, the bulk of which tend to be lead-rich. The predominance of lead in quartz porphyry deposits, based on production records and drill hole intercepts, correlates with the greater abundance of galena relative to sphalerite observed in sulfide samples. Replacement deposits associated with each intrusion contain approximately the same proportions of silver and gold, although some deposits spatially related to quartz porphyry are rich in gold, and a few granodiorite-related deposits contain relatively higher silver abundances. In agreement with sphalerite textures and compositions and with field relationships, metal ratios suggest that sulfide deposition is associated with each intrusion.

FLUID PHYSICAL CHARACTERISTICS, COMPOSITIONS, AND COMPONENT SOURCES

Data on the temperatures, pressures, and chemical and isotopic compositions of the fluids involved in the formation of hydrous skarn, veins in hydrous skarn, and sulfide replacement deposits throughout the district were obtained from microthermometric measurements of fluid inclusions, and isotope analyses of silicate, sulfide, and carbonate minerals. These data allow temperatures, pressures, and depths of formation of the several hydrothermal mineral assemblages to be estimated and compared. Sulfur and lead isotope compositions also provided permissive sources for components.

Fluid Inclusion Microthermometry

Petrographic observations and microthermometric measurements were recorded for fluid inclusions in: (1) quartz and calcite veins in granodiorite, and quartz, dolomite, calcite, and sphalerite from contact zone hydrous skarn and marble; (2) sphalerite, dolomite, calcite, and barite from replacement deposits, mainly north of Ruby Hill; (3) quartz phenocrysts in quartz porphyry; and (4) quartz in vein deposits south of Ruby Hill (figs. 2 and 6). Entrapment temperatures, entrapment pressures, and major solute concentrations of mineralizing fluids were estimated from these observations and measurements. Only a few data were collected from replacement deposits in Prospect Mountain and no usable fluid inclusions from replacement deposits on Mineral Point were found.

Veins in granodiorite, hydrous skarn, and marble

Primary fluid inclusions in quartz from the three vein types in granodiorite, quartz-microcline-pyrite veins, quartz-sericite-pyrite veins, and carbonate veins, comprise two populations based on the phases present at room temperature: (1) vapor carbon dioxide (VCO_2)+liquid carbon dioxide (LCO_2)+liquid saline solution (LH_2O), and, (2) LCO_2+LH_2O. Numerous planes of secondary fluid inclusions also occur in the samples but were not measured because of small size and uncertain origin. The primary fluid inclusions, which range in size from <5 to 25 μm, occur as isolated individuals and as small groups in quartz growth planes. The presence of CO_2 was initially recognized by phase relations (two nested spherical phases, VCO_2 in LCO_2, in LH_2O), and by rapid expansion of the spherical phases when inclusions were crushed. In VCO_2+LCO_2+LH_2O inclusions the vapor bubble occupies ~5 to 10 vol.% (visual estimate) of the inclusion. In LCO_2+LH_2O inclusions and in VCO_2+LCO_2+LH_2O inclusions after CO_2 homogenization, LCO_2 makes up 20 to 25 vol.% (visual estimate) of the inclusions.

Primary fluid inclusions in quartz, dolomite, calcite, and sphalerite from hydrous skarn and marble adjacent to the Ruby Hill stock constitute the same populations as veins in granodiorite. Contact zone fluid inclusions are generally <15 μm in maximum dimension, occur mostly as isolated individuals in quartz, and occur largely along growth planes in dolomite, calcite and sphalerite.

Carbon dioxide homogenization (to LCO_2) in fluid inclusions in quartz-sericite-pyrite veins (type 2) in granodiorite and in hydrous skarn minerals takes place over the temperature range 23.3 to 27.8°C (table 7A), corresponding, by graphical solution, to CO_2 densities of 0.68 to 0.73 g/cm^3 (Bodnar and others, 1985), and vol.% CO_2 of <20 to 25 (Schwartz, 1989). LCO_2 in these inclusions homogenizes (to liquid) at 225 to 273°C (table 7A), and salinities (wt.% $NaCl_{eq}$), determined by clathrate melting (Collins, 1979), range from ~6 to 13 (X_{NaCl} ≈ 0.020 to 0.044, table 7A). LCO_2+LH_2O+VCO_2 inclusions in carbonate veins (type 3) in granodiorite, and in marble distal to the Ruby Hill stock homogenize to liquid in the temperature range 230 to 274°C (table 7A). Salinities for the one sample measured are within the same range as those measured for the quartz-dominated veins in granodiorite.

For H_2O+CO_2+6 wt.% $NaCl_{eq}$ (X_{NaCl} ≈ 0.02) fluids the measured CO_2 concentrations and homogenization temperatures give minimum entrapment pressures of ~1,000 to 1,600 bars (Schwartz, 1989; Bowers and Helgeson, 1983). A similar pressure estimate of ~1,000 bars (at 700°C, assuming

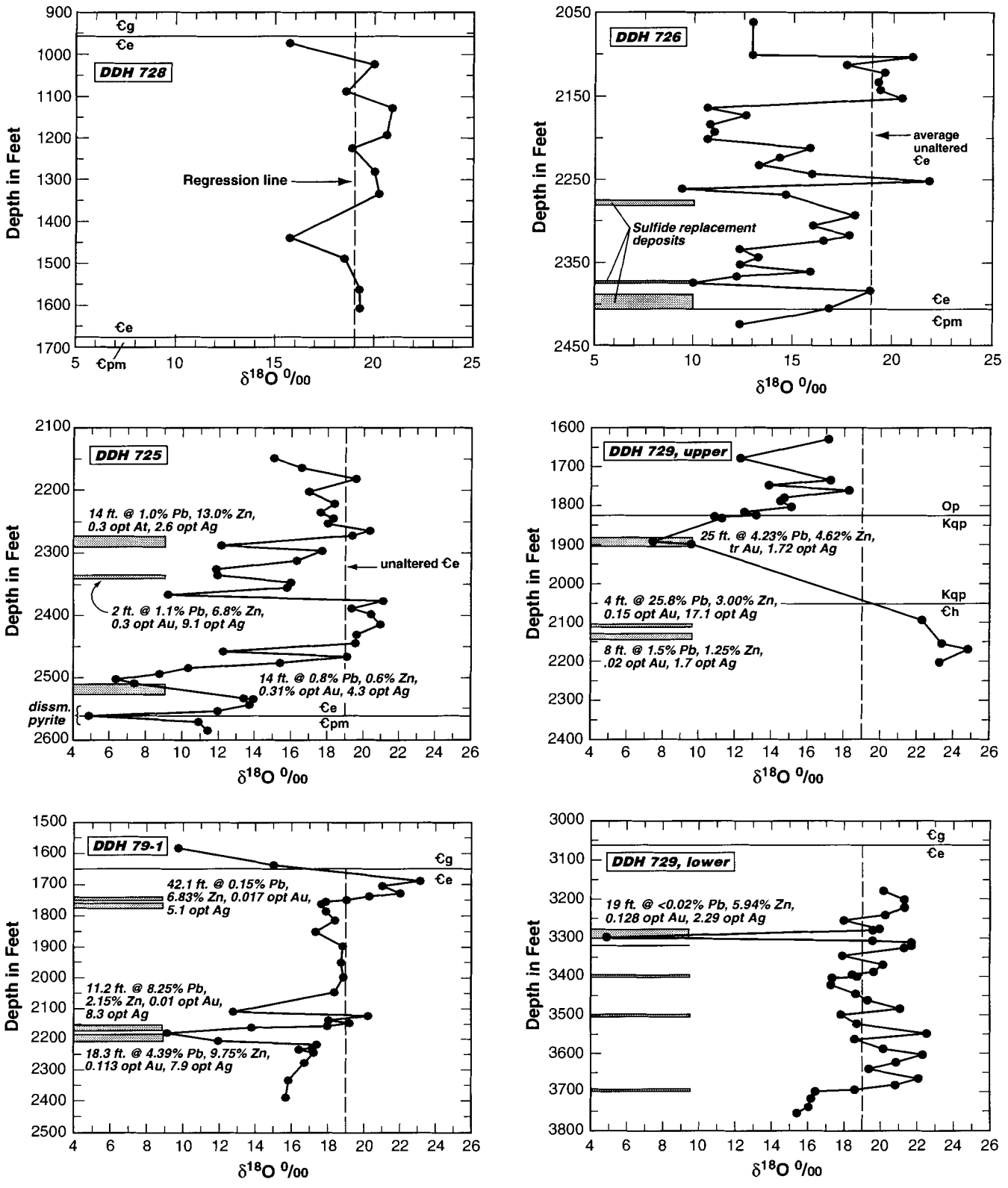

Figure 10. Variations with depth below the surface of whole rock oxygen isotope compositions and metal concentrations (gold, silver, lead, and zinc) in diamond drill holes DDH 728, 726, 725, 729, and 79-1, which penetrate unmineralized Eldorado Dolomite (€e, DDH 728) and sulfide replacement deposits (shaded horizontal bars) in Eldorado dolomite (€e) and quartz porphyry (Kqp; DDH 726, 725, 729, and 79-1) in the down-dropped block north of Ruby Hill (figs. 2A and 3). Other lithologies: €pm = Prospect Mountain Quartzite, €g = Geddes Formation, Op = Pogonip Group. DDH locations are shown in figure 2A. Isotope data are from table 8. Regression of oxygen isotope analyses gives a whole rock composition of 19‰±3‰ for unmineralized Eldorado Dolomite. The average abundances of lead and zinc in unmineralized carbonate rocks are 9 and 20 ppm, respectively.

Figure 10. ***Continued***

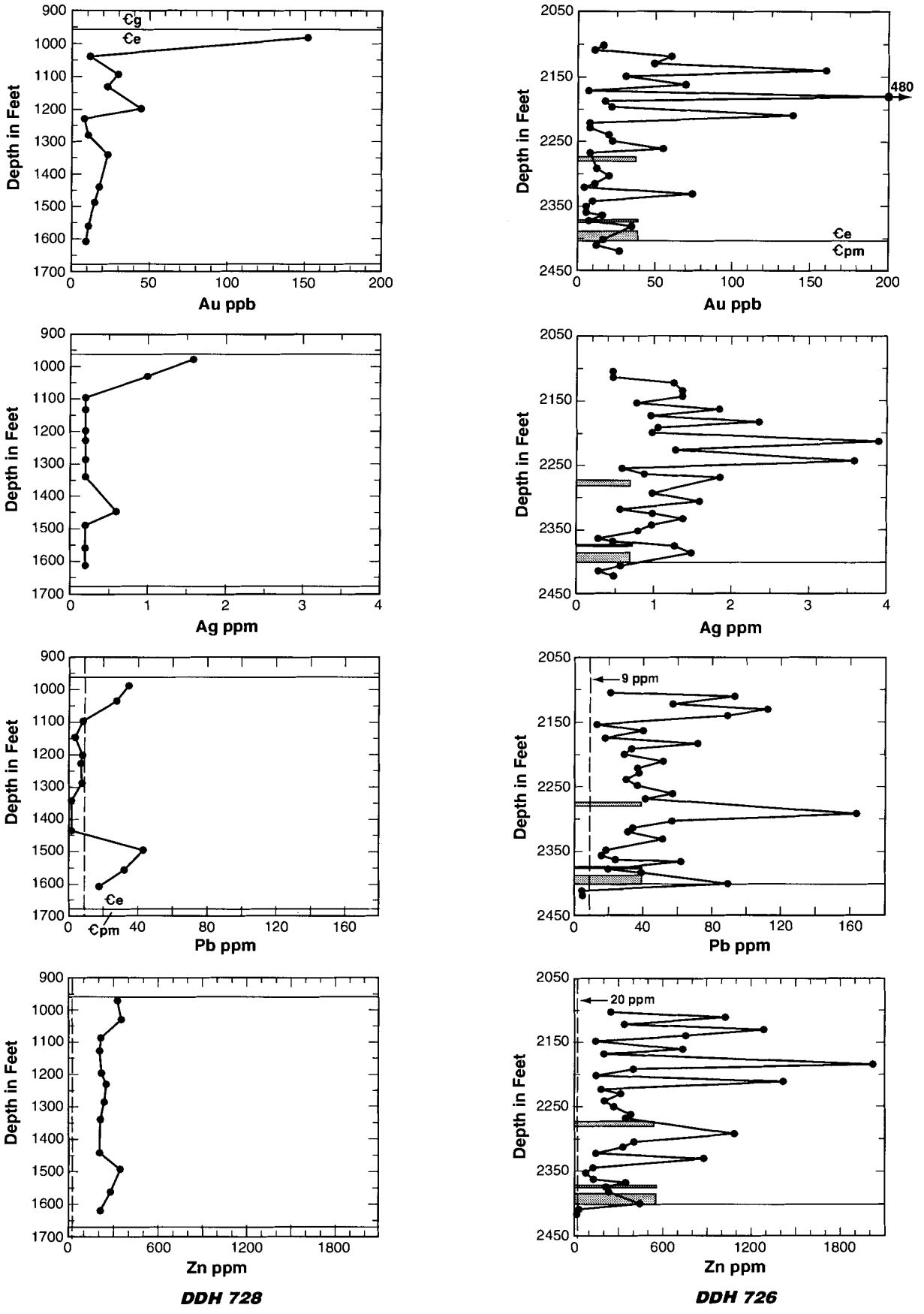

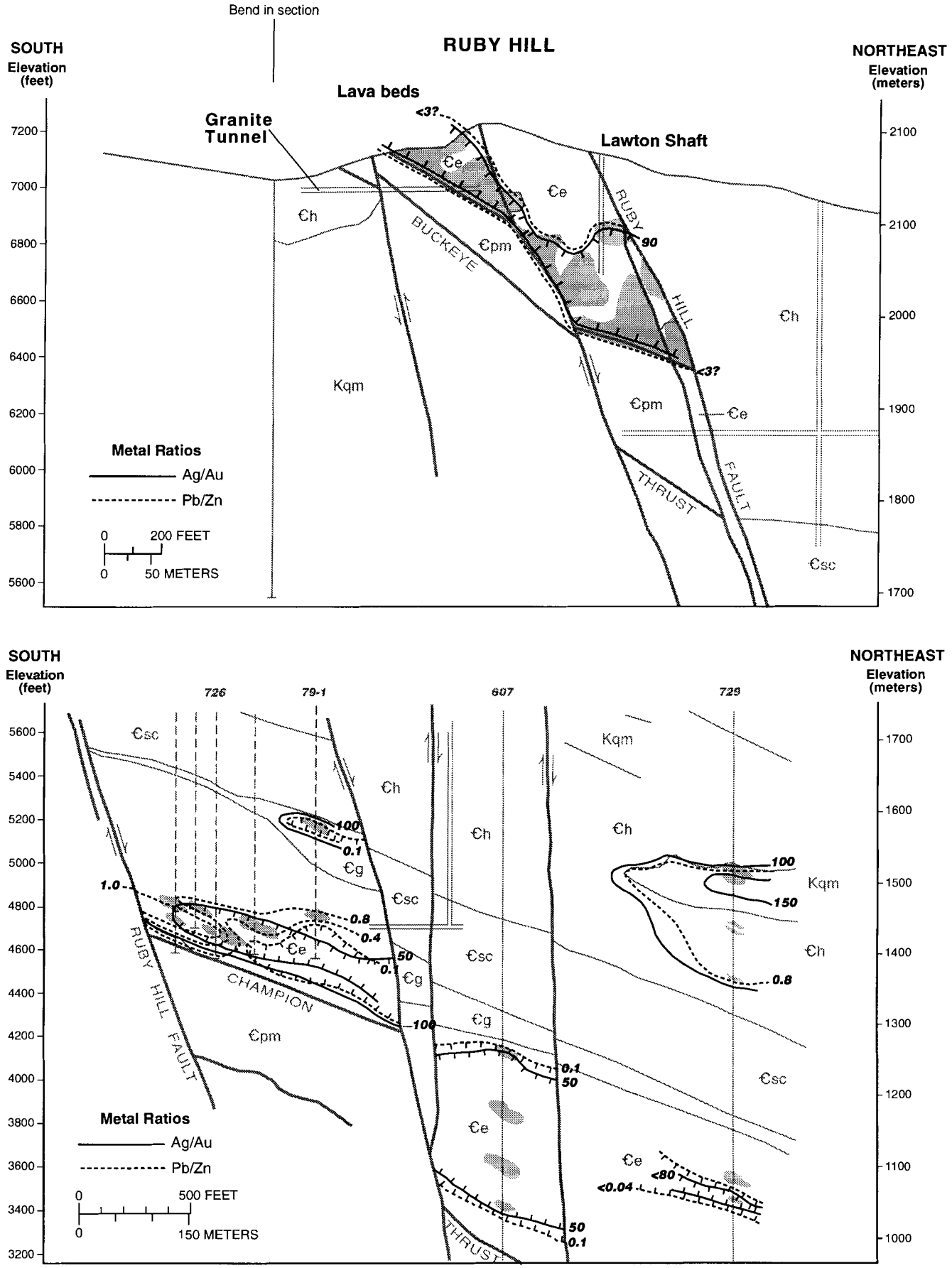

Figure 11. Parts of section A-A' (fig. 3) showing Ag/Au and Pb/Zn contoured around replacement deposits in Eldorado Dolomite in Ruby Hill, and at depth north of Ruby Hill. Metal abundances were derived from drill hole logs provided by the Ruby Hill Mining Co.

all iron is Fe^{2+}) for granodiorite emplacement is based on Al^T in amphiboles in granodiorite (DDH 730, table 3; Blundy and Holland, 1990). The fluid inclusion pressure estimates, assuming lithostatic gradient, correspond to minimum depths of emplacement of granodiorite and skarn of 3.8 to 6.1 km (2.3 to 3.7 miles). For higher salinity fluids indicated for many samples (table 7) the minimum entrapment pressure could be several hundred bars higher and the minimum depth of granodiorite emplacement several hundreds of meters deeper. Under a hydrostatic gradient the depth of granodiorite emplacement increases several times over the lithostatic pressure depth estimates. Isotope analyses of hydrous skarn and replacement mineral fluid inclusion waters (presented in a later section) show that meteoric water circulated in and adjacent to the Ruby Hill stock. Therefore, total pressure (minimally 1 to 1.6 kilobars) must include an increment of hydrostatic pressure, and the depth of emplacement is greater than the minimum (3.8 km) derived from fluid inclusion microthermometry. Ambient pressure is directly related to permeability which typically changes from lithostatic to hydrostatic in the evolving thermal regime of intrusive environments (Hanson, 1995).

Adding pressure corrections to homogenization temperatures of +90 to +110°C (Potter and others, 1978) gives a minimum entrapment temperature range of 340 to 383°C for fluid inclusions in granodiorite veins and in hydrous skarn minerals. These fluid inclusion entrapment temperatures are ~40 to 80° lower than maximum temperatures of hydrous skarn formation based on mineral equilibria (see below), and the pressure corrections applied my be somewhat insufficient.

XCO_2 in fluid inclusions in veins in granodiorite and in hydrous skarn minerals averages about 0.075 (table 7), which places the minimum temperature at 1 kilobar of the hydrous skarn minerals tremolite and antigorite at ≥420°C (Einaudi and others, 1981, figs. 5 and 6). If $XCO_2 = 0.075$ is valid for the early skarn mineral assemblage of pyroxene (average $Di_{75.1}$ $Hd_{24.3}$ $Jo_{0.6}$) + garnet (average Gr_{72} Al_{27} $(Sp+Py+Uv)_1$), the minimum temperature stability range for that assemblage is about 470°C. If XCO_2 was much higher (e.g., 0.1), and/or total pressure was >2 kilobars, then minerals less abundant (andradite) or unobserved (anorthite, talc, magnesite) would be stable in the skarns; therefore, the XCO_2 value based on fluid inclusion measurements (0.075) is preferred. By way of comparison, grossularite in Cretaceous tungsten skarn in the Osgood Mountains, Nevada, formed from fluids with similar XCO_2 (≤ 0.035), based on carbon and oxygen isotope systematics (Taylor and O'Neil, 1977).

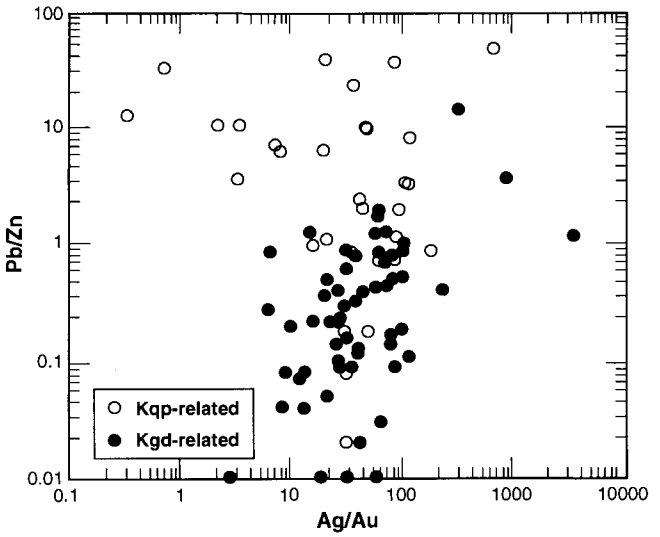

Figure 12. Pb/Zn plotted against Ag/Au for sulfide replacement deposits in Ruby Hill, north of Ruby Hill, and on Mineral Point, distinguished by spatial proximity to quartz porphyry (Kqp) and granodiorite (Kgd, Ruby Hill stock). Data include drill hole analyses (obtained from logs provided by the Ruby Hill Mining Company), production records (Nolan, 1962), reserve data (Love, 1966), and dump sample analyses of unoxidized sulfide minerals.

Replacement deposits

Primary fluid inclusions in hydrothermal dolomite, calcite, and sphalerite from sulfide replacement deposits north of Ruby Hill consist of two liquid phases, LCO_2 and LH_2O. LCO_2 uniformly comprises ~25 vol.% (visual estimate) of the inclusions. The inclusions are generally <15 μm in maximum dimension, and occur largely as individuals and in small groups in growth planes. Primary inclusions in quartz and barite from sulfide replacement deposits on Prospect Mountain consist of VH_2O and LH_2O. They occur in growth zones but are not always distinguishable from younger inclusions in numerous crosscutting planes, and many barite inclusions appear to have necked.

Fluid inclusions in hydrothermal dolomite, calcite, sphalerite, quartz, and barite (one sample) intergrown with pyrite, sphalerite, and galena, and in sphalerite in sulfide replacement deposits north of Ruby Hill and in Prospect Mountain homogenize to liquid at temperature modes ranging from 212 to 360°C (table 7B). Homogenization temperature modes of fluid inclusions in most sulfide replacement deposit minerals north of Ruby Hill range from 253 to 292°C. Homogenization temperature modes in Prospect Mountain replacement deposits are somewhat lower than those north of Ruby Hill, ranging from 212 to 263°C. Modes are defined as the midpoints (rounded upward) of groups (selected by inspection) of contiguous homogenization temperature histograms that have been compiled on 5°C intervals. Maximum salinities of inclusions in both groups of deposits are similar and fall within the range 3.5 to 10.4 wt.% $NaCl_{eq}$ (~0.011 to 0.035 X_{NaCl}, table 7A). Because no VCO_2 is present in these inclusions, true inclusion salinities are less than the range measured and lower than the range of salinities in hydrous skarn minerals. XCO_2 was not measured, but it is presumably higher than about 0.05 at the depositional temperatures of replacement deposits, as no calc-silicate minerals occur in replacement deposits.

At an estimated entrapment pressure of 1,300 bars, based on hydrous skarn and granodiorite vein pressures, corrections of +90 to +110°C were added to homogenization temperatures, giving an estimated entrapment temperatures range for replacement deposits of 302 to 470°C. In sulfide replacement deposits north of Ruby Hill, the lowest entrapment temperature of 358°C is from dolomite in a sulfide replacement deposit

Table 7A. Fluid inclusion types, sources, microthermometric measurements, and graphical solutions of CO_2 density, CO_2 volume percent, and CO_2 mole percent, and entrapment pressures and temperatures for $VCO_2+LCO_2+LH_2O$ fluid inclusions and LCO_2+LH_2O inclusions in types 2 and 3 veins in granodiorite, and in hydrous skarn minerals near the Ruby Hill granodiorite stock.

Sample number	No. incl.	Type	Host mineral; Rock	VCO_2 homog.T°C	$LCO_2 \Rightarrow LH_2O$ homog. mode T°C	XNaCl (No.)[1]	σCO_2 g/cm[2,3]	σ f.i.[4]	VCO_2[5]	XCO_2[1]	Pe(bars)[6]	Te°C[7]
GRANODIORITE AND SKARN												
713-2284	16	$VCO_2+LCO_2+LH_2O$	quartz, vein type 2; gd	24.9 to 27.8	261	0.031-0.034(4)	0.69	0.90	22	0.08	1200	371;320
713-2387	14	$VCO_2+LCO_2+LH_2O$	quartz, vein type 2; gd	23.3 to 24.0	273		0.73	0.88	25	0.10	1600	383
720-1073	18	$VCO_2+LCO_2+LH_2O$	quartz; sphalerite; contact zone	25.4 to 26.6	248; 220	0.034(2) 0.020-0.022(3)[8]	0.68	0.92	<20	0.06	1000	338;310
706-1333	21	$VCO_2+LCO_2+LH_2O$	c. grnd. quartz+pyrite; contact zone vein	23.9 to 24.7	245	0.025-0.029(10)	0.71	0.92	<20	0.07	1000	345
706-1384	4	$VCO_2+LCO_2+LH_2O$	quartz; contact zone	24.6 to 26.4	260		0.71	0.92	22	0.08	1400	365
EDT92-06c	3	$VCO_2+LCO_2+LH_2O$	quartz; contact zone	17.7 to 18.5	249		0.79	0.85	<20	0.08	1400	354
706-791	11	$VCO_2+LCO_2+LH_2O$	calcite, calcite+pyrite vein type 3; contact zone (marble)	24.6 to 26.4	e230		0.70	0.90	<20	0.06	1000	335
713-950.4	15	$LCO2+LH_2O+VCO2$	calcite, calcite+pyrite vein type 3; granodiorite		245							340
713-1269	26	$LCO2+LH_2O$	calcite, calcite vein type 3; granodiorite		245; 168							340
722-346	12	$LCO2+LH_2O$	quartz; quartz vein in contact zone (marble)		e 225[9]							e325
727-396	14	LCO_2+LH_2O	quartz; quartz vein in contact zone (marble)		e 274[9]	0.035-0.044(7)						e355

see footnotes below Table 7B

Table 7B. Fluid inclusion homogenization temperatures and salinities, and estimated entrapment temperatures for sulfide replacement deposits north of Ruby Hill, and for sulfide replacement and vein deposits in Prospect Mountain. Deposit locations are shown on figures 1, 2, and 6.

Sample number	No. incl.	Type	Host mineral; Rock	$LCO_2 \Rightarrow LH_2O$ homog. mode T°C	XNaCl (No.)[1]	Te°C[7]
RUBY HILL SULFIDE REPLACEMENT						
79-1-1740	26	LCO2+LH_2O	dolomite; sulfide replacement in DDH north of Ruby Hill	253	0.011-0.027(15)	358
EUD91-11G	23	LCO2+LH_2O	dolomite; sulfide replacement in FAD Shaft north of Ruby Hill	288		393
DDH8-2125	19	LCO2+LH_2O	calcite; sulfide replacement in DDH north of Ruby Hill	292		397
729-1896	9	LCO2+LH_2O	sphalerite; sulfide replacement in DDH north of Ruby Hill	290		395
729-3034	21	LCO2+LH_2O	dolomite; sulfide replacement in DDH north of Ruby Hill	360[9]	0.018-0.026(7)	470
PROSPECT MOUNTAIN VEIN AND SULFIDE REPLACEMENT						
EDT92-01A	27	V+LH_2O	quartz; sulfide replacement in which gn>sl>>py, Diamond mine dump	212		317
EDT92-06C1	17	V+LH_20	quartz; galena+quartz replacement; Prospect Mountain Tunnel dump	226	0.031-0.035(11) 0.009-0.011(3)	
EDT92-14A	35	V+LH_2O	barite; Wabash sulfide replacement	263		368
EDT92-08	40	V+LH_2O	quartz; quartz+dolomite+tennantite vein above Ruby Hill Tunnel	268; 253; 198[10]	0.023-0.026(6)	(boiling curve P?)
EDT92-16A	7	V+LH_2O	quartz; quartz+gn+sulfosalt vein, Dead Broke tunnel dump	e260[9]		e365
EUD92-10P2	17	V+LH_2O	quartz; quartz+st+gn+sulfide vein, Grant mine dump, Mineral Hill	e248[10]		(boiling curve P?)

[1] mole fraction CO_2; true salinities for inclusions containing VCO_2, maximum salinities where VCO_2 absent (Collins, 1979)
[2] Bodnar, and others (1985)
[3] average of range
[4] bulk density, assuming σ H_2O = 1.0 g/cm^3, and negligible (CO_2) in H_2O
[5] Schwartz (1989)
[6] estimated minimum entrapment pressure (Schwartz, 1989; Bowers and Helgeson, 1983)
[7] pressure-corrected minimum entrapment temperature (Potter, and others, 1978; Bowers and Helgeson, 1983), includes +90 to 110°C pressure correction
[8] no LCO_2
[9] large Th°C range
[10] variable phase ratios, large Th°C range

~530 m (~1,740 feet) below the present surface. The highest entrapment temperature in a sulfide replacement deposit north of Ruby Hill, 470°C, is from hydrothermal dolomite ~1,000 m (3,304 feet) below the present surface north of the Fad Shaft (DDH 729, fig. 3). The large range in hydrothermal dolomite and calcite temperatures may have resulted from unrecognized volume increases during heating of fluid inclusions in carbonate minerals, particularly in one dolomite sample. The homogenization temperature mode for sphalerite inclusions is within the range of modes determined for three of the four carbonate minerals (table 7B), and the more probable entrapment temperature range for replacement deposits north of Ruby Hill is 358 to 395°C. Pressure-corrected entrapment temperatures for sulfide replacement deposits in Prospect Mountain are 302 to 373°C. Upon cooling, fluid inclusions in barite from one deposit in Prospect Mountain exsolved VCO_2, suggesting that some stretching occurred during heating. Temperature variability also may have been caused by unrecognized necking of inclusions.

The temperature limit of ≤420°C for hydrous skarn adjacent to the Ruby Hill stock, based on mineral equilibria and XCO_2, is ~25 to 80°C higher than the temperatures based on H_2O+CO_2+NaCl fluid systematics in fluid inclusions in veins in granodiorite, in hydrous skarn minerals, and in sulfide replacement deposits north of Ruby Hill. It is also ~100°C greater than sulfide replacement deposit temperatures indicated by average compositions of arsenopyrite coexisting with sphalerite+pyrite. Emplacement of the Ruby Hill stock was virtually contemporaneous with the formation of contact zone skarns and sulfide replacement deposits, according to spatial relationships between granodiorite and skarns, radioisotopic ages, common mineralogy, sphalerite textures and compositions, and metal zoning presented earlier. Although temperature gradients around a cooling intrusion would be expected, the relatively large temperature discrepancies may be partially attributed to fluid inclusion entrapment temperature minima (insufficient pressure corrections), nonequilibrium among the hydrous skarn minerals tremolite and antigorite, or a combination of both.

Quartz porphyry

Secondary fluid inclusions in quartz phenocrysts in quartz porphyry consist of four phases, vapor, LH_2O, NaCl daughter mineral, and KCl daughter mineral, which occur in three inclusion types: $V+LH_2O$, $V+LH_2O+NaCl$, and $V+LH_2O+NaCl+KCl$. Unsaturated ($V+LH_2O$) inclusions homogenize to liquid over the temperature range 225 to 305°C and have no clear temperature modes. The homogenization temperature range of saturated inclusions ($V+LH_2O+NaCl$ and $V+LH_2O+NaCl+KCl$) is smaller at 245 to 275°C with a mean of ~252°C. NaCl dissolution temperatures correspond to 27.5 to 40 wt.% NaCl and average 36 wt.% NaCl, assuming vapor saturation and the absence of significant amounts of other components (e.g., $CaCl_2$). KCl dissolution temperatures correspond to 22 to 31 wt.% KCl and average 26 wt.% KCl, using the same assumptions. These average salt concentrations imply equilibrium temperatures of ~400°C (Sterner and others, 1988). Applying the same pressure corrections as above places the quartz porphyry-related hydrothermal fluids in the same range of entrapment temperatures as those of granodiorite vein, hydrous skarn, and most replacement deposits (~340 to 395°C) in the vicinity of Ruby Hill. Entrapment temperature similarities between fluid inclusions in quartz porphyry quartz phenocrysts and fluid inclusions in hydrothermal phases that resulted from intrusion of granodiorite suggests that the quartz porphyry inclusions are associated with the deposition of base metal sulfide minerals in quartz porphyry.

Veins south of Ruby Hill

Fluid inclusions in vein deposits in marble on Mineral Hill and in dolomite on Prospect Mountain (figs. 1, 2A, and 6) contain variable amounts of VH_2O and LH_2O. Some fluid inclusions are entirely filled with liquid and may be necked. Fluid inclusion homogenization temperatures in veins on Prospect Mountain (fig. 6; table 7B) range from 198 to 268°C, commonly with several modes per sample, perhaps a result of unrecognized necking. Because of the variable V/L within fluid inclusion populations and the absence of vein deformation, many of the veins can be interpreted to have precipitated on or near a boiling temperature-pressure curve and require no pressure correction. The veins on Prospect Mountain occur at elevations both above and below the elevations of replacement deposits and small pockets of skarn (fig. 6) that lie minimally hundreds of meters above the southern part of the Ruby Hill stock, based on magnetic contours (fig. 2B) and relatively abundant skarn encountered in the Prospect Mountain and Ruby Hill Tunnels (fig. 6). Postmineralization faulting (e.g., Silver Connor fault, fig. 6) may have juxtaposed some veins, replacement deposits, and skarn, but other veins are not significantly displaced relative to replacement deposits and skarn (e.g., Grant Mine, fig. 2A; Gordon Mine, fig. 6). Some of the vein deposits contain abundant stibnite, a mineral not found in replacement deposits or hydrous skarn (table 4), and gold appears to be rare in the veins. Vein ages relative to replacement deposits and skarn on Prospect Mountain cannot be determined, as no cross-cutting relationships were observed and no vein has been dated. However, the proximity of the veins to granodiorite and close juxtaposition of veins and higher temperature skarn and replacement deposits (fig. 6) suggests that the veins are not a distal part of zoned Cretaceous hydrothermal assemblages. Vein temperatures and the presence of stibnite, therefore, are permissive evidence that the veins belong to a separate and, given the absence of vein deformation, younger hydrothermal event.

Fluid Isotope Compositions

In order to determine the source(s) and evolution of fluids involved in alteration of granodiorite and sedimentary rocks of the contact zone, and in sulfide replacement and vein deposition, the isotopic compositions of hydrogen, oxygen, and carbon were analyzed in hydrothermal minerals and in water extracted from fluid inclusions in hydrothermal minerals. Oxygen isotope analyses of dolomite and siliciclastic rocks were also used to

clarify structural relationships on Ruby Hill, and to identify fluid circulation haloes around sulfide replacement deposits north of Ruby Hill. Isotope data, collected from dolomite, quartzite, shale, quartz, pyroxene, garnet, sphalerite, pyrite, galena, and pyrrhotite (tables 8 and 9), are plotted on δD, $\delta^{18}O$, and $\delta^{13}C$ axes and geologic sections (figs. 4, 10, 13, and 14). The measured and calculated deuterium and oxygen isotope water compositions require salinity and pressure corrections, which have only been partially quantified at elevated temperatures and pressures (e.g. Horita and others, 1993). At a depositional pressure of 1 kilobar a pressure correction of 10‰ was added to all deuterium measurements (Dreisner, 1997).

Chemical and isotopic disequilibrium between hydrous fluids that circulated in sedimentary wall rocks following intrusion of the Ruby Hill granodiorite stock resulted not only in the formation of skarn assemblages in the contact zone proximal to the stock, but also in oxygen isotope exchange between fluid water and wall rocks both proximally and distally to the stock. The large differences in oxygen isotope compositions between water involved in wall-rock alteration and sedimentary wall rocks that have not extensively exchanged oxygen with water were used to assess relative amounts of water circulation in dolomite adjacent to replacement deposits that is megascopically unaltered.

Prospect Mountain Quartzite, Pioche Shale, and Eldorado Dolomite that have not extensively exchanged oxygen with meteoric water have oxygen isotope compositions of ~13.7 to 19 ‰ (table 8; fig. 4). These isotopic compositions may not be representative of totally unaltered compositions, as unaltered Paleozoic carbonate rocks in the Great Basin may have somewhat heavier oxygen isotope compositions in the range 22 to 26 ‰ (e.g., lower parts of DDH 729, table 8). In the Eureka district, the lighter gray, coarser-grained, and textureless variety of Eldorado Dolomite, that which largely encloses the sulfide replacement deposits, was thought by Nolan (1962) to be a product of hydrothermal recrystallization. Therefore, some Eldorado Dolomite (and Hamburg Dolomite) may have undergone oxygen isotope exchange with water prior to intrusion of the Ruby Hill stock. However, regardless of dolomitization processes, oxygen isotope compositions of megascopically unaltered Eldorado Dolomite and Prospect Mountain Quartzite (DDH 728; fig. 2A, table 8) have a limited range of a few per mil. Average $\delta^{18}O$ compositions of Eldorado Dolomite in DDH 728, located 700 m northwest from known sulfide replacement deposits north of Ruby Hill, and in several surface samples (table 8) provide a regional datum against which extensive oxygen isotope exchange adjacent to the Ruby Hill stock and adjacent to replacement deposits can be measured.

Ruby Hill structure

Oxygen isotope analyses of Prospect Mountain Quartzite, Pioche Shale, and Eldorado Dolomite in the Granite Tunnel, which extends several hundred meters through skarn assemblages and granodiorite in Ruby Hill, show that significant oxygen isotope depletion (relative to less exchanged compositions) occurred in Prospect Mountain Quartzite, Pioche Shale, and granodiorite throughout the footwall of the Champion and Buckeye thrust faults (fig. 4). Less exchanged (and megascopically unaltered) Eldorado Dolomite at the hanging-wall contact of the Champion thrust fault supports the interpretation that Eldorado Dolomite was positioned adjacent to altered rocks of the contact zone after intrusion of the Ruby Hill stock. However, as replacement stopes in Eldorado Dolomite in the Granite Tunnel are approached, the oxygen isotopic composition of dolomite shows increasing depletion (fig. 4), a local characteristic of replacement deposits that is documented more fully below.

Isotope exchange haloes

Oxygen isotope analyses of dolomite in diamond drill core adjacent to sulfide replacement deposits north of the Ruby Hill fault reveal marked $\delta^{18}O$ depletions in Eldorado Dolomite over distances ranging from a few to more than 10 m from sulfide-dolomite contacts. Depletion is defined by $\delta^{18}O$ values lower than those of unmineralized Eldorado Dolomite, which is about 19±3‰ in DDH 728 (fig. 10; table 8). As noted above, oxygen isotope compositions of completely unexchanged Eldorado Dolomite, Hamburg Dolomite and other Cambrian sedimentary rocks may not have been fully determined, and a regional $\delta^{18}O$ datum has only been established for Eldorado Dolomite. Therefore, except in the cases of extreme depletion, $\delta^{18}O$ contours around sulfide replacement deposits in formations other than Eldorado Dolomite may not be completely analogous to those around replacement deposits in Eldorado Dolomite (figs. 10 and 13).

Depletion of up to 15‰ was measured in Eldorado Dolomite adjacent to sulfide replacement deposits (fig. 10). Most shells of depleted dolomite are approximately symmetrically distributed around sulfide replacement masses, although some are slightly offset, and several sulfide replacement masses show no wall-rock depletion (fig. 10). Asymmetrical depletion shells may have resulted from sulfide replacement that did not coincide with the geometric centers of replacement sites as determined by premineralization fracturing and permeability. Other depleted intervals unrelated to massive sulfides intersected by drill holes suggest the nearby presence of additional sulfide replacement masses. The absence of wall-rock depletion near the sulfide replacement in DDH 79-1 and the upper part of DDH 729 (fig. 10) may be attributable to the occurrence of this sulfide zone within, or suspected to be near, quartz porphyry which intrudes carbonate rocks above Eldorado Dolomite. Without full three-dimensional knowledge of sulfide replacement deposits and depletion haloes it is difficult to correlate all drill hole dolomite depletion with sulfide replacement deposits. The dimensions of Eureka district depletion haloes are considerably smaller that those reported by Kesler and others (1996), although differences may relate to dolomite versus limestone host rocks, the baseline applied for unexchanged carbonate rocks, and fluid pH.

Coupled with gold, silver, lead, and zinc abundances in drill core (described above), and regardless of symmetry, oxygen isotope depletion shells and metal enrichment in dolomite enclosing sulfide replacement deposits north of the Ruby Hill fault effectively, for exploration purposes, enlarge

Table 8. $\delta^{18}O$ (‰) in Eldorado (Ce), Geddes (Cg), and Hamburg (Ch) Dolomites and Prospect Mountain Quartzite (Cpm). Drill hole sample numbers consist of the diamond drill hole number and depth below the surface. Hole locations are shown in figures 2A and 3. Analyses are by Coastal Science Laboratories, Inc., Austin, TX.

DRILL HOLE SAMPLES

Sample Number	$\delta^{18}O_{SMOW}$‰	Lithology	Sample Number	$\delta^{18}O_{SMOW}$‰	Lithology	Sample Number	$\delta^{18}O_{SMOW}$‰	Lithology
725-2152	15.0	Ce	725-2554	12.0	Ce	729-2156	23.4	Ch
725-2169	16.6	Ce	725-2560	4.8; 5.1	Ce	729-2173	24.8	Ch
725-2187	19.6	Ce	725-2570	10.8	Cpm	729-2205	23.2	Ch
725-2205	17.0	Ce	725-2587	11.4	Cpm	79-1-1585	9.6	Cg
725-2223	18.4	Ce	728-980	15.8	Ce	79-1-1643	14.9	Cg
725-2239	17.7	Ce	728-1030	20.1	Ce	79-1-1690	23.2	Ce
725-2249	18.3	Ce	728-1090	18.6	Ce	79-1-1706	20.9	Ce
725-2258	18.0	Ce	728-1130	21.0; 20.8	Ce	79-1-1729	22.0	Ce
725-2268	20.4(2)	Ce	728-1196	20.6	Ce	79-1-1739	20.3	Ce
725-2277	19.3	Ce	728-1226	19.0	Ce	79-1-1750	19.0	Ce
725-2291	12.2	Ce	728-1283	20.0	Ce	79-1-1753	17.8	Ce
725-2302	17.7	Ce	728-1339	20.3	Ce	79-1-1760	17.6	Ce
725-2315	16.3	Ce	728-1394	17.2	Ce	79-1-1787	17.9	Ce
725-2328	11.9	Ce	728-1440	15.8	Ce	79-1-1821	18.4	Ce
725-2337	12.0	Ce	728-1489	18.5	Ce	79-1-1850	17.3	Ce
725-2347	16.0	Ce	728-1558	19.3	Ce	79-1-1899	18.8	Ce
725-2358	15.8	Ce	728-1610	19.3	Ce	79-1-1950	18.7	Ce
725-2368	9.4; 9.1	Ce	728 ave.	19.0	Ce	79-1-1999	18.8	Ce
725-2378	21.2	Ce				79-1-2052	18.3	Ce
725-2390	19.3	Ce	729-1633	17.0	Ch	79-1-2110	12.6	Ce
725-2400	20.5	Ce	729-1680	12.3	Ch	79-1-2123	20.2	Ce
725-2415	21.0	Ce	729-1735	17.2	Ch	79-1-2136	18.0	Ce
725-2430	19.6	Ce	729-1750	13.8	Ch	79-1-2146	19.2	Ce
725-2445	19.6	Ce	729-1765	18.3	Ch	79-1-2156.5	17.9	Ce
725-2458	12.3	Ce	729-1781	14.7	Ch	79-1-2160.5	13.7	Ce
725-2468	19.1	Ce	729-1795	14.5	Ch	79-1-2177	9.1	Ce
725-2477	15.4	Ce	729-1808	15.1	Ch	79-1-2204	11.9	Ce
725-2487	10.3	Ce	729-1820	12.4	Ch	79-1-2214	17.3	Ce
725-2496	8.8	Ce	729-1829	13.0	Ch	79-1-2226	17.0	Ce
725-2505	6.3; 6.5	Ce	729-1832	10.8	Ch	79-1-2232	16.3	Ce
725-2510	7.3	Ce	729-1835	11.3	Ch	79-1-2244	17.2	Ce
725-2531	13.5	Ce	729-1894	7.41[1]	Kqp	79-1-2278	16.6	Ce
725-2534	13.9(2)	Ce	729-1902	9.46[1]	Kqp	79-1-2338	15.7	Ce
725-2544	13.7	Ce	729-2095	22.4	Ch	79-1-2390	15.6	Ce

SURFACE SAMPLES

Sample Number	$\delta^{18}O_{SMOW}$‰	Location	Lithology
EUD91-15		Ratto Canyon haul road	Ce
SPP95-6	13.66	Prospect Peak, 30 m N of relay stations	Cpm
SPP95-7	16.27	SW ridge of Prospect Peak	Cpm
SPP95-8	18.64	Ratto Canyon haul road	Ce
SPP95-9	18.41	Ratto Canyon haul road	Ce
SPP95-10	12.07	Ruby Hill, centimeters from stope	Ce
SPP95-11	15.04	Ruby Hill, 60 cm from stope	Ce
SPP95-12	15.95	Ruby Hill, 3 m above upper Buckeye thrust	Ce

[1] Kqp altered to quartz, muscovite, kaolinite, pyrite

Table 9. A. Hydrogen, oxygen and carbon isotopic compositions of fluids in quartz, diopside, garnet, dolomite, and sulfide minerals, or calculated to be in equilibrium with silicate and carbonate minerals, from skarns and sulfide replacement deposits. B. Whole rock and mineral deuterium and oxygen isotope compositions of quartz porphyry, granodiorite, dolomite (Ꞓe), and quartzite (Ꞓpm), from surface and diamond drill hole core samples. Hole locations are shown on fig. 2. Some equilibrium temperatures are estimated (e) from similar samples. Fluid isotope samples consisted of up to several grams of mineral separate. Deuterium and fluid oxygen in sulfide minerals, and deuterium in silicate and carbonate minerals were analyzed in fluid extracted by vacuum crushing. qtz = quartz; musc = muscovite; kaol = kaolinite; py = pyrite

Sample no.	Mineral	$T_{H.}$ °$C_{f.i.}$	δD_{H2O}‰	$\delta^{18}O_{min.}$	$\delta^{18}O_{H20}$‰[5]	δ^{13}Cdolomite‰	Analyst
A. Fluids							
713-588	quartz	e345	-118	13.02	7.5		1
713-1269	quartz	355	-107	15.00	9.8		1
713-1287	quartz	e355	-111	13.42	8.2		1
713-2386	quartz	505	-91	17.97	15.7		1
722-346	quartz	e320	-116	16.24	9.9		1
718-608	diopside	e550	-95	10.72	11.4		1
720-1907.3	garnet	e375	-92	9.17	12.4		1
EDT92-04	quartz	e350	-107	17.48	12.1		1
EDT91-16	quartz	e350	-113[3]	13.77	8.4		1
721-442	dolomite	e355	-141	17.51	10.9	1.65	1
722-353	dolomite	e320	-121	19.63	12.0	-0.17	1
DH8-2125	dolomite	402	-139	14.50	9.0	0.11	1
729-3034	dolomite	485	-119	15.91	11.8	1.56	1
726-2278	sphalerite		-96		4.8[3]		1
726-2393	sphalerite		-94		5.0[3]		1
729-1897	sulfides	395-415[4]	-98		2.0[3]		1
729-3034	pyrite + sphalerite	e480[4]	-102		3.2[3]		1
79-1-2158	galena		-126		1.2[3]		1
79-1-1740	sphalerite	260-280[4]	-118		too small		1
EDT92-01	galena	e320[4]	-101		4.8		1
EDT92-06	galena	e350[4]	-109		4.3		1
718-529	pyrrhotite	520	-77		5.2		1
718-764	pyrrhotite	727	-86		4.7		1
718-991	pyrite	e700	-100		3.3		1
729-1896	sphalerite	395-415[4]	-84		2.6		1
B. Whole rock/mineral							
729-1894	quartz porphyry whole rock (qtz, musc, kaol, py)			7.41			1
729-1902	quartz porphyry whole rock (qtz, musc, kaol, py)			9.46			1
706-1385	granodiorite			13.22			1
713-1180	granodiorite (igneous biotite)		-73	7.26			1
713-1229	granodiorite			13.22			1
SPP95-8	dolomite (Ꞓe)			18.64		1.01	1
SPP95-9	dolomite (Ꞓe)			18.41		0.54	1
SPP95-10	dolomite (Ꞓe)			12.07		-1.17	1
SPP95-11	dolomite (Ꞓe)			15.04		0.59	1
SPP95-12	dolomite (Ꞓe)			15.95		0.21	1
EUD91-15	dolomite (Ꞓe)			14.4			2
79-1-2123	dolomite (Ꞓe)			20.2		-0.8	2
79-1-2146	dolomite (Ꞓe)			19.2		-0.3	2
79-1-2177	dolomite (Ꞓe)			9.1		-1.3, -1.1	2
79-1-2204	dolomite (Ꞓe)			11.9		1.0, 1.1	2
79-1-2232	dolomite (Ꞓe)			16.3		0.1	2
79-1-2278	dolomite (Ꞓe)			16.6		0.2	2
725-2400	dolomite (Ꞓe)			20.5		-0.1	2
725-2445	dolomite (Ꞓe)			19.6		0.0	2
725-2496	dolomite (Ꞓe)			8.8		-0.2	2
725-2510	dolomite (Ꞓe)			7.3		0.1	2
725-2534	dolomite (Ꞓe)			13.9		1.2	2
SPP95-6	quartzite (Ꞓpm)			13.66			1
SPP95-7	quartzite (Ꞓpm)			16.27			1

[1] Kevin Shelton, University of Missouri, Columbia
[2] Coastal Science Laboratories, Austin, Texas
[3] Small samples
[4] f.i. entrapment temperatures of coexisting dolomite, sphalerite, quartz

[5] Fractionation equations:

quartz-water	Matsuhisa and others (1979)
dolomite-water	Northrup and Clayton (1966)
garnet-water	Bottinga and Javoy (1973; 1975)
pyroxene-water	Bottinga and Javoy (1973; 1975)

the size of most known deposits by 3 to 4 volumes (figs. 10 and 13). Correlation of depletion and metal enrichment in drill holes where sulfide replacement was not encountered, for example, anomalous gold and zinc and $\delta^{18}O$ depletion 650 to 665 m (~2,160 to 2,200 feet) below the surface in DDH 726 (fig. 10), are a favorable indication of an nearby sulfide replacement. The near absence of metal anomalies and limited fluctuation of $\delta^{18}O$ in unmineralized DDH 728 (fig. 10) argue for further lateral investigation of all metal enrichment and oxygen isotope depletion in unmineralized dolomite.

Several percent of very fine-grained pyrite are locally disseminated in dolomite and limestone penetrated by diamond drill holes north of Ruby Hill. In drill core these pyritic intervals seldom exceed 1 m in thickness and contain subeconomic base and precious metals. A few are near sulfide replacement masses but many have no close spatial relationship to massive sulfide replacement deposits encountered in drill holes. The pyrite was apparently hydrothermally deposited because dolomite in which it is disseminated has been depleted in $\delta^{18}O$, similar to the margins of sulfide replacement masses. Three-dimensional exposure of pyritic dolomite during mining may reveal a spatial relation between the two sulfide occurrences.

Ore and alteration fluids

Deuterium, oxygen, and carbon isotope analyses of fluid inclusion waters and sulfide. silicate, and carbonate minerals in pyroxene+garnet skarn, hydrous skarn, veins in granodiorite and hydrous skarn, and sulfide replacement deposits reveal distinct groupings of waters (figs. 14A and 14B, table 9). Coarse-grained hydrothermal dolomite, intergrown with pyrite, galena, sphalerite, and other sulfides in replacement deposits in Eldorado Dolomite, precipitated from water having very low δD values, ~ <-110‰, and calculated $\delta^{18}O$ values that range from 9.0 to 12.0‰. Water that deposited pyrite, galena, and sphalerite in sulfide replacement deposits has a larger, mostly heavier range in δD, and significantly lower $\delta^{18}O$ values, clustered at 1 to 5‰, than hydrothermal dolomite. Quartz, pyroxene, and garnet waters from contact zone skarns have calculated $\delta^{18}O$ compositions of 7.5 to 15.7‰, similar to hydrothermal dolomite, and a δD range, -71 to -98‰, similar to that of replacement sulfide minerals. Fluid inclusion water in pyrrhotite from hydrous skarn is most enriched in δD (-67 and -76‰) and has $\delta^{18}O$ compositions similar to water in replacement sulfide minerals. Carbon isotope compositions of hydrothermal dolomite and Eldorado Dolomite, ranging from ~ 1.7 to -1.2‰ (table 9), were determined for ~ 25% as many dolomite samples as were used to construct the isotope depletion haloes around sulfide replacement deposits (table 8; fig. 10).

Based on the most depleted water deuterium detected in other Cretaceous magmatic-hydrothermal deposits (Osgood Mountain stock, Nevada, Taylor and O'Neil, 1977; Rochester district, Nevada, unpub. analyses), Cretaceous meteoric water in Nevada was characterized by $\delta D \approx -130 \pm 20$‰ and $\delta^{18}O \leq -16$‰. The low deuterium compositions of fluid inclusions in hydrothermal dolomite indicate that Cretaceous meteoric water circulated in the vicinity of the Ruby Hill stock (fig. 14A). Magmatic water, or water in equilibrium with magmas, is characterized by deuterium abundances greater than -80‰ (e.g., Taylor, 1979). Deuterium in skarn and replacement mineral fluid inclusions either exceeds -80‰ or is intermediate between -80‰ and

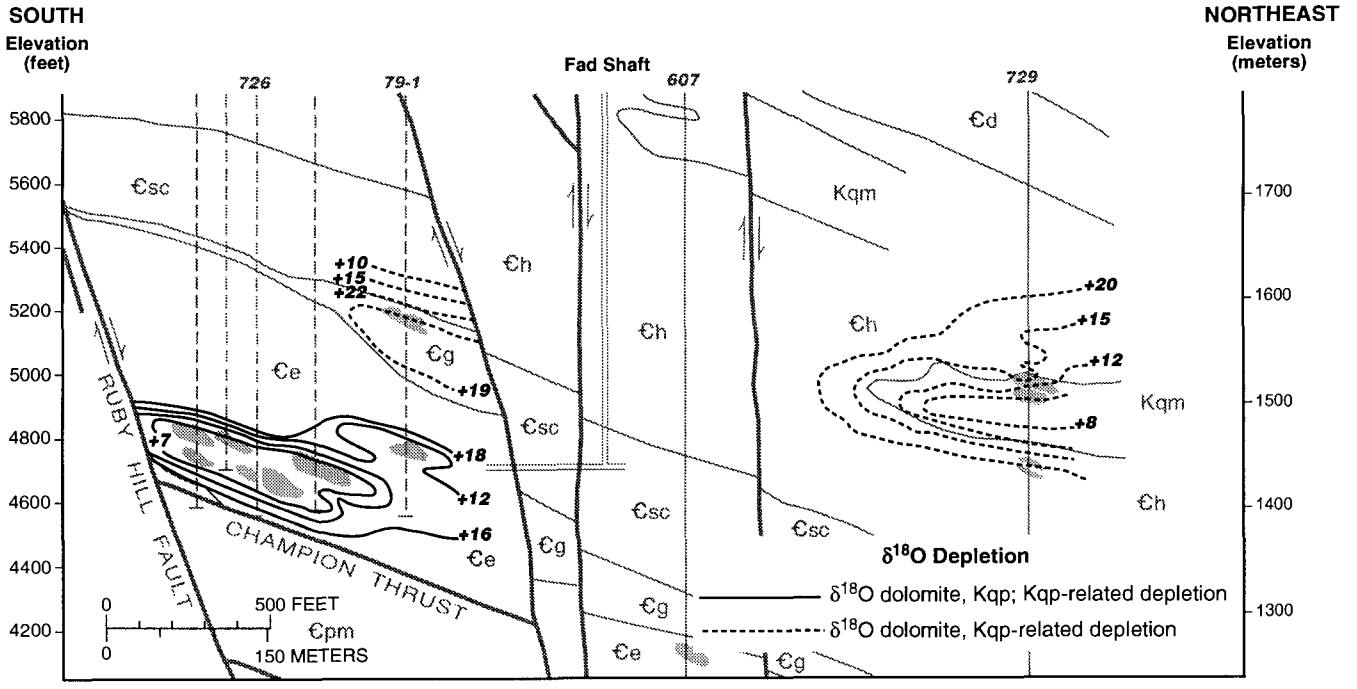

Figure 13. Part of section A-A' (fig. 3) on which whole-rock oxygen isotope compositions of Eldorado Dolomite (€e) and quartz porphyry (Kqp) near sulfide replacement deposits have been contoured. Thin dashed and solid lines are diamond drill holes. DDH locations are shown in figure 2A. Data are from table 8.

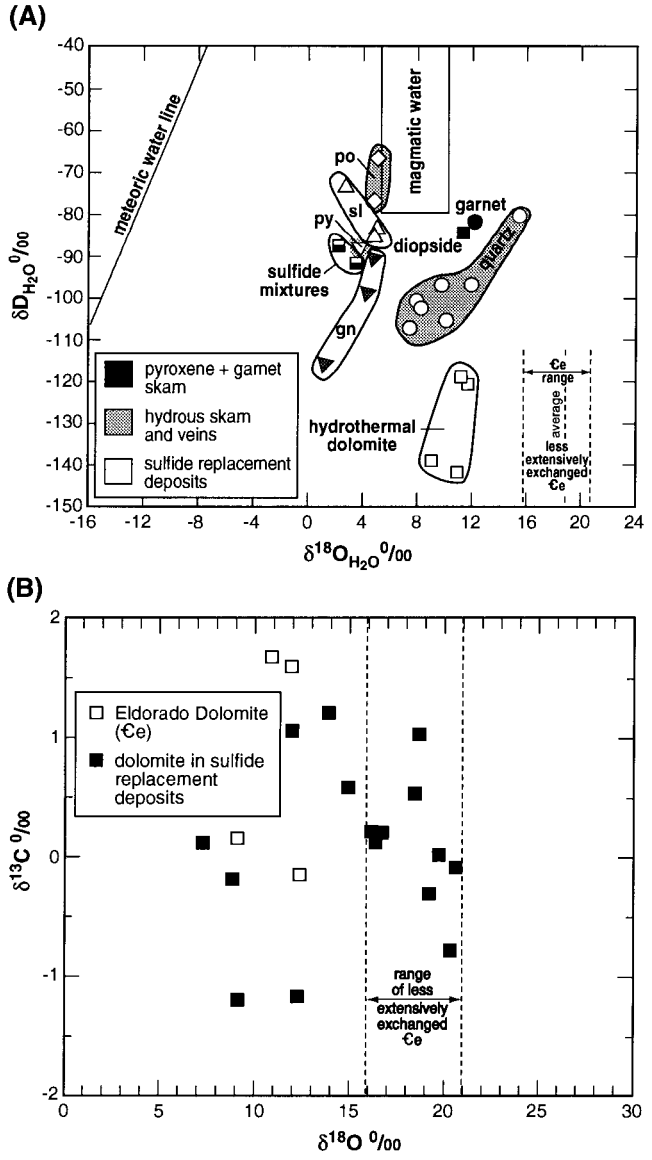

Figure 14. (A) Hydrogen isotope compositions (δD‰) of water extracted from fluid inclusions in sulfides, silicates and dolomite versus oxygen isotope compositions ($\delta^{18}O$‰) of water extracted from sulfides and calculated to be in equilibrium with silicates and dolomite, using the fractionation equations of Northrup and Clayton, (1966), Bottinga and Javoy (1973; 1975), Matsuhisa, and others, (1979), and those given in Field and Fifarek (1985). Data are from table 9, although a 10‰ pressure correction (1 kilobar; Dreisner, 1997) has been added to all deuterium values in this figure. po = pyrrhotite, sl = sphalerite, py = pyrite, gn = galena, and Ce is Eldorado Dolomite. The average and range in oxygen isotope compositions for Eldorado Dolomite (Ce) are from figure 10 and table 8. Magmatic water compositions are after Taylor (1979). (B) $\delta^{13}C$ and $\delta^{18}O$ compositions (in ‰) of Eldorado Dolomite (filled squares) and hydrothermal dolomite (open squares) in sulfide replacement deposits. Data are from table 9.

lower deuterium values indicative of Cretaceous meteoric water. Water $\delta^{18}O$, calculated to be in equilibrium with skarn and replacement minerals, exchanged variable amounts of oxygen with wall-rock dolomite, resulting in oxygen isotope compositions that are between the two oxygen sources. These water isotope compositions indicate that skarn and replacement minerals precipitated largely from mixtures of meteoric and magmatic waters.

Oxygen, deuterium, and carbon isotope compositions of hydrothermal dolomite and hydrothermal dolomite water permit interpretation of component sources. The range of oxygen isotope compositions of hydrothermal dolomite is similar to the range of the oxygen isotope analyses that define isotope depletion haloes (table 9; fig. 14B). None of the hydrothermal dolomite samples have $\delta^{18}O$ values that are the same as those of less extensively exchanged Eldorado Dolomite (fig. 10), and all were apparently recrystallized from Eldorado Dolomite ($\delta^{18}O \approx 19‰$) by Cretaceous meteoric water ($\delta^{18}O \leq 16‰$) that exchanged oxygen with Eldorado Dolomite. Based on deuterium abundances, little if any magmatic water was involved in the recrystallzation of hydrothermal dolomite. Carbon isotope compositions (~ 1.7 to -1.2‰, table 9; fig. 14B) are very similar to the range of carbon isotope compositions of marine carbonate rocks (1.65 to -1.3‰, Ohmoto and Rye, 1979). There is no significant difference between $\delta^{13}C$ in hydrothermal dolomites and wall-rock dolomite, nor is there a relationship apparent between $\delta^{13}C$ and degree of $\delta^{18}O$ exchange in hydrothermal dolomite. The absence of carbon isotope exchange indicates that carbon, in addition to much of the oxygen, in hydrothermal dolomite was derived from adjacent Eldorado Dolomite.

Pyrite, galena, and sphalerite in sulfide replacement deposits precipitated from water that is composed of isotopically heavier hydrogen and isotopically lighter oxygen than hydrothermal dolomite, and isotopically lighter oxygen than skarn waters (fig. 14A). Sulfide replacement water is a mixture of magmatic and meteoric waters, as most analyses plot between magmatic and partially exchanged Cretaceous meteoric water compositions. Silicate minerals in both pyroxene+garnet and hydrous skarn also precipitated from mixtures of magmatic water and partially exchanged Cretaceous meteoric water, the former indicated by δD that is heavier than Cretaceous meteoric water. The two analyzed skarn pyrrhotite samples precipitated largely from magmatic water (fig. 14A). However, oxygen in water from which diopside, garnet, and hydrous skarn quartz precipitated is less exchanged than sulfide replacement water, perhaps reflecting relatively limited water circulation in, and/or less oxygen isotope exchange with Hamburg Dolomite adjacent to the Ruby Hill stock.

It should be noted that differences in the isotopic composition of hydrothermal dolomite water, sulfide replacement water, and skarn water, which form the basis of the preceding water source interpretation, may have, in part, also resulted from: (1) isotopic modification of water during analysis, and (2) mixing of waters from several sources during analysis. Regarding explanation (1), during extraction of fluids from inclusions in sulfide minerals Whelan and Shaw (1987) found that organic contamination and absorption of freed water

on sulfide mineral surfaces resulted in negative shifts in deuterium compositions of up to tens of permils. If a negative deuterium shift occurred during analysis of Eureka district sulfide mineral inclusions, restored deuterium would coincide with magmatic water deuterium, reinforcing, if not increasing the proposed magmatic water contribution. However, no other studies of surface contamination and absorption of sulfide inclusion water have been published, and the accuracy of direct deuterium analyses of fluid inclusions in sulfide minerals cannot be fully addressed. However, the composition of skarn pyrrhotite water is more similar to sulfide replacement water than to skarn silicate water, suggesting either that all sulfide minerals were precipitated from isotopically distinct water, or that analytical procedures modified the water isotope compositions of all sulfide minerals.

Regarding explanation (2), fluid inclusion water, recovered by crushing milligrams of sample and vacuum extraction of released water, likely consists of waters from primary, pseudosecondary, and secondary inclusions, and, therefore, may represent uneven mixtures of several fluids (e.g., Foley and others, 1989). Visual confirmation of more than one fluid inclusion population in Eureka district replacement sulfide minerals is restricted to sphalerite which contains numerous planes of pseudosecondary inclusions, only a few of which are optically resolvable for microthermometry. The close paragenetic association of the pyrite and galena with sphalerite allows for those minerals to also contain pseudosecondary (and secondary) fluid inclusions. Mixing of inclusion waters of differing origin during bulk analysis should also have affected the isotopic compositions of waters extracted from skarn silicates, and hydrothermal dolomite during bulk analysis, as these minerals also contain pseudosecondary and secondary fluid inclusions. Although mixing of isotopically distinct fluids during analyses cannot be directly evaluated, the relatively tight grouping of analyses from related minerals suggests that such mixing was limited. Therefore, mixtures of magmatic water and meteoric waters having undergone variable amounts of oxygen isotope exchange with Eldorado Dolomite and Hamburg dolomite characterize the isotope composition of all hydrothermal minerals associated with emplacement of the Ruby Hill granodiorite stock. The relatively high fluid temperature and pressure estimates, and proximity of hydrothermal silicate and sulfide minerals to granodiorite support magmatic-meteoric water mixing.

Sulfur Isotopes

Isotopic compositions of sulfide minerals in sulfide replacement deposits, in hydrous skarn, in veins in dolomite, and in veins in granodiorite, were determined for calculation of depositional temperatures, as well as for assessment of possible sulfur provenances. Sulfur isotope compositions of pyrite, sphalerite, galena, and several other sulfide minerals range from 7.21 to 20.08 ‰ and average ~14‰ (table 10). Some sulfide minerals in replacement deposits appear to be texturally coeval and others, although paragenetically distinct, are intimately mixed in masses consisting of 50 to >75% sulfide minerals.

Temperatures

Temperature estimates from coexisting pairs of pyrite, sphalerite, and galena, calculated using the fractionation equations tabulated in Field and Fifarek (1985), span a considerable range. Some mineral pairs do not display clear textural equilibrium, rendering average temperatures meaningless, but modes at ~350 and 270°C may be indicative of equilibrium temperatures. Causes of the large temperature range and reversed fractionations include isotope disequilibrium, unrecognized sample impurity, and possibly, marginal oxidation of galena to sulfate. Isotopic disequilibrium among sulfide minerals may result when dissolved metal complex concentrations exceed that of H_2S, causing Rayleigh isotopic fractionation between early precipitating sulfides which consume most H_2S, such as pyrite in the sulfide replacement deposits, and late-forming sulfides which precipitate from a H_2S depleted fluid (Ohmoto and Goldhaber, 1997). The relatively narrow range in $\delta^{34}S$ of all sulfides in the district suggests, however, that sphalerite, galena, and pyrite all derived sulfur from the same source at approximately the same temperature. Sulfur isotope temperature modes are broadly similar to minimum entrapment temperatures determined from fluid inclusion microthermometry, and broadly similar to average temperatures derived from arsenopyrite+sphalerite+pyrite equilibria.

Provenance

All sulfide sulfur in Eureka district intrusions, hydrous skarn, quartz veins on Prospect Mountain and Mineral Hill, and replacement deposits is isotopically heavy, averaging 14.7‰ in granodiorite sulfide minerals, 14.0‰ in hydrous skarn sulfide minerals, 17.5‰ in quartz vein sulfide minerals, and 13.7‰ in replacement deposit sulfide minerals (table 10). Sulfide sulfur in disseminated gold deposits is also heavy and averages 14.4‰ (table 10). Eureka district sulfur is considerably heavier than sulfur normally associated with igneous sources, and is far less variable than biogenic sulfur (Ohmoto and Rye, 1979).

Isotopically heavy sulfide sulfur also occurs in the replacement and vein deposits at Pioche, Lincoln County, Nevada (Armstrong-Reinthal, 1983; unpub. data), 225 km (135 miles) southeast of Eureka, and in most metal deposits of all types in central and eastern Nevada Paleozoic rocks (Vikre, 1998). The Pioche deposits are in the same or stratigraphically equivalent lower Cambrian sedimentary rocks as the deposits at Eureka, and are, in part, spatially associated with Cretaceous intrusions. The existence of a regional source of heavy sulfur may be postulated for the ores of both districts, and for most deposits in central and eastern Nevada. Possible sources of heavy sulfur in pre-Cretaceous strata in eastern Nevada are: (1) sulfate-bearing evaporite beds, and (2) syngenetic or diagenetic sulfides in sedimentary rocks.

Gypsum beds occur in Permian rocks in southeastern Nevada (Tschanz and Pampeyan, 1970 ; Stewart, 1980) which, assuming the presence of a complete Paleozoic section, were

positioned at least 2,600 m (~8,600 feet) and as much as 5,900 m (~19,500 feet) over lower Cambrian rocks at Eureka (and Pioche) in the Cretaceous, a large vertical distance for access by hydrothermal fluids that mineralized only Early Cambrian rocks. Tectonic foreshortening, however, could have placed Permian gypsum and lower Cambrian rocks in closer proximity by the Cretaceous, and Permian gypsum cannot be ruled out as a source of the heavy sulfur at Eureka.

A more proximal source for heavy sulfur that requires no tectonism is disseminated pyrite in Late Proterozoic-Early Cambrian siliciclastic rocks which underlie most of central and eastern Great Basin, and which are up to thousands of meters thick in Nevada, southeastern California and western Utah (Stewart, 1980; Link and others, 1993). These rocks are generally deeply oxidized, but several oil exploration wells in Nevada penetrated sections of Pioche Shale, Prospect Mountain Quartzite, Cambrian quartzite and shale, and Late Proterozoic quartzites and shales hundreds to thousands of meters below the surface. The siliciclastic rocks ubiquitously contain small amounts of disseminated pyrite that have sulfur isotopic compositions of 11.44 to 34.10‰ (table 11), a range that encompasses nearly all sulfide sulfur isotope compositions from both the Eureka and Pioche districts.

Lead Isotopes

Lead isotope compositions were analyzed in several sulfide minerals in order to assess lead sources in Eureka district deposits. Lead isotope compositions were determined for galena, pyrite, and realgar from sulfide replacement and disseminated gold deposits, and for feldspars from Cretaceous and Oligocene igneous rocks (fig. 15, table 12). Four lead isotope compositions were also determined for disseminated pyrite, retrieved from exploratory oil wells in central and eastern Nevada, and western Utah, in Late Proterozoic-Early Cambrian shale and quartzite that underlie the Eureka district. The oil well leads were determined for the same samples in which the sulfur isotopes were analyzed (previous section).

As a group Eureka district sulfide and feldspar leads are highly radiogenic, with elevated values of ^{206}Pb, ^{207}Pb, and ^{208}Pb derived from radioactive decay of two uranium isotopes and thorium, respectively. Eureka leads are similar to, or slightly less uranogenic than, leads in pyrite from Late Proterozoic-Early Cambrian siliciclastic rocks. These siliciclastic rocks were never cratonized, which would have homogenized leads to less radiogenic isotopic compositions (Doe and Zartman, 1979). The uranogenic leads in Late Proterozoic-Early Cambrian rocks are, therefore, a likely source of most lead in the Eureka district deposits. A small portion of Eureka lead must have been derived from a less uranogenic source, most likely deeper crust. Thus, both the lead and sulfur isotope compositions of Eureka district ores permit derivation of the bulk of lead and sulfur at Eureka from immediately subjacent sedimentary rocks (Vikre, 1998).

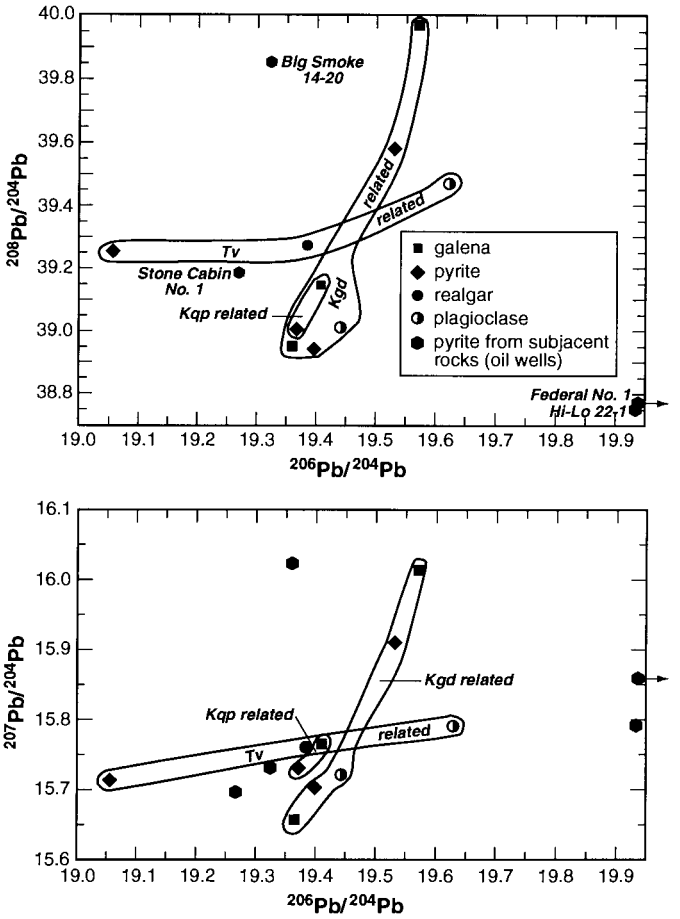

Figure 15. Lead isotope ratios of: plagioclase from Cretaceous granodiorite (Ruby Hill stock) and Oligocene quartz latite, sulfide minerals from deposits spatially related to Cretaceous granodiorite and to quartz porphyry, sulfide minerals from gold deposits considered Oligocene in age, and pyrite from subjacent Late Proterozoic-Early Cambrian siliciclastic rocks. Data are from table 12. Symbol size encompasses analytic error.

FORMATION OF SKARNS AND REPLACEMENT DEPOSITS

Eureka District

Based on the distribution and compositions of hydrothermal minerals (common sulfide minerals, sphalerite textures, sphalerite compositions, and arsenopyrite compositions), and depositional temperatures and pressures (similar fluid inclusion characteristics) of Eureka district deposits, the formation of pyroxene+garnet skarn, hydrous skarn, veins in granodiorite and hydrous skarn, and replacement deposits in Cambrian dolomites nearly synchronously followed intrusion of Cretaceous granodiorite. The presence of pyrrhotite inclusions in pyrite in sulfide replacement deposits supports formation of a sulfur-deficient iron sulfide assemblage in distal replacement sites concurrently with sulfidation of pyroxene+garnet±magnetite skarn, which is marked by

Table 10. Sulfur isotope compositions (‰) and temperatures (°C) of sulfide mineral pairs and barite from replacement deposits, skarn, quartz veins (on Prospect Mountain), veins in granodiorite, and gold deposits in the Eureka district.

Sample number	Location	Mineral	$\delta^{34}S$‰	T°C$\delta^{34}S$ py-sl	sl-gn	py-gn	Analyst
Replacement Deposits							
EUD91-11Bp	Fad Shaft	pyrite	15.2	952	348	376	2
EUD91-11Bs	stockpile	sphalerite	15.0				2
EUD91-11Bg		galena	12.8				2
EUD91-11A		sphalerite	14.95	572			1
EUD91-11A		pyrite	15.37				1
EUD91-11B		sphalerite	14.91	428	326	309	1
EUD91-11B		pyrite	15.52				1
EUD91-11B		galena	12.54				1
EUD91-11M		sphalerite	14.48		436		1
EUD91-11M		galena	12.79				1
726-2370	DDH in sulfide resource	pyrite	15.58	582	1086	804	2
726-2370	(Hole No.-depth below surface)	sphalerite	15.17				2
726-2370		galena	14.71				2
726-2393		pyrite	15.82	246	280	236	2
726-2393		sphalerite	14.71				2
726-2393		galena	11.93				2
729-1897		sphalerite	13.75	211	245	204	2
729-1897		galena	10.59				2
729-1897		pyrite	15.03				2
729-1903		galena	9.10		268		2
729-1903		sphalerite	12.00				2
729-3304		sphalerite	13.37	(inv.)[3]			1
729-3304		pyrite	12.70				1
729-3307		sphalerite	12.89	251			1
729-3307		pyrite	13.98				1
79-1-1748		sphalerite	13.63	275			1
79-1-1748		pyrite	14.63				1
79-1-2158		sphalerite	14.77	(inv.)[3]	283	(inv.)[3]	1
79-1-2158		pyrite	14.38				1
79-1-2158		galena	12.03				1
79-1-2190		pyrite	17.33	(inv.)[3]	237	(inv.)[3]	2
79-1-2190		sphalerite	14.94				2
79-1-2190		galena	11.67				2
79-1-2195		pyrite	14.54	(inv.)[3]	475	(inv.)[3]	1
79-1-2195		sphalerite	14.03				1
79-1-2195		galena	12.51				1
EUD91-16	Top of Ruby Hill	galena	11.75				2
		galena	12.14				1
EDT92-20sl	Richmond dump	sphalerite	15.60				1
-20py		pyrite	14.82	(inv.)[3]	363	(inv.)[3]	1
-20gn		galena	13.50				1
EDT92-21py	KK dump	pyrite	13.88			1003	1
-21gn		galena	13.26				1
EDT92-22py	Lizette dump	pyrite	15.57			424	1
-22gn		galena	13.49				1
EDT92-01	Diamond Tunnel dump	galena	14.39				1
EDT92-06	Prospect Mountain Tunnel dump	galena	17.16				1
EUD91-1Ap	T.L. Mine	pyrite	12.1				2
EUD91-1Ag	stockpile	galena	12.7			(inv.)[3]	2
EUD91-1Bg		galena	10.5(2)			327	2
EUD91-1Bp		pyrite	13.3				2
EUD91-1Cp		pyrite	13.7(2)	(inv.)[3]			2
EUD91-1Cs		sphalerite	14.6				2

Table 10. ***Continued***

Sample number	Location	Mineral	$\delta^{34}S‰$	T°Cδ^{34}S py-sl	T°Cδ^{34}S sl-gn	T°Cδ^{34}S py-gn	Analyst
EUD91-2Ap	Bullwacker	pyrite	14.3			476	2
EUD91-2Clg	Mine dumps	galena	12.5				2
EUD91-2C2g		galena	10.9			272	2
EUD91-3p	Holly Shaft dump	pyrite	16.9				2
Skarn							
713-222	DDH Ruby Hill	pyrite	14.89				2
713-558		pyrite	16.22				2
718-764py	DDH Phoenix Shale	pyrite	10.80				1
718-519		pyrite	14.72				2
718-519		molybdenite	13.20				2
718-764		pyrrhotite	11.26				1
720-1265	DDH Mineral Hill	barite	7.80				2
720-1947py		pyrite	15.09				1
720-1947		pyrite	14.58				2
720-1947		pyrrhotite	14.25				1
722-346	DDH Zulu Canyon	pyrite	14.85				2
724-761py	DDH Zulu Canyon	pyrite	13.96				1
724-761		pyrrhotite	14.89				1
724-793		pyrite	13.75				2
EUD91-7p	N. Mineral	pyrite	9.2				2
EUD91-7pl	Hill	pyrite	14.7				2
EDT93-1	Connolly Mine	barite	8.46				2
Veins							
EDT92-14	Wabash dump	pyrite	20.08				1
EDT92-16	Dead Broke dump	galena	17.07				1
EDT92-19	Silver Conner dump	silver sulfides	7.21				1
727-396	DDH Zulu Canyon	galena	14.48				2
EUD91-6t	Eureka Tunnel dump	tennantite	18.2(2)				2
Veins in Granodiorite							
713-1162	DDH Ruby Hill	pyrite	14.22				2
713-1287		pyrite	14.78				2
713-2386		pyrite	15.09				2
717-1938		pyrite	14.82				2
717-1938		molybdenite	14.63				2
Gold Deposits							
EUD91-10Dr	Windfall Mine	realgar	10.0; 8.7				2
EUD91-10Bp	Rustler Pit	pyrite	13.2				2
EUD91-12r	Ratto Canyon Mine	realgar	17.9; 19.5				2
EUD91-12p		pyrite	17.22				1

[1] Kevin Shelton, University of Missouri, Columbia
[2] Coastal Science Laboratories, Inc., Austin, Texas
[3] Inverse fractionation

Mean ± standard deviation

	py-sl	sl-gn	py-gn
T°Cδ^{34}S	366 ± 179	352 ± 119	371 ± 410
No. of pairs	8	11	10

Table 11. Sulfur isotope compositions (‰) of disseminated pyrite in Late Proterozoic-Early Cambrian sedimentary rocks encountered in oil wells in central and southern Nevada. Well cuttings and lithologic logs were provided by the Nevada Bureau of Mines and Geology.

Sample no: interval depth (ft.)	Operator and well name	Location	Lithology	$\delta^{34}S‰$
H-14-20:4810-4860	Harper Oil Co. Big Smoke No. 14-20	S20, T13N, R44E Nye County, Nevada	Cambrian quartzite and shale	19.62
H-14-20:5120-5210A	Harper Oil Co. Big Smoke No. 14-20	S20, T13N, R44E Nye County, Nevada	Cambrian quartzite and shale	34.10
H-14-20:5120-5210B	Harper Oil Co. Big Smoke No. 14-20	S20, T13N, R44E Nye County, Nevada	Cambrian quartzite and shale	31.08
HI-LO 22-1: 4800-5160	Maxus Exploration Co. Hi-Lo #22-1	S1, T7S, R50E Lincoln County, Nevada	Cambrian shale, phyllite, quartzite	16.25
Soda Springs Unit No. 1: 7970-8090	Marathon Oil Co. Soda Springs Unit No. 1	S15, T8N, R57E Nye County, Nevada	Late Proterozoic-Early Cambrian Prospect Mountain Quartzite	11.44
Kog No. 1: 6600-6760	Kamarden Oil and Gas Ltd. Kog No. 1	S22, T22S, R60E Clark County, Nevada	Cambrian Pioche Shale	31.44
Stone Cabin No. 1: 9630-9660	BTA Oil Producers Stone Cabin No. 1	S6, T5N, R48E Nye County, NV	Cambrian Gold Hill Formation	12.25
Federal No. 1: 8250-8550	Bridger Petroleum Company Federal No. 1	S15, T26S, R17W Beaver County, UT	Late Proterozoic-Early Cambrian Prospect Mountain Quartzite	22.20

Table 12. Lead isotopic compositions of galena, pyrite, realgar and plagioclase from sulfide replacement deposits, contact zone skarn, and granodiorite in the Eureka district, and of pyrite in Late Proterozoic-Early Cambrian siliciclastic rocks in oil exploration wells in Nevada and Utah. Analyses by S. Bowring (Cambridge, MA).

Sample no.	Location	Mineral	$^{206}Pb/^{204}Pb$	$^{207}Pb/^{204}Pb$	$^{208}Pb/^{204}Pb$
EUREKA DISTRICT					
713-1287p	DDH, Ruby Hill	pyrite	19.399	15.701	38.939
713-1430	DDH, Ruby Hill	plagioclase	19.442	15.722	39.008
720-1265g	DDH, Zulu Canyon	galena	19.570	16.012	39.967
726-2393	DDH, Fad Shaft	galena	19.363	15.653	38.952
726-2393p	DDH, Fad Shaft	pyrite	19.532	15.909	39.581
729-1897	DDH, N. of Fad Shaft	galena	19.410	15.766	39.146
729-1897p	DDH, N. of Fad Shaft	pyrite	19.370	15.730	39.002
EUD91-10p	Windfall Mine	pyrite	19.057	15.712	39.251
EUD91-12r	Ratto Canyon Mine	realgar	19.388	15.761	39.271
EUD91-13	Locan Shaft	plagioclase	19.625	15.789	39.465
OIL WELLS					
HI-LO 22-1	S1, T7S, R50E Lincoln County, NV	pyrite	19.932	15.793	38.749
Big Smoke 14-20	S20, T13N, R44E Nye County, NV	pyrite	19.321	15.731	38.852
USA 1-30	S30, T1N, R6E Lincoln County, NV	pyrite	18.556	15.616	39.136
Stone Cabin No. 1	S6, T5N, 48E Nye County, NV	pyrite	19.267	15.699	39.177
Federal No. 1	S15, T26S, R17W Beaver County, UT	pyrite	20.548	15.860	38.777

widespread replacement of magnetite by pyrrhotite. The post-pyrrhotite paragenetic position of sphalerite and galena in hydrous skarn and marble also correlates with sulfide mineral paragenesis in replacement deposits. Mineral assemblages and stabilities, coupled with fluid inclusion microthermometric measurements, indicate that pyroxene+garnet skarn proximal to the Ruby Hill granodiorite stock formed at ~470°C, at ~ 1 to 1.6 kilobars of pressure, and at relatively low XCO_2, as dolomite was unstable relative to pyroxene. Hydrous skarn, characterized by quartz, amphibole, sulfide minerals, serpentine, carbonate minerals, and chlorite, resulted from alteration of pyroxene, garnet, and dolomite at temperatures of ~400°C, and by aqueous fluid containing similar XCO_2, according to fluid inclusion microthermometry. Fluid inclusion microthermometric, sulfur isotope, and sulfide mineral compositional data show that distal replacement deposits composed mainly of pyrite, sphalerite, and galena formed at sub-400°C temperatures, and with fluid XCO_2 and salinities comparable to those of hydrous skarn fluid. Temperature (and pressure) gradients of similar magnitude have been measured in other intrusion-related, carbonate rock-hosted hydrothermal systems (Sawkins, 1964; Meinert, 1987; 1993; Newberry and others, 1991). Based on stable isotope analyses of fluid inclusion waters and host minerals, hydrous skarn and sulfide replacement minerals were deposited from variable mixtures of magmatic and Cretaceous meteoric water that partially exchanged oxygen with Cambrian dolomites (and also created oxygen isotope depletion shells around the replacement deposits), possibly under contrasting hydrologic permeabilities. Therefore, a temperature gradient coupled with fluid mixing were apparently the major physical controls of skarn and sulfide mineral replacement of dolomite at Eureka.

A semiquantitative reconstruction of the Eureka district (fig. 16) summarizes igneous and hydrothermal events that occurred during the mid-Cretaceous. These events are based on structural and stratigraphic interpretations, radioisotopic ages, stable isotope, igneous, and hydrothermal mineral compositions and stabilities, and fluid inclusion microthermometry. At about 107 Ma granodiorite and quartz porphyry were emplaced into deformed lower Paleozoic carbonate rocks, minimally about 4 to 6 km beneath the surface. At ancestral Ruby Hill, granodiorite intruded a recumbent synform of Cambrian dolomites and siliciclastic rocks, elevating local meteoric water to temperatures exceeding 400°C. This meteoric water, combined with increments of magmatic water, altered Hamburg Dolomite adjacent to granodiorite to pyroxene+garnet and hydrous skarn mineral assemblages. It also circulated in Eldorado Dolomite distal to granodiorite north of ancestral Ruby Hill and recrystalized dolomite to coarse-grained hydrothermal dolomite in the structural sites of replacement deposits. Subsequently, a mixture of magmatic and meteoric water circulated through the replacement sites, resulting in replacement of hydrothermal dolomite and Eldorado Dolomite by economic quantities of base and precious metal sulfide minerals. Following the intrusive and hydrothermal events the sulfide replacement deposits were thrust hundreds to thousands of meters southward along subparallel low-angle faults, juxtaposing them apically to the granodiorite intrusion. A series of high-angle, normal faults, probably Miocene and younger, displaced the sulfide replacement deposits tens to hundreds of meters down to the north, and replacement deposits nearest the surface, those mined at Ruby Hill, were oxidized during late Tertiary erosion.

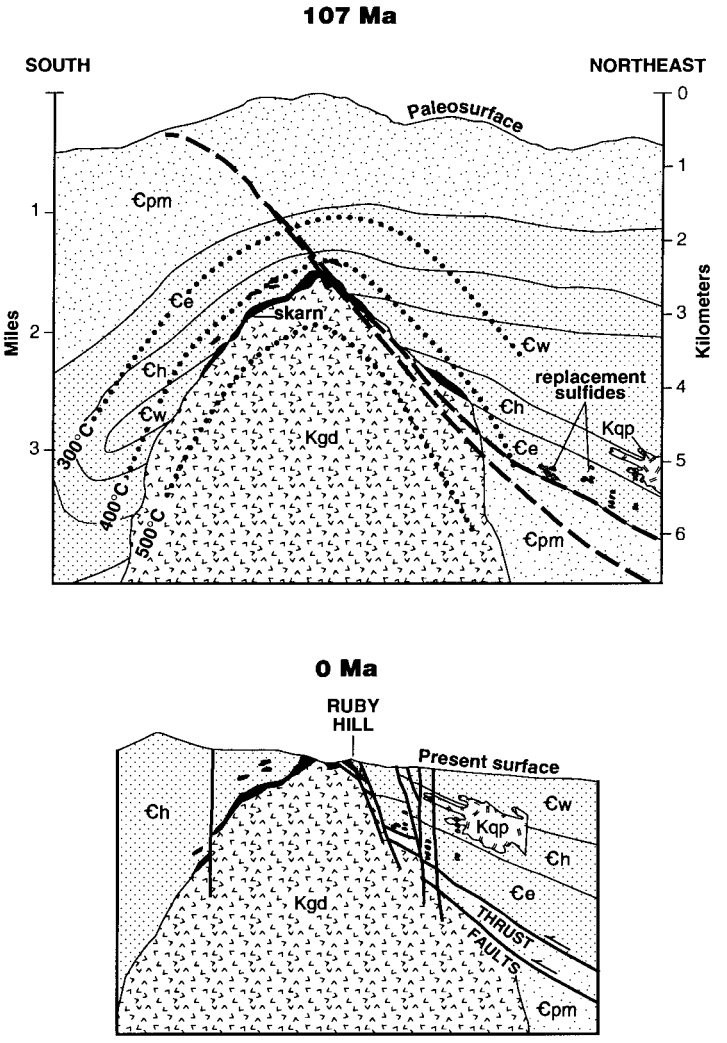

Figure 16. Section A-A' (fig. 3) showing proposed Cretaceous igneous and hydrothermal events in the vicinity of ancestral Ruby Hill (top), and part of section A-A' showing Ruby Hill today (bottom). Positions of post-intrusion low-angle thrust faults are dashed (top section). The disparity in thickness of Hamburg Dolomite (Ch) between the two sections is caused by the present (0 Ma) steep northerly dip that was omitted from the mid-Cretaceous section in order to emphasize the pre-intrusion recumbent synform of Cambrian carbonate rocks (107 Ma). Scale of lower section is the same as the upper section.

Regional Comparison

Such characteristics of carbonate rock-hosted replacement deposits as age, igneous affiliation, metal grades, metal ratios, and isotopic compositions of sulfides and fluid inclusion waters vary among individual deposits, whereas structure, geometry of ore bodies, alteration, and Paleozoic host rock compositions are more common characteristics (Megaw and others, 1988; Titley, 1993). Regional variations in lead grades and lead isotope compositions among replacement deposits in the North American cordillera show that the deposits are geographically distinguishable (fig. 17). Deposits in the Great Basin of the western United States (Nevada, western Utah, and southeastern California), including the Eureka district, are rich in lead and their leads are relatively uranogenic. Deposits in Colorado, Arizona, and Mexico have lower average lead grades and tend to be rich in zinc. Arizona deposits are generally lead deficient (but copper rich), and their leads are, in part, distinctly non-radiogenic. Although lead grades may be biased by the inclusion of productions records of oxidized ores (lead enrichment), many major carbonate replacement deposits in the North American cordillera can be characterized on the basis of $^{207}Pb/^{206}Pb$ (fig. 17). Regional contrasts among lead grades and lead isotope compositions apparently relate to age and composition of underlying Precambrian basement (Zartman, 1974; Wooden and others, 1988; Vikre, 1998).

Based on sulfur and lead isotope compositions a permissive source for the sulfur and lead acquired by the Cretaceous intrusions at Eureka are subjacent Late Proterozoic-Early Cambrian siliciclastic rocks. The Eureka district, as well as other skarn and replacement deposits in Paleozoic rocks in the central, eastern, and southern Great Basin, overlie extended cratonic basement as bounded by the ^{706}Sr line, and few significant carbonate replacement districts overlie crust composed of accreted terranes or island arcs to the west. The thick sequence of Late Proterozoic siliciclastic rocks that overlies crystalline basement of the craton must be considered as a source for lead and sulfur in other eastern Nevada, western Utah, and southwestern California metal deposits (Vikre, 1998).

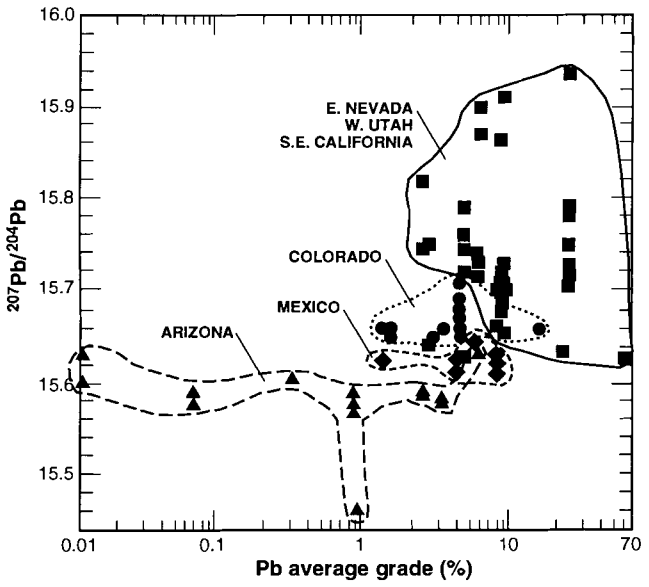

Figure 17. Average lead grade versus $^{207}Pb/^{204}Pb$ in carbonate rock-hosted replacement deposits in the North American cordillera. Sources of data: Delevaux and others (1966), Stacey and others (1968), Rye and others (1974), Zartman (1974), Stacey and Zartman (1978), Cumming and others (1979), Titley (1993), Bouse (1995), J. Tingley (personal commun., 1996), and unpublished data.

ACKNOWLEDGMENTS

This research could not have been undertaken and completed without the compliance and assistance of the following companies and individuals: ASARCO, Incorporated, Quentin J. Browne, Ruby Hill Mining Company, Homestake Mining Company, Bill Stanley, Bill Wright, Sam Monteleone, and Tom Johnston. Significant improvements to earlier manuscript drafts were provided by M.D. Barton, M.T. Einaudi, B.J. Maher, J. Margolis, J. Muntean, T.B. Thompson, and W. Wright.

REFERENCES

Armstrong, R.L., 1970. K-Ar dating using neutron activation for Ar analysis: comparison with isotope dilution Ar analysis: Geochimica et Cosmochimica Acta, v. 34, p. 233–236.

Armstrong-Reinthal, C.A., 1983, A stable isotope, petrographic, and fluid inclusion investigation of the Pioche mining district, Nevada [M.S. thesis]: University of Wisconsin-Madison, 166 p.

Barton, P.B., and Skinner, B.J., 1979, Sulfide mineral stabilities, *in* Barnes, H.L., ed., Geochemistry of Hydrothermal Ore Deposits, 2nd edition: John Wiley and Sons, New York, p. 278–403.

Binyon, E.O., 1946, Exploration of the gold, silver, lead, and zinc properties, Eureka Corporation, Eureka Co., Nev.: U.S. Bureau of Mines Report of Investigation 3949, 18 p.

Blake, M.C., McKee, E.H., Marvin, R.F., Silberman, M.L., and Nolan, T.B., 1975, The Oligocene volcanic center at Eureka, Nevada: U.S. Geological Survey Journal of Research, v. 3, no. 5, p. 605–612.

Blundy, J.D., and Holland, T.J.B., 1990, Calcic amphibole equilibria and a new amphibole-plagioclase geothermometer: Contributions to Mineralogy and Petrology, v. 104, p. 208–224.

Bodnar, R.J., Reynolds, T.J., and Kuehn, C.A., 1985, Fluid inclusion systematics in epithermal systems: *in* Berger, B.R. and Bethke, P.M. (eds.), Geology and Geochemistry of Epithermal Systems: Reviews in Economic Geology, v. 2, p. 73–97.

Bottinga, Y., and Javoy, M., 1973, Comments on oxygen isotope geothermometry: Earth and Planetary Science Letters, v. 20, p. 250–265.

Bottinga, Y., and Javoy, M., 1975, Oxygen isotope partitioning among minerals in igneous and metamorphic rocks: Reviews in Geophysics and Space Physics, v. 13, p. 401–418.

Bouse, R.M., 1995, Pb isotopic compositions of ore deposits and their host rocks in Arizona: implications for the crustal inheritance of metals [Ph.D. dissertation]: University of Arizona, 205p.

Bowers, T.S., and Helgeson, H.C., 1983, Calculation of the thermodynamic and geochemical consequences of nonideal mixing in the system H_2O-CO_2-NaCl on phase relations in geologic systems: metamorphic equilibria at high pressures and temperatures: American Mineralogist, v. 68, p. 1059–1075.

Collins, P.L.F., 1979, Gas hydrates in CO_2-bearing fluid inclusions and the use of freezing data for estimation of salinity: Economic Geology, v. 74, p. 1435–1444

Curtis, J.S., 1884, Silver-lead deposits of Eureka, Nev.: U.S. Geological Survey Monograph 7, 200 p.

Cumming, G.L., Kesler, S.E., and Kristic, D., 1979, Isotopic composition of lead in Mexican mineral deposits: Economic Geology, v. 74, p. 1395–1407.

Delevaux, M.H., Pierce, A.P., and Antweiler, J.C., 1966, New isotopic measurements of Colorado ore leads: U.S. Geological Survey Professional Paper 550C, p. C178–C186.

Dilles, P.A., Wright, W.A., Monteleone, S.E., Russell, K.D., Marlowe, K.E., Wood, R.A., and Margolis, J., 1996, The geology of the West Archimedes deposit: a new gold discovery in the Eureka mining district, Eureka County, Nevada: Geological Society of Nevada, Geology and ore deposits of the American Cordillera, Symposium Proceedings, p. 159–171.

Doe, B.R., and Zartman, R.E., 1979, Plumbotectonics, the Phanerozoic, *in* Barnes, H.L., ed., Geochemistry of Hydrothermal Ore Deposits, second edition: John Wiley and Sons, New York, p. 22–70.

Dreisner, T., 1997, The effect of pressure on deuterium-hydrogen fractionation in high-temperature water: Science, v. 277, p. 791–794.

Einaudi, M.T., Meinert, L.D., and Newberry, R.J., 1981, Skarn deposits: Economic Geology Seventy-Fifth Anniversary Volume, 1905-1980, p. 317–391.

Field, C.W., and Fifarek, R.H., 1985, Light stable-isotope systematics in the epithermal environment: *in* Berger, B.R., and Bethke, P.M., Geology and Geochemistry of Epithermal Systems: Reviews in Economic Geology, v. 2, p. 99–128.

Foley, N.K., Bethke, P.M., and Rye, R.O., 1989, A reinterpretation of the δDH_2O of inclusion fluids in contemporaneous quartz and sphalerite, Creede mining district, Colorado: a generic problem for shallow orebodies?: Economic Geology, v. 84, p. 1966–1977.

Hague, A., 1883, Abstract of report on the geology of the Eureka district, Nevada: U.S. Geological Survey 3rd Annual Report, p. 237–272.

Hague, A., 1892, Geology of the Eureka district, Nev., U.S. Geological Survey Monograph 20 (with atlas), 419 p.

Hanson, R.B., 1995, The hydrodynamics of contact metamorphism: Geological Society of America Bulletin, v. 107, p. 595–611.

Hemley, J.J., Cygan, G.L., and d'Angelo, W.M., 1986, Effect of pressure on ore mineral solubilities under hydrothermal conditions: Geology, v. 14, p. 377–379.

Horita, J., Cole, D.R., and Wesolowski, D.J., 1993, The activity-composition relationship of oxygen and hydrogen isotopes in aqueous salt solutions: II. vapor-liquid water equilibrium of mixed salt solutions from 50 to 100°C and geochemical implications: Geochimica et Cosmochimica Acta, v. 57, p. 4703–4711.

Johnson, A. C., 1958, Shaft-sinking methods and costs at the T.L. shaft, Eureka Corp., Ltd., Nev.: U.S. Bureau of Mines Information Circular 7835, 25 p.

Kesler, S.E., Vennemann, T.W., Vasquez, R., Stenger, D.P., and Fredrickson, G.C., 1996, Application of large-scale oxygen isotope haloes to exploration for chimney-manto Pb-Zn-Cu-Ag deposits, *in* Coyner, A.R., and Fahey, P.L., eds., Geology and ore deposits of the American cordillera: Geological Society of Nevada Symposium Proceedings, p. 1383–1396.

King, C.E., 1878, Systematic geology: U.S. Geological Exploration of the 40th Parallel, U.S. Government Printing Office, Washington, D.C., v. 1., 803 p.

Langlois, J.D., 1971, Hydrothermal alteration of intrusive igneous rocks in the Eureka mining district, Nevada [M.S. thesis]: University of Arizona, 113 p.

LeMaitre, R.W., ed., 1989, A classification of igneous rocks and glossary of terms: Blackwell Scientific Publications, London, 191 p.

Link, P.K., Christie-Blick, N., Stewart, J.H., Miller, J.M.G., Devlin, W.J., and Levy, M., 1993, Late Proterozoic strata of the United States Cordillera, *in* The Geology of North America, Volume C-2, Precambrian: Conterminous U.S.: The Geological Society of America, p. 536–558.

Love, W.H., 1966, The Ruby Hill project, Eureka, Nevada: Nevada Bureau of Mines and Geology Report 13, p. 85–107.

Marvin, R.F., and Cole, J.C., 1978, Radiometric ages; compilation A, U.S. Geological Survey: Isochron/West, no. 22, p. 3–16.

Matsuhisa, Y., Goldsmith, J.R., and Clayton, R.N., 1979, Oxygen isotope fractionation in the system quartz-albite-anorthite-water: Geochimica et Cosmochimica Acta, v. 43, p. 1131–1140.

Maxwell, J.C., and Verall, P., 1953, Expansion and increase in permeability of carbonate rocks on heating: American Geophysical Union Transactions. v. 34, p. 101–106.

Megaw, P.K.M., Ruiz, J., and Titley, S.R., 1988, High-temperature, carbonate-hosted Ag-Pb-Zn(Cu) deposits of northern Mexico: Economic Geology, v. 83, p. 1856–1885.

Meinert, L.D., 1987, Skarn zonation and fluid evolution in the Groundhog Mine, Central mining district, New Mexico: Economic Geology, v. 82, p. 523–545.

Meinert, L.D., 1993, Igneous petrogenesis and skarn deposits: *in* Kirkham, R.V., and others, Mineral Deposit Modeling: Geological Association of Canada, Special Paper 40, p. 569–583.

Miesch, A.T., and Nolan, T.B., 1958, Geochemical prospecting studies in the Bullwacker mine area, Eureka district, Nevada: U.S. Geological Survey Bulletin 1000-H, p. 397–408.

Murowchick, J.B., 1992, Marcasite inversion and the petrographic determination of pyrite ancestry: Economic Geology, v. 87, p.1141–1152.

Newberry, R.J., Einaudi, M.T., and Eastman, H.S., 1991, Zoning and genesis of the Darwin Pb-Zn-Ag skarn deposit, California; a reinterpretation based on new data: Economic Geology, v. 86, p. 960–982.

Nolan, T.B., 1962, The Eureka mining district, Nevada: U.S. Geological Survey Professional Paper 406, 78 p.

Nolan, T.B., and Hunt, R.N., 1968, The Eureka mining district, Nevada; *in* Ridge, J.D., ed., Ore deposits of the United States: American Institute of Mining, Metallurgy and Petroleum Engineers, Inc., New York, p. 966–991.

Nolan, T.B., Merriam, C.W., and Blake, M.C., Jr., 1974, Geologic map of the Pinto Summit Quadrangle, Eureka and White Pine Counties, Nevada: U.S. Geological Survey Miscellaneous Geological Investigations Map I-793.

Nolan, T.B., Merriam, C.W., and Brew, D.A., 1971, Geologic map of the Eureka quadrangle, Eureka and White Pine Counties, Nevada: U.S. Geological Survey Miscellaneous Geological Investigations Map I-612.

Nolan, T.B., Merriam, C.W., and Williams, J.S., 1956, The stratigraphic section in the vicinity of Eureka, Nevada: U.S. Geological Survey Professional Paper 276, 77 p.

Northrup, D.A., and Clayton, R.N., 1966, Oxygen isotope fractionations in systems containing dolomite: Journal of Geology, v. 74, p. 174–196.

Ohmoto, H., and Goldhaber, M.B., 1997, Isotopes of sulfur and carbon, *in* Barnes, H.L., ed., Geochemistry of Hydrothermal Ore Deposits, third edition: John Wiley and Sons, New York, p. 517–612.

Ohmoto, H., and Rye, R.O., 1979, Isotopes of sulfur and carbon, *in* Barnes, H.L., ed., Geochemistry of Hydrothermal Ore Deposits, 2nd edition: John Wiley and Sons, New York, p. 509–567.

Potter, R.W., Clynne, M.A., and Brown, D.L., 1978, Freezing point depressions of aqueous sodium chloride solutions: Economic Geology, v. 73, p. 284–285.

Rye, R.O., Doe, B.R., and Wells, J.D., 1974, Stable isotope and lead isotope study of the Cortez, Nevada, gold deposit and surrounding area: U.S. Geological Survey Journal of Research, v. 2, no. 1, p. 13–23.

Sawkins, F.J., 1964, Lead-zinc ore deposition in the light of fluid inclusions, Providencia, Zacatecas, Mexico: Economic Geology, v. 69, p. 883–919.

Schwartz, M.O., 1989, Determining phase volumes of mixed CO_2-H_2O inclusions using microthermometric measurements: Mineralium Deposita, v. 24, p. 43–47.

Scott, S.D., 1983, Chemical behavior of sphalerite and arsenopyrite in hydrothermal and metamorphic environments: Mineralogical Magazine, v. 47, p. 427–435.

Sharp, W., 1947, The story of Eureka: American Institute of Mining and Metallurgical Engineers Technical Publication 2196, 12 p.

Silberman, M.L., and McKee. E.H., 1971, K-Ar ages of granitic plutons in north-central Nevada: Isochron/West, no. 1, p. 15–32.

Stacey, J.S., and Zartman, R.E., 1978, A lead and strontium isotopic study of igneous rocks and ores from the Gold Hill mining district, Utah: Utah Geology, v. 5, no. 1, p. 1–15.

Stacey, J.S., Zartman, R.E., and N'Komo, I.T., 1968, A lead isotope study of galenas and selected feldspars from mining districts in Utah: Economic Geology, v. 63, p. 796–814.

Sterner, S.M., Hall, D.L., and Bodnar, R.J., 1988, Synthetic fluid inclusions. V. Solubility relations in the system NaCl-KCl-H_2O under vapor-saturated conditions: Geochimica et Cosmochimica Acta, v. 52, p. 989–1005.

Stewart, J.H., 1980, Geology of Nevada: Nevada Bureau of Mines and Geology Special Publication 4, 136 p.

Taylor, B.E., and O'Neil, J.R., 1977, Stable isotope studies of metasomatic Ca-Fe-Al-Si skarns and associated metamorphic and igneous rocks, Osgood Mountains, Nevada: Contributions to Mineralogy and Petrology, v. 63, p. 1–49.

Taylor, H.P., Jr., 1979, Oxygen and hydrogen isotope relationships in hydrothermal mineral deposits, *in* Barnes, H.L., ed., Geochemistry of Hydrothermal Ore Deposits, second edition: John Wiley and Sons, New York, p. 236–277.

Thompson, T.B., and Arehart, G.B., 1990, Geology and origin of ore deposits in the Leadville district, Colorado: Part 1. Geologic studies of orebodies and wall rocks, *in* Beaty, D.W., Landis, G.P., and Thompson, T.B., eds., Carbonate-hosted sulfide deposits of the central Colorado mineral belt: Economic Geology Monograph 7, p.130–155.

Titley, S.R., 1993, Characteristics of high-temperature, carbonate-hosted massive sulphide ores in the United States, Mexico and Peru, *in* Kirkham, R.V., and others, Mineral Deposit Modeling: Geological Association of Canada Special Paper 40, p. 585–614.

Toulmin, P., III, and Barton, P.B., Jr., 1964, A thermodynamic study of pyrite and pyrrhotite: Geochimica et Cosmochimica Acta, v. 28, p. 641–671.

Tschanz, C.M., and Pampeyan, E.H., 1970, Geology and mineral deposits of Lincoln County, Nevada: Nevada Bureau of Mines and Geology Bulletin 73, 188 p.

Vanderburg, W.O., 1938, Reconnaissance of mining districts in Eureka County, Nev.: U.S. Bureau of Mines Information Circular 7022, 66 p.

Vikre, P.G., 1998, Subjacent crustal sources of sulfur and lead in central and eastern Great Basin metal deposits: submitted for publication.

Walcott, C.D., 1884, Paleontology of the Eureka district: U.S. Geological Survey Monograph 8, 298 p.

Wheeler, H.E., and Lemmon, D.M., 1939, Cambrian formations of the Eureka and Pioche districts, Nevada: Nevada Bureau of Mines and Geology Bulletin 31, 60 p.

Whelan, J.F., and Shaw, C.A., 1987, Reliability of δD and $\delta^{18}O$ values of inclusion fluids from sulfides: U.S. Geological Survey Open-File Report 87-138, 10 p.

Wooden, J.L., Stacey, J.S., Howard, K.A., Doe, B.R., and Miller, D.M., 1988, Pb isotopic evidence for the formation of Proterozoic crust in the southwestern United States, *in* Ernst, W.G., ed., Metamorphism and crustal evolution of the western United States, Rubey Volume VII: Prentice-Hall. Englewood Cliffs, New Jersey, p. 68–86.

Zartman, R.E., 1974, Lead isotopic provinces in the cordillera of the western United States and their geologic significance: Economic Geology, v. 69, p. 792–805.

APPENDIX

Major oxide compositions in weight percent of Eldorado Dolomite and Limestone, Hamburg Dolomite (Wheeler and Lemmon, 1939), and the Ruby Hill granodiorite stock (analyses by XRL, Mississauga, Ontario).

	Oxide	Weight Percent
Eldorado Dolomite (4)		
(DDH A, FAD Shaft area)	$CaCO_3$	55.08–57.10
	$MgCO_3$	39.50–42.07
	Al_2O_3	0.13–0.30
	Fe_2O_3	0.05–0.50
	insol.	0.22–0.76
Eldorado Limestone (1)	$CaCO_3$	95.78
(DDH A, FAD Shaft area)	$MgCO_3$	2.03
	Al_2O_3	0.14
	Fe_2O_3	0.02
	insol.	0.20
Hamburg Dolomite (2)	$CaCO_3$	55.09–56.00
(Windfall Canyon)	$MgCO_3$	41.07–43.22
	Al_2O_3	0.17–0.19
	Fe_2O_3	0.03
	insol.	0.02–0.78
stoichiometric dolomite	$CaCO_3$	54.35
$CaMg(CO_3)_2$	$MgCO_3$	45.65

Ruby Hill granodiorite	Oxide	Weight Percent	
		EUD91-4 (Rogers Tunnel)	713-1180 (DDH 713, Granite Tunnel)
	SiO_2	62.10	65.10
	TiO_2	0.45	0.62
	Al_2O_3	16.90	15.00
	FeO	2.60	1.80
	Fe_2O_3	5.88	4.72
	MgO	1.70	0.94
	CaO	4.74	4.60
	Na_2O	2.71	2.55
	K_2O	2.81	3.52
	P_2O_5	0.30	0.39
	MnO	0.13	0.07
	TOTAL	100.49	99.24

The Nevada Bureau of Mines and Geology

The Nevada Bureau of Mines and Geology (NBMG) is a research and public service unit of the University of Nevada and is the state geological survey. NBMG is part of the Mackay School of Mines at the University of Nevada, Reno. NBMG scientists conduct research and publish reports on mineral resources, engineering geology, environmental geology, hydrogeology, and geologic mapping.

Individuals interested in Nevada geology are encouraged to visit, call, or write NBMG or visit our World Wide Web home page (www.nbmg.unr.edu). When visiting NBMG by car please stop at the information booth just inside the Center Street entrance on the south end of the Reno campus of the University of Nevada. The attendant will issue you a temporary parking permit and give you directions to parking areas and to the NBMG offices in the west wing of the Scrugham Engineering-Mines Building. The publications sales office (room 310) and the information office (room 311) are open from 7:30 a.m. to 2:30 p.m., Monday through Friday. Orders for publications or requests for information may be made by telephone (702-784-6691, x2 for orders, x133 for information) from 7:30 a.m. to 4:00 p.m., M-F, or by fax (702-784-1709) or e-mail (info@nbmg.unr.edu for orders and ddavis@nbmg.unr.edu for information) anytime. Please address mail to: Nevada Bureau of Mines and Geology, Mail Stop 178, University of Nevada, Reno, NV 89557-0088.